

Developing Emission Models for Fugitive Particulate Matter in Arid and Semi-Arid Regions



Global Centre for Clean Air Research (GCARE)
Department of Civil and Environmental Engineering
Faculty of Engineering and Physical Sciences
University of Surrey
Guildford, Surrey, UK

A thesis submitted for the fulfilment of
Doctor of Philosophy
by
Hala Hassan

Copyright © Hala Hassan, 2020

Declaration of Originality

This thesis and the work to which it refers are the results of my own efforts. Any ideas, data, images or text resulting from the work of others (whether published or unpublished) are fully identified as such within the work and attributed to their originator in the text, bibliography or in footnotes. This thesis has not been submitted in whole or in part for any other academic degree or professional qualification. I agree that the University has the right to submit my work to the plagiarism detection service Turnitin UK for originality checks. Whether or not drafts have been so-assessed, the University reserves the right to require an electronic version of the final document (as submitted) for assessment as above.

Hala Hassan

University of Surrey, UK

Wednesday, 18th December, 2019

Abstract

There is substantial evidence that airborne particulate matter (PM) contributes to haze, acid rain, global climate change, and decreased life expectancy. Many recent studies have reported that a large fraction of airborne PM could be attributed to fugitive PM (fPM). The developing arid and semi-arid regions, in particular, are facing the biggest brunt of fPM usually ascribed to the regionally transported dust. On the other hand, the rapid expansion of their metropolitan cities is contributing a considerable amount of locally induced fPM which makes it a prominent environmental and health stressor in these areas. Based on field measurements and dispersion modelling, this thesis aims to: (i) measure fPM from two common sources (loose soils and non-exhaust traffic) in areas with arid desert climates, (ii) derive representative emission models, and (iii) assess their overall environmental and health impacts.

For this thesis, on site measurements and samples of PM (<10 μm diameter) were collected. Source apportionment was performed to determine the contributions of individual sources. Dispersion modelling and regression analysis were used to derive emission models for loose Calcisols (a prominent soil in the subject areas) and vehicle-induced fPM (VfPM). Finally, our derived models were used along with the state-of-the-art practices (i.e., regional emission models and the World Health Organization's (WHO) Environmental Burden of Disease (EBD) method) to determine the environmental and health impacts of local fPM. Several important findings were extracted from the above analysis: (i) fPM from different origins contribute more than 60% of the urban PM in arid areas, (ii) power law emission models with wind speed dependence were derived for loose Calcisols soil, (iii) emission factors were derived for VfPM using linear regression and were close to values reported in USA, (iv) EBD estimates found that fPM may lead to ~ 11.0 times higher short-term excess mortalities compared to constant database measurements.

Acknowledgments

Firstly, I would like to express my sincere gratitude to my principal supervisor Professor Prashant Kumar and co-supervisor Dr. Konstantinos Kakosimos for their continuous support during my Ph.D. study, and for their patience, motivation, and immense knowledge that helped me in all the time of research and writing of this thesis.

Besides my supervisors, I wish to thank Dr. Dikaia Saraga and Dr. Thomas Maggos from the Environmental Research Laboratory, INRASTES, NSCR Demokritos, of Greece for their help in conducting the elemental analysis needed to carry out the modelling tasks of this thesis.

I greatly acknowledge the NPRP award [NPRP 7 - 649 - 2 - 241] from the Qatar National Research Fund (a member of The Qatar Foundation) that made this work possible. I would like to thank the Qatar Foundation, the Ministry of Public Health, the Public Work Authority and the Ministry of Transport and Communications of Qatar for facilitating the permissions needed to conduct the field experiments presented in this thesis.

Last but not least, I would like to thank my family: my parents, brother and sister for their unparalleled love, help and constant prayers. My deepest gratitude goes to my loving husband, Nader, whose patience and support made this achievement possible, and to my beautiful son, Omar, for his smile that washed away my misery and kept me going through the hardest times.

Publications

The work described in this thesis appeared in the following published/under review articles and presentations:

Journal Articles

Hassan, H.A., Kumar, P., Kakosimos, K.E., 2016. Flux estimation of fugitive Particulate Matter emissions from loose Calcisols at construction sites. *Atmospheric Environment* 141, 96-105.

Saraga, D., Maggos, T., Sadoun, E., Fthenou, E., **Hassan, H.**, Tsiouri, V., Karavoltos, S., Sakellari, A., Vasilakos, C., Kakosimos, K., 2017. Chemical characterization of indoor and outdoor Particulate Matter (PM_{2.5}, PM₁₀) in Doha, Qatar. *Aerosol and Air Quality Research* 17, 1156–1168.

Argyropoulos, C.D., **Hassan, H.**, Kumar, P., Kakosimos, K.E., 2019. Measurements and modelling of particulate matter building ingress during a severe dust storm event. *Building and Environment*. 167, 106441.

Hassan, H.A., Saraga, D., Kumar, P., Kakosimos, K.E., 2020. Vehicle-induced fugitive Particulate Matter emissions in a city of arid desert climate. *Atmospheric Environment* (revised version under review).

Hassan, H.A., Kumar, P., Kakosimos, K.E., 2020. The impact of local fugitive Particulate Matter and emission inventories on air quality and health impact assessment in dry and arid areas. (ready to be submitted to the Atmospheric Environment journal)

Book Chapters:

Hassan, H., Abraham, M., Kumar, P., Kakosimos, K.E., 2017. Sources and emissions of fugitive Particulate Matter. In: Kumar, P. (Ed.), *Airborne Particles: Origin, Emissions and Health Impacts*. Nova Science Publishers, Inc., pp. 21-35.

Conference Papers and Presentations

Hassan, H., Kumar, P., Kakosimos, K., 2018. Emission models for Particulate Matter in hot-dry environments. Paper presented at the 11th International Conference on Air Quality – Science and Applications, Barcelona, Spain.

Hassan, H., Kumar, P., Kakosimos, K., 2017. Emissions modelling and impact assessment of fugitive Particulate Matter in arid and semi-arid region. Paper presented at the 18th International Conference on Harmonisation within Atmospheric Dispersion Modelling for Regulatory Purposes, Bologna, Italy.

Argyropoulos, C.D., Abraham, M., **Hassan, H.**, Ashraf, A., Fthenou, E., Sadoun, E., Kakosimos, K.E., 2016. Modelling of PM₁₀ and PM_{2.5} building infiltration during a dust event in Doha, Qatar. Paper presented at the 2nd International Conference on Atmospheric Dust (DUST2016), Taranto, Italy.

Hassan, H., Tsiouri, V., Kakosimos, K.E., 2015. Developing emission factors of fugitive Particulate Matter emissions for construction sites in the Middle East area”. Paper presented at the ICAPC 2015: XIII International Conference on Air Pollution and Control, Paris, France.

Hassan, H., Kumar, P., Kakosimos, K., 2016. Fugitive Particulate Matter emissions from loose soils rich in carbonates. Poster presented at the 2nd International Conference on Atmospheric Dust (DUST2016), Taranto, Italy.

Hassan H, Kumar P, Liora N, Melas D, Kakosimos KE. The impact of fugitive particulate matter on the environmental health and sustainability of dry and arid regions. In: Proceedings of the 2016 AIChE Annual Meeting, November 2016. San Francisco, US.

Table of Content

| | | |
|-----------|--|----|
| Chapter 1 | Introduction..... | 17 |
| 1.1 | Background and Motivation..... | 17 |
| 1.2 | Aims and Objectives | 18 |
| 1.3 | Research Significance | 19 |
| 1.4 | Research Approach | 19 |
| 1.4.1 | Flux Estimation of fPM from Loose Soils (Calcisols) at Construction Sites | 20 |
| 1.4.2 | Estimate Vehicle-Induced PM Emissions in An Area with Arid Desert Climate .. | 20 |
| 1.4.3 | Estimate the Impact of Local fPM on Air Quality and Health in Dry and Arid Areas | 21 |
| 1.5 | Thesis Outline | 21 |
| Chapter 2 | Literature Review..... | 24 |
| 2.1 | Introduction | 24 |
| 2.2 | Sources and Mechanisms | 33 |
| 2.3 | Quantification of Emissions | 37 |
| 2.3.1 | Experimental | 37 |
| 2.3.2 | Field Measurements | 37 |
| 2.3.3 | Dispersion Modelling..... | 40 |
| 2.3.4 | Emission Inventories..... | 41 |
| 2.4 | Health Impacts..... | 43 |
| 2.5 | Environmental Impacts and Control | 46 |
| 2.6 | Chapter Summary..... | 48 |
| Chapter 3 | Materials and Methods..... | 50 |
| 3.1 | Introduction | 50 |
| 3.2 | Instrumentation..... | 51 |
| 3.2.1 | Grimm Enviro Check 365 – Environmental Dust Monitor | 51 |
| 3.2.2 | Grimm MicroPNS – Microprocessor Controlled Sampling System..... | 52 |
| 3.3 | Gravimetric Analysis of PM Samples | 52 |
| 3.4 | Models | 53 |
| 3.4.1 | Positive Matrix Factorisation (EPA PMF 5.0) Model | 53 |

| | | |
|-----------|---|-----|
| 3.4.2 | Fugitive Dust Model (FDM)..... | 55 |
| 3.4.3 | CALPUFF Model..... | 55 |
| 3.5 | Chapter Summary..... | 56 |
| Chapter 4 | Flux Estimation of fPM Emissions from Loose Soils (Calciols)..... | 58 |
| 4.1 | Introduction..... | 58 |
| 4.2 | Methodology..... | 63 |
| 4.2.1 | Site Description..... | 63 |
| 4.2.2 | Data Collection..... | 64 |
| 4.2.3 | Atmospheric Dispersion Modelling..... | 67 |
| 4.2.4 | Source Characterization..... | 68 |
| 4.2.5 | Evaluation of EFs..... | 69 |
| 4.3 | Results and Discussion..... | 71 |
| 4.3.1 | Measurements..... | 72 |
| 4.3.2 | Correlations between the Measured Concentrations and Wind Speeds..... | 74 |
| 4.3.3 | Estimation of the Emission Fluxes..... | 75 |
| 4.4 | Chapter Summary and Conclusions..... | 79 |
| Chapter 5 | Vehicle-Induced fPM Emissions..... | 81 |
| 5.1 | Introduction..... | 81 |
| 5.2 | Methodology..... | 84 |
| 5.2.1 | Derivation of the VfPM Emissions..... | 84 |
| 5.2.2 | Field Campaign..... | 89 |
| 5.2.3 | Source Apportionment..... | 90 |
| 5.2.4 | Estimation of Traffic Intensities..... | 92 |
| 5.2.5 | fPM Emissions from Barren Lands and Construction Sites..... | 92 |
| 5.2.6 | Dispersion Modelling of PM..... | 93 |
| 5.3 | Results and Discussion..... | 94 |
| 5.3.1 | Measurements..... | 94 |
| 5.3.2 | Source Apportionment..... | 100 |
| 5.3.3 | Derived Emission Factors..... | 103 |
| 5.4 | Chapter Summary and Conclusions..... | 106 |
| Chapter 6 | The Impact of fPM on Air Quality and Health in Dry-Arid Areas..... | 108 |

| | | |
|------------|---|-----|
| 6.1 | Introduction | 108 |
| 6.2 | Methodology | 112 |
| 6.2.1 | Study Area and fPM Sources | 112 |
| 6.2.2 | Emissions Modelling | 113 |
| 6.2.2.2 | Road Traffic fPM | 115 |
| 6.2.3 | Land-use Characterization and Surface Properties | 115 |
| 6.2.4 | Dispersion Modelling..... | 116 |
| 6.2.5 | Health Impact Assessment Criteria..... | 117 |
| 6.2.6 | Modelling Cases..... | 120 |
| 6.3 | Results and Discussion..... | 121 |
| 6.3.1 | Emission Fluxes | 121 |
| 6.3.2 | Modelled Concentrations | 127 |
| 6.3.3 | Contribution to Airborne PM levels | 133 |
| 6.3.4 | Sensitivity of the Health Impact Assessment..... | 134 |
| 6.4 | Chapter Summary and Conclusions | 138 |
| Chapter 7 | Summary, Conclusions and Future Work..... | 140 |
| 7.1 | Summary | 140 |
| 7.1.1 | Flux Estimation of fPM Emissions from loose Soils (Calcisols) | 141 |
| 7.1.2 | Estimation of Vehicle-Induced fPM Emissions..... | 141 |
| 7.1.3 | The Impact of fPM on Air Quality and Health in Dry-Arid Areas..... | 142 |
| 7.2 | Conclusions | 142 |
| 7.3 | Recommendations for Future Research | 143 |
| References | | 146 |
| Appendix A | | 168 |
| Appendix B | | 169 |
| Appendix C | | 171 |

List of Figures

| | |
|---|----|
| Figure 1.1 Flow chart presenting the structure of the thesis through its main chapters | 22 |
| Figure 2.1 PM levels observed in selected developing areas with arid climates. Blue horizontal line: annual limits according to the EU air quality directive (2008/EC/50). Marron horizontal line: annual recommended guidelines by WHO. | 27 |
| Figure 2.2 Schematic figure showing the movement of particles during wind erosion as taken from Schaap et al. (2009). As seen in the figure, the smaller particles engage in direct suspension while the larger fractions tend to saltate and creep..... | 35 |
| Figure 2.3 Process of rock crushing showing the potential sources of fPM emissions, as taken from Cowherd Jr. and Kinsey (1986) | 36 |
| Figure 2.4. Potential pathways for PM within the human body as taken from Pope III and Dockery (2006)..... | 46 |
| Figure 4.1 Map showing main worldwide areas and the Middle East (inset) covered by Calcisols (FAO, 2014)..... | 61 |
| Figure 4.2 The study area showing: (a) Qatar geological map and sites locations, (b) outline of the construction site and the formed 23 area sources (Section 4.2.3)..... | 65 |
| Figure 4.3. (a) Wind rose for the construction site station during the studied period. Polar plots of PM ₁₀ mean concentration ($\mu\text{g m}^{-3}$) by wind speed (m s^{-1}), (b) for the construction site station during the study period, and (c) for the background station during the study period. | 66 |
| Figure 4.4 Particle size analysis of the five collected soil samples (SS). Soil SS1 to SS3 are from within the construction site and SS4 and SS5 are from the nearby area..... | 71 |
| Figure 4.5 A time series showing the change of mass concentration and the wind (at the construction site station) for an indicative period (~1 week) and after the exclusion of invalid data as described in Section 4.3.1..... | 73 |
| Figure 4.6. Comparison between this study (estimated emission fluxes), the proposed function and AP-42 emission fluxes for (a) PM _{2.5} , and (b) PM ₁₀ . Dashed lines show the 90% confidence and prediction bands | 78 |
| Figure 4.7. Scatter plot of modelled versus measured (net) mass concentrations for: (a) PM ₁₀ , and (b) PM _{2.5} . Plots also indicate the data filtered according to wind sectors. Solid line indicates perfect agreement and dashed lines show a difference of a factor of two (FAC2)..... | 78 |

| | |
|---|-----|
| Figure 5.1 Outline of the methodologies for the estimation of VEX EFs (orange pathway), VfPM EFs (green pathway), and the interconnections with the employed methods (blue blocks; in brackets the corresponding section number). Other results (white blocks w/ blue outline) and non-studied phenomena (greyed blocks) are also displayed | 88 |
| Figure 5.2 A map of Doha's major roads network showing the sampling site and the adjacent roads | 90 |
| Figure 5.3 Windrose diagram at the sampling site during the campaign period | 95 |
| Figure 5.4 Time series of the hourly measured PM _{2.5} and PM ₁₀ concentrations using the particle counter..... | 98 |
| Figure 5.5 Pollution roses of the PMCs ($\mu\text{g m}^{-3}$) hourly measurements (PM ₁₀ <1000 $\mu\text{g m}^{-3}$).... | 98 |
| Figure 5.6 Mean diurnal and weekly variations of (a) PM _{2.5} and (b) PM ₁₀ concentrations using two subsets of the data (PM ₁₀ <200 $\mu\text{g m}^{-3}$ & PM ₁₀ <160 $\mu\text{g m}^{-3}$). The shaded areas indicate the 95% confidence intervals. | 99 |
| Figure 5.7 Factor contributions (constrained) to the total PM and the elemental profiles for each of the PMF factors as percentage contributions and absolute concentrations (ASS: aged sea salt, SEA: secondary aerosol, FSS: fresh sea salt, RESUS: resuspension, VEX: vehicle exhaust, FO/SHP: fuel oil/shipping) | 102 |
| Figure 5.8 Correlation heatmap for the estimated PMF factors (ASS: aged sea salt, SEA: secondary aerosol, FSS: fresh sea salt, RESUS: resuspension, VEX: traffic, FO/SHP: fuel oil/shipping, and Total), meteorological quantities (ws: wind speed, T: temperature, u*: friction velocity, and humidity), and dispersion modelled quantities (AR10: barren lands and construction, VfPM: RESUS-AR10, c_ldv: contribution of light-duty vehicles, c_hdv: contribution of heavy-duty vehicles, and road: contribution of road surface)..... | 104 |
| Figure 5.9 Scatter plot examples of the measured vs predicted (a) exhaust (VEX) and (b) non-exhaust (VfPM) PM ₁₀ concentration levels with the proposed (linear) EFs. Vectors correspond to the daily wind speed and prevailing direction, and colors corresponde to the average relative humidity [%].. | 106 |
| Figure 6.1 The LULC maps of the study area (a) GLCC (standard practice), (b) OWN (modified). The OWN land-use map shows the soil HWSD classifications of soils: SL= Solonchanks, SD = Sand Dunes, LP = Leptosols, CL= Calcisols..... | 117 |

| | |
|--|-----|
| Figure 6.2. Map showing the major roads network (230 segments) in the Doha metropolitan area and the discrete receptors..... | 118 |
| Figure 6.3 Gridded population of 2015 over Doha’s metropolitan area..... | 120 |
| Figure 6.4 Mean emission fluxes of windblown PM ₁₀ ($\mu\text{g m}^{-2} \text{s}^{-1}$) over Qatar for the modelling period (January-December, 2015) – (a) Case 1, (b) Case 2, (c) Case 3 – as shown in Table 6.2. | 124 |
| Figure 6.5 Mean emission fluxes of windblown PM _{2.5} ($\mu\text{g m}^{-2} \text{s}^{-1}$) over Qatar for the modelling period (January-December, 2015). (a) Case 1, (b) Case 2, (c) Case 3..... | 125 |
| Figure 6.6 Mean emission fluxes of PM ₁₀ ($\mu\text{g m}^{-2} \text{s}^{-1}$) emitted from VEX (left) and VfPM (right) along Doha’s major road network. (a and b) show Cases 1 and 2, (c and d) show Case 3. | 126 |
| Figure 6.7 Mean emission fluxes of PM _{2.5} ($\mu\text{g m}^{-2} \text{s}^{-1}$) emitted from exhaust (left) and non-exhaust (right) traffic along Doha’s major road network. (a) and (b) Case 1&2, (c) and (d) Case 3 | 127 |
| Figure 6.8 The annual mean PM ₁₀ ($\mu\text{g m}^{-3}$) contributions from barren lands predicted by CALPUFF model over Doha. (a) Case 1, (b) Case 2, (c) Case 3. | 129 |
| Figure 6.9 The annual mean PM _{2.5} ($\mu\text{g m}^{-3}$) contributions from barren lands predicted by CALPUFF model over Doha. (a) Case 1, (b) Case 2, (c) Case 3. | 130 |
| Figure 6.10 The annual mean PM ₁₀ ($\mu\text{g m}^{-3}$) contributions from VEX (left) and VfPM (right) predicted by CALPUFF model over Doha. Case 1 (a & b), Case 2 (c & d), Case 3 (e & f). The highest emissions roads are marked in (a). | 131 |
| Figure 6.11 The annual mean PM _{2.5} ($\mu\text{g m}^{-3}$) contributions from VEX (left) and VfPM (right) predicted by CALPUFF model over Doha. Case 1 (a & b), Case 2 (c & d), Case 3 (e & f). | 132 |
| Figure 6.12 Time series comparing modelled and measured concentrations of (a) PM _{2.5} and (b) PM ₁₀ | 136 |
| Figure 6.13 Pollution roses showing the measured and modelled (Case 3) concentration by wind direction. The right side shows polar plots of the standard deviation of modelled concentrations (normalised by the mean)..... | 137 |
| Figure 6.14 The ratio of Case 3 to Case 0 (WHO) expected mortalities (per 0.25 km ²) attributable to outdoor fugitive PM ₁₀ | 138 |
| Figure A1 Contribution plot showing the contribution (%) from each wind sector to the mean PM ₁₀ | 168 |
| Figure B1 PM _{2.5} weekday pollution roses (with PM ₁₀ threshold <160 $\mu\text{g m}^{-3}$)..... | 169 |

Figure B2 Scatter plot examples of the measured vs predicted (a) VEX and (b) VfPM PM_{2.5} concentration levels with the estimated EFs. Vectors correspond to the daily wind speed and prevailing direction, and colours the average relative humidity [%]..... 170

Figure C1 Wind roses comparing the meteorology data from CALMET and WRF models two locations within Doha city: (i) monitoring site and (ii) Doha International Airport.....172

Figure C2 Scatter plots of wind speeds (u_{10}) predicted by CALMET and WRF models at two urban sites in Doha city: (i) the monitoring site and (ii) Doha International Airport.....173

List of Tables

| | |
|--|-----|
| Table 2.1 Measured PM concentrations in different sites of the developing arid region | 26 |
| Table 2.2 Overview of source apportionment studies conducted in developing arid countries, showing the percentage source contribution to PM _{2.5} and PM ₁₀ | 29 |
| Table 3.1 Instruments and models used in chapters (4-6) of the thesis | 51 |
| Table 4.1 Parameters of emission flux function ($E = Q_0 u^w$; $\text{g m}^{-2} \text{s}^{-1}$) for four particle size class and the goodness of fit results (for hourly averages dataset)..... | 75 |
| Table 5.1 Literature Emission Factors (EFs) for Traffic PM [mg VKT^{-1}] | 86 |
| Table 5.2 Statistical results of the measured meteorological parameters | 95 |
| Table 5.3 Statistical analysis of the daily measured PMC data | 96 |
| Table 6.1 Examples of emission inventory studies in areas with arid or semi-arid climates | 111 |
| Table 6.2 The four modelling scenarios formulated to study the sensitivity of the health impact assessment criteria | 121 |
| Table 6.3 Total Annual PM emission from barren lands, VEX, and VfPM road traffic | 123 |

List of Acronyms

| | |
|------------------------------|---|
| CALPUFF | California Puff Model |
| CMB | Chemical Mass Balance |
| EBD | Environmental Burden of Disease |
| EEA | European Environment Agency |
| EF | Emission Factor |
| EMEP | European Monitoring and Evaluation Program |
| FDM | Fugitive Dust Model |
| fPM | Fugitive Particulate Matter |
| PM ₁₀ | Particulate matter less than 10 µm in aerodynamic diameter |
| PM _{2.5} | Particulate matter less than 2.5 µm in aerodynamic diameter |
| PMF | Positive Matrix Factorisation |
| PMCs | Particles Mass Concentrations |
| PNCs | Particles Number Concentrations |
| PSA | Particle Size Analysis |
| Q _o | Proportionality Constant |
| QGIS | Quantum Geographic Information System |
| USEPA | United States Environmental Protection Agency |
| u [*] | Wind Friction Velocity |
| u _{th} [*] | Threshold Friction Velocity |
| VfPM | Vehicle-induced fugitive Particulate Matter |
| w | Wind Speed Dependence Factor |
| wd | Wind Direction |

| | |
|-----|---------------------------|
| WHO | World Health Organization |
| ws | Wind Speed |
| XRD | X-ray Powder Diffraction |
| XRF | X-ray Fluorescence |

Chapter 1 Introduction

This chapter provides an overview of the research in the context of particulate matter pollution in arid areas, especially from fugitive (uncontrolled) sources. It provides a background and the motivation to explore the subject, the aims and objectives of this research project and a brief overview of the research approach and structure.

1.1 Background and Motivation

Outdoor air pollution is one of the world's biggest environmental challenges, accounting for the loss of 4.2 million lives worldwide every year (WHO, 2016b). Ambient Particulate Matter (PM), in particular, had become a topic of increasing concern, due to its deleterious impacts to humans and the environment. Cities in the developing arid and semi-arid regions (i.e., North Africa, Middle East and Central Asia) have been recording remarkable levels of atmospheric PM, frequently exceeding international standards (Khodeir et al., 2012; Saraga et al., 2017; Shaltout et al., 2013). A study conducted in the city of Tehran (Iran) documented 2197 excess deaths in a year owing to short-term exposure to more than $10 \mu\text{g m}^{-3}$ PM_{10} (particles $\leq 10 \mu\text{m}$ in aerodynamic diameter) (Naddafi et al., 2012). As reported by several studies, a large portion of PM_{10} in arid environments come from fugitive sources, such as aeolian dust, vehicles tyre and brake markers, and dust resuspensions (Abu Allaban et al., 2007; Engelbrecht and Jayanty, 2013; Massoud et al., 2011; Sowlat et al., 2013). Nonetheless, there are relatively few studies that focus on the fugitive part of airborne PM in these regions, and most of the available ones focus on the regional influence rather than local sources (Prakash et al., 2015).

Determination of fugitive Particulate Matter (fPM) emissions has been an ongoing challenge for the air quality research community because of the induced health effects and the large uncertainty on their determination (Neuman et al., 2009; Roney and White, 2006). Different techniques such as field measurements (Brown et al., 2008; Kouyoumdjian and Saliba, 2006; Shahsavani et al., 2012), laboratory scale testing (Neuman et al., 2009; Roney and White, 2006) and dispersion modelling (Ono et al., 2011) have been used in the past for the adequate determination of fPM emissions. These techniques were also used for the development of empirical emission factors (EFs) (Sanf elix et al., 2015). Most of the currently available EFs, however, were developed for certain geographical areas and weather conditions of Europe and North America, which may lead to inaccuracies when applied to other surfaces of interest (Sanderson et al., 2014).

1.2 Aims and Objectives

fPM emissions in dry and arid regions generate from natural sources (e.g., windblown dust and sea salt) or anthropogenic sources (e.g., construction and non-exhaust traffic emissions). The overall objective of this research is to investigate the effect of fPM in an area with a typical arid desert climate representative of the wider developing region, and derive representative emission models to quantify fPM from common local sources in these areas. The specific objectives of this project are to:

1. Design and perform field studies to: (i) collect source related information, (ii) measure ambient PM concentrations from selected fPM sources (barren lands and non-exhaust traffic), and (iii) collect soil and ambient PM samples from different sites for the purpose of source characterization

2. Use dispersion modelling to calculate PM concentrations from loose soils and obtain their emission fluxes in an iterative procedure. The aim is to derive emission flux functions for the estimation of fPM from local loose soils that express their wind speed dependence.
3. Use the elemental data of the ambient samples to run source apportionment modelling to identify the individual source contributions.
4. Use the sources apportionment results, coupled with dispersion modelling and regression analysis to derive EFs for vehicle-induced PM – or in other words exhaust and non-exhaust traffic emissions.
5. Perform dispersion modelling to estimate the impact of local fPM on air quality and health in dry and arid areas, using our own developed models and literature emission inventories.

1.3 Research Significance

Lack of information on fPM sources is critical, given that many of these sources can be seen close to residential areas and could have a direct impact on sensitive groups such as children and elderly. At the same time, fPM emission rates introduce the largest uncertainty in air quality assessment (i.e., dispersion modelling). This study creates a new knowledge and experimental insights concerning the release of fPM, especially in dry-arid regions where the meteorological and soil conditions play a significant role. Finally, new emission models (i.e., emission flux functions and factors) will be developed for fPM with the capacity to improve regional and local air quality and climate modelling efforts.

1.4 Research Approach

To achieve objective 1, a field campaign was conducted from April to June 2015 at a sampling site ~ 50 m away from a busy road to measure traffic PM. In addition, measurements taken earlier (April to May 2014) from a construction site at rest (and a background location) were

used to represent the exposed urban barren lands (Hassan, 2015). The measurements collected from both sites include: (i) continuous particle number (PNC) and mass (PMC) concentrations, (ii) composite soil samples collected from the construction site, and (iii) integrated ambient samples collected at the road-adjacent site.

To achieve the rest of the objectives, the following step by step research approach was followed:

1.4.1 Flux Estimation of fPM from Loose Soils (Calcisols) at Construction Sites

To achieve objective 2, PM concentrations collected from the construction site (i.e., loose soils) were combined with dispersion modelling to develop the specific functions for the emission fluxes (i.e., emission rates per area). A dispersion model - Fugitive Dust Model (FDM) - was implemented to calculate PM concentrations and obtain their emission fluxes in an iterative procedure. The model results were fitted to a power function, which expresses the wind velocity dependence. The results of this analysis and derived functions are presented in Chapter 4.

1.4.2 Estimate Vehicle-Induced PM Emissions in An Area with Arid Desert Climate

To achieve objective 3, the elemental data of the ambient samples collected at the road-adjacent site were used to run source apportionment modelling using Positive Matrix Factorisation (PMF) model. The PMF results provide the contributions of vehicle exhaust emissions, and dust resuspensions (which include the contribution of barren lands, non-exhaust traffic and transboundary emissions). This leads to objective 4, where dispersion modelling is performed to obtain two sets of contributions (i) the contribution of local barren lands and constructions sites (in order to eventually estimate the non-exhaust traffic contributions), and (ii) the traffic contribution of light-duty vehicles and heavy-duty vehicles estimated using a unity EF. Finally, regression analysis was performed to investigate linear and non-linear relations of the variables,

and derive the EFs and models for exhaust and non-exhaust traffic PM. The results of this study are presented in Chapter 5.

1.4.3 Estimate the Impact of Local fPM on Air Quality and Health in Dry and Arid Areas

Finally, objective 5 is achieved by running dispersion modelling and comparing four distinct modelling cases. The first case (baseline or Case 0) reflects the standard practice of the World Health Organisation (WHO) with one health impact assessment criteria utilized for the whole population based on an annual average concentration obtained from the local monitoring network or satellite data. The other three cases improve, in principle, the baseline case by assigning to the population location-specific average concentrations. Case 1 and Case 2 estimate emissions using regional models and inventories developed for other regions, and Case 3 incorporates our locally developed models from the previous objectives. Finally, the health outcomes associated with the modelling cases are assessed following the WHO's environmental burden of disease (EBD) method. The modelling and health impact results are presented in Chapter 6.

1.5 Thesis Outline

This thesis comprises 7 chapters as presented in Figure 1.1. Chapter 1 discusses the motivation, objectives and significance behind this research, and outlines the approaches followed to achieve each objective.

Chapter 2 provides a background on fPM pollution in dry-arid areas, discusses their sources, concepts of entrainment, means of measurements and control. It also highlights the shortcomings of the existing knowledge on the topic.

Chapter 3 discusses the methodologies and the experimental set-ups used in this project. It includes descriptions of the instruments used for measuring fPM, and the models used for source characterization and calculating the dispersion of emissions.

Chapter 4 presents the results of measuring fPM emissions from loose soils. In this chapter, measurements are coupled with dispersion modelling to obtain the emission flux functions of fPM produced by a specific type of soil – the Calcisols – common in dry and semi-dry regions of North Africa, Middle East, Central Asia and Australia.

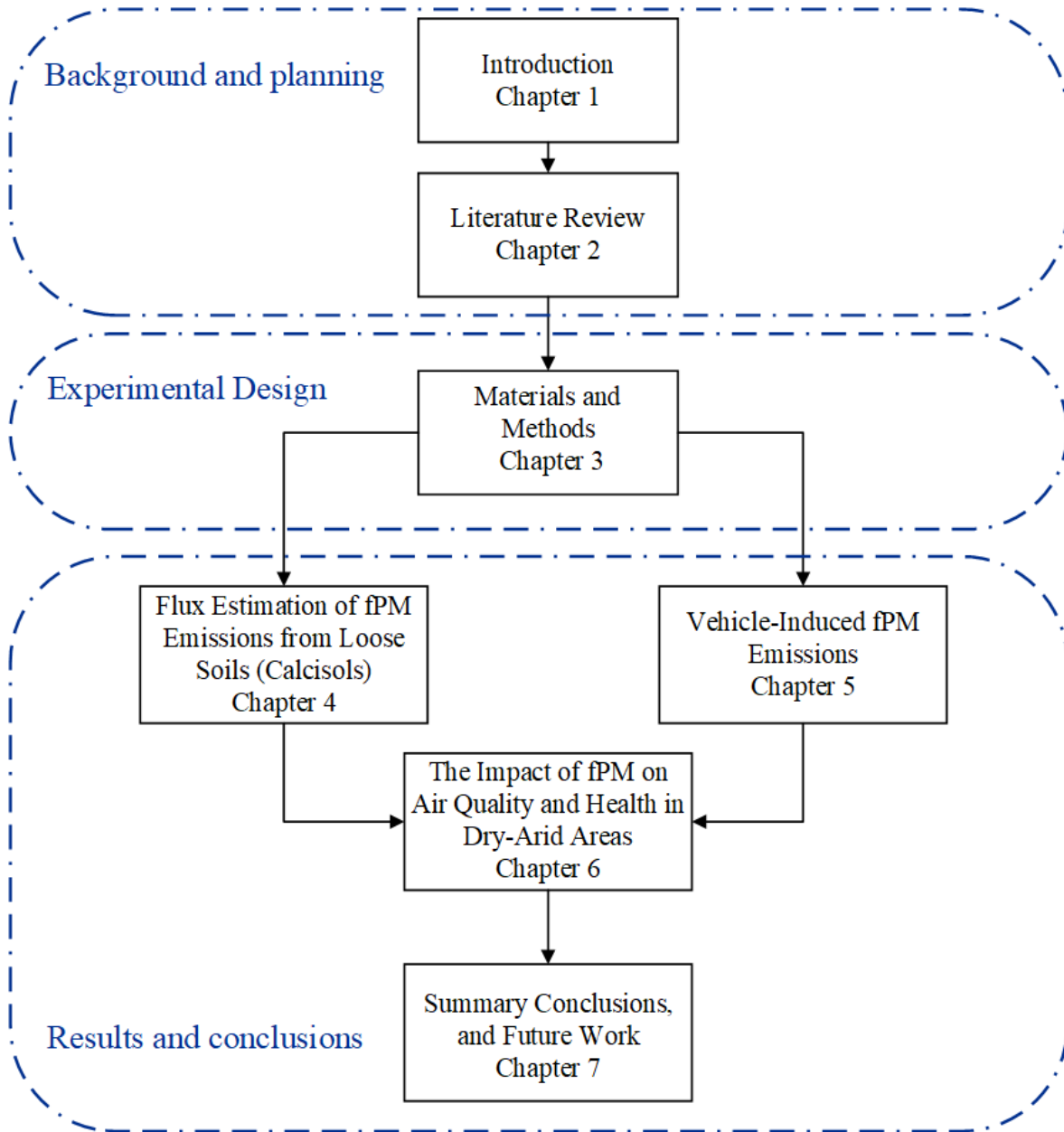


Figure 1.1 Flow chart presenting the structure of the thesis through its main chapters

Chapter 5 presents the results of measuring fPM from road traffic. In this chapter, a combination of field measurements, source apportionment, dispersion modelling and regression analysis were used to obtain EFs and emission models for vehicle-induced exhaust (VEX) and fugitive (non-exhaust) particulate matter (VfPM).

Chapter 6 presents the results of employing the derived EFs and models from chapters 4 and 5 to assess the impact of local fPM from common sources in a typical arid and dry area in Middle East. The results assess the sensitivity of different emission models, surface data (land use) and determines the health impact in the exposed urban areas.

Chapter 7 reviews the stated objectives of this research and presents a summary of the thesis, followed by a conclusion of the findings and suggestions for the direction of future work.

Chapter 2 Literature Review

The aim of this chapter is to define fPM and explain their significance in urbanizing arid environments. Firstly, the chapter discusses the types (natural and anthropogenic) and origins (regional and local) of fPM sources in the developing arid regions. Next, it explains the mechanisms and factors governing the fPM entrainment. Thereafter, the methods of quantification (laboratory experiments, field measurements and dispersion modelling) and the applicability of the currently available emission inventories are discussed. Finally, the chapter throws the light on the main health risks associated with fPM exposure and the common methods of control. This work appeared in (Hassan et al., 2017a).

2.1 Introduction

Ambient PM, referring to the mix of solid and liquid particles suspended in the air, is a prominent component of air pollution in urban environments. PM is a complex pollutant that varies greatly in size, composition and origin. It is often categorized in research as ultrafine particles (UFP; ≤ 100 nm in aerodynamic diameter), fine particles (PM_{2.5}; ≤ 2.5 μm in aerodynamic diameter), and coarse particles (PM_{2.5-10}; > 2.5 μm and ≤ 10 μm in aerodynamic diameter); PM₁₀ is the sum of fine and coarse particles. These sizes are small enough to stay airborne longer, have lower deposition rates and are easily inhalable compared to larger particles, posing a higher risk to human health (Heal et al., 2012). PM can also be classified as primary (i.e., released directly from the source to the atmosphere) or secondary (i.e., formed in the atmosphere due to reactions between gaseous pollutants) (USEPA, 2009). There is substantial evidence that airborne PM contributes to haze, acid rain, global climate change, and decreased life expectancy (Heal et al.,

2012; Kumar et al., 2014). The WHO had set annual mean guidelines for PM₁₀ and PM_{2.5} at 20 µg m⁻³ and 10 µg m⁻³, respectively (WHO, 2005). Nonetheless, recent data shows that 92% of the world's population live in areas where PM_{2.5} levels exceeded those guidelines (WHO, 2016a).

The developing arid and semi-arid regions (i.e., North Africa, Middle East and Central Asia; ~ 19% of the world's total area), exhibit remarkable levels of atmospheric PM arising primarily from wind erosion of surface soil (Tsiouri et al., 2015). On the other hand, anthropogenic sources in these regions continue to significantly feed these levels through the speedy growth of the metropolitan cities, populations, road traffic and industries (Saab, 2017). Populations exposed to such levels suffer increased respiratory and cardiovascular diseases (Bener et al., 2009; Nasser et al., 2015), exposure to carcinogenic constituents (Alghamdi, 2016), and risk of mortality (Harrison et al., 2017). Table 2.1 presents PM concentrations from published field studies conducted in several urban and rural sites across the developing arid regions. The reported PM levels in these studies show a large variation between the sites, and they often far exceed those of international standards (Khodeir et al., 2012; Saraga et al., 2017; Shaltout et al., 2018). For example, a one year study conducted in Jeddah city revealed that 90.0%, 88.9%, 95.9% and 91.8% of the mean 24-h PM₁₀ concentrations exceeded WHO's maximum daily guidelines during summer, autumn, winter, and spring, respectively, of the studied year (Lim et al., 2018). Annual average concentrations of PM_{2.5} observed in Islamabad ranged between 47.8 µg m⁻³ to 93.0 µg m⁻³ during 2007-2011, exceeding not only the WHO's guidelines but even the Pakistan National Environmental Quality Standards (Rasheed et al., 2015). Figure 2.1 shows a comparison of the mean levels reported in selected arid areas compared to WHO's guidelines and the annual limits of the European Union (EU) air quality directive (2008/EC/50).

Table 2.1 Measured PM concentrations in different sites of the developing arid region

| Country | Site/City | PM ₁₀ ($\mu\text{g m}^{-3}$) | PM _{2.5} ($\mu\text{g m}^{-3}$) | Year recorded | Reference |
|--------------|-----------------|--|---|---------------|---------------------------------|
| Lebanon | Beirut | 84±27 | 31±9 | 2004-2005 | (Kouyoumdjian and Saliba, 2006) |
| Iraq | Balad | 184 | 56 | 2006-2007 | (Engelbrecht et al., 2009a) |
| | Baghdad | 250 | 103 | 2006-2007 | |
| | Tallil | 303 | 65 | 2006-2007 | |
| | Tikrit | 298 | 111 | 2006-2007 | |
| | Taji | 213 | 81 | 2006-2007 | |
| | Al Asad | 95 | 37 | 2006-2007 | |
| | UAE | UAE | 140 | 52 | |
| Qatar | Qatar | 165 | 67 | 2006-2007 | |
| Afghanistan | Bagram | 108 | 38 | 2006-2007 | |
| | Khowst | 127 | 75 | 2006-2007 | |
| Kuwait | Northern Kuwait | 211 | 67 | 2006-2007 | |
| | Central Kuwait | 298 | 87 | 2006-2007 | |
| | Coastal Kuwait | 176 | 60 | 2006-2007 | |
| | Southern Kuwait | 199 | 62 | 2006-2007 | |
| Djibouti | Djibouti | 72 | 35 | 2006-2007 | |
| Palestine | Haifa | - | 19.9 | 2007 | (Sarnat et al., 2010) |
| Jordan | Amman | - | 34.9 | 2007 | |
| Egypt | Cairo | - | 27±7 | 2014-2015 | (Shaltout et al., 2018) |
| | Cairo | 99 | 40 | 2002 | (Abu Allaban et al., 2007) |
| Saudi Arabia | Jeddah | 108 | 22 | 2011-2012 | (Lim et al., 2018) |
| | Makkah | 45 | 23 | 2014-2015 | (Munir et al., 2017) |
| Bahrain | Muharaq | 185 | 43 | 2012 | (Coskuner et al., 2018) |
| Alegria | Constantine | 49 | - | 2010 | (Terrouche et al., 2015) |
| Iran | Tehran | - | 30.9-33.2 | 2012-2013 | (Taghvaei et al., 2018) |

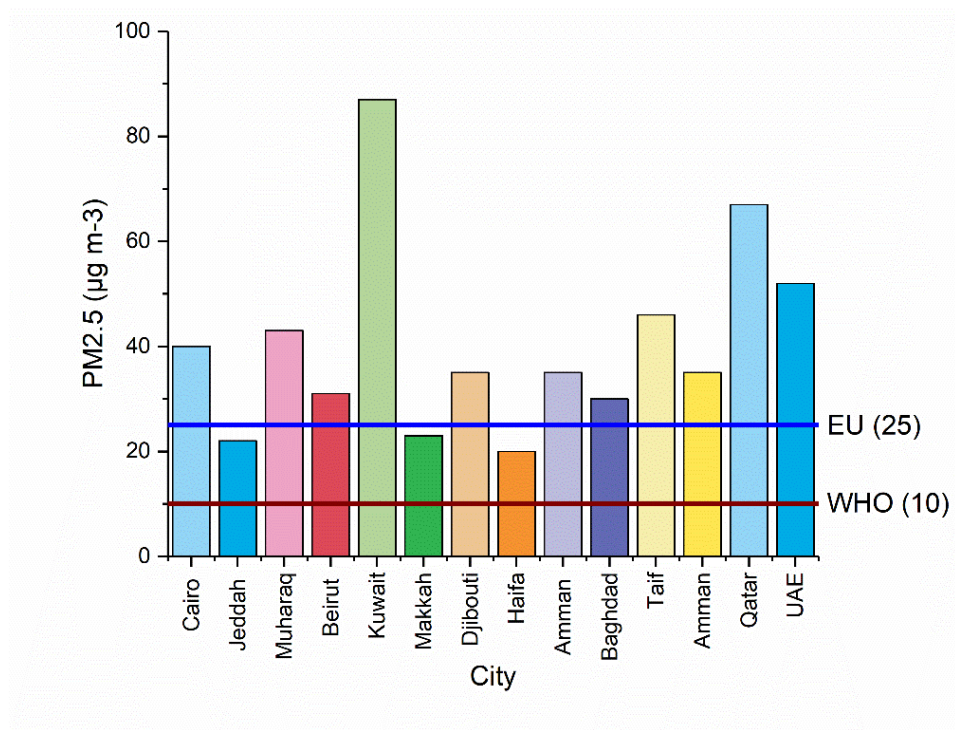
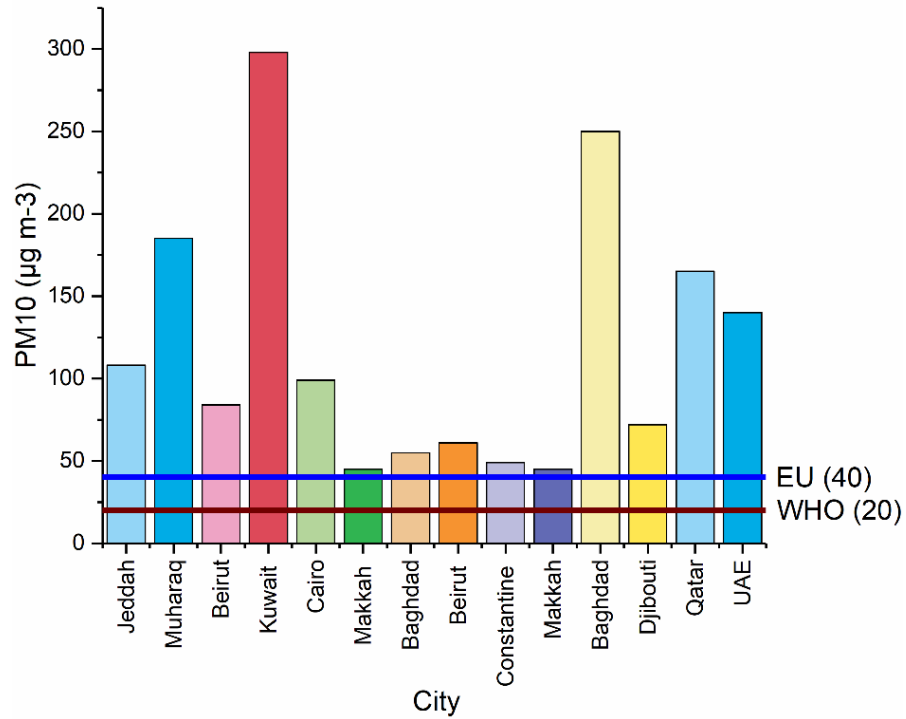


Figure 2.1 PM levels observed in selected developing areas with arid climates. Blue horizontal line: annual limits according to the EU air quality directive (2008/EC/50). Marron horizontal line: annual recommended guidelines by WHO.

Fugitive PM (fPM) are the primary particles that escape directly to the atmosphere, without passing through a controlling duct, when applying a mechanical force on an exposed surface (USEPA, 1995). fPM sources are usually categorised into open dust sources (e.g., unpaved and paved roads, exposed areas and handling of materials) and process-based sources (e.g., crushing, grinding, furnacing, blasting and the like). fPM can also be distinguished as natural and anthropogenic depending on their origin (Lenschow, 2001). Source characterization studies conducted in several developing cities have found that fPM (e.g., loose soil, road dust and marine aerosols) contribute heavily to PM levels at urban sites (Sowlat et al., 2013). For example, Khodeir et al. (2012) analysed ambient PM samples collected from multiples sites in Jeddah city using XRF and SPlus Factor Analysis model with Varimax rotations, and showed that 64% of PM₁₀ mass come from soil resuspensions. Another study by Engelbrecht and Jayanty et al. (2013) used PMF to model the chemical data of ambient PM samples collected from six cities in Iraq. Their results identified five factors (sources) of PM in which four of them were attributed to geological dust, while one factor pointed to exhaust emissions from gasoline vehicles. Studies also suggest that fPM is strongly associated with the coarse fraction of PM₁₀ (Hamdan et al., 2015). For example, Alolayan et al. (2013) performed a combined source apportionment and back trajectory profiles analysis of PM_{2.5} samples collected from an urban site in central Kuwait. Their results showed that while 54% of PM_{2.5} came from sand dust, its profile belayed regional origins. Another recent study by Lim et al. (2018), where PM_{2.5} and PM₁₀ samples were collected for one year (June 2011-May 2012) at an urban site in Jeddah city, showed that soil dust contributed 27% and 77% of PM_{2.5} and PM_{2.5-10}, respectively. Table 2.2 presents the results of previous source apportionment studies conducted at different sites featuring the typical arid climate found in the subject areas (i.e., hot and humid summers, mild winters, and minimal rainfall; (Shraim et al., 2016)).

Table 2.2 Overview of source apportionment studies conducted in developing arid countries, showing the percentage source contribution to PM_{2.5} and PM₁₀

| Reference | Location (type) | Sampling Instruments | Measured PM fraction | Source Apportionment Method | Sources identified (contribution of each source to the total apportioned PM) |
|---------------------------------|--|--|---|-----------------------------|--|
| (Nayebare et al., 2018) | Makkah, Saudi Arabia (mix of residential and urban/semi industrial sites) | Low volume air sampling pump, ambient samples collected on Whatman PTFE, 46.2 mm filters | PM _{2.5} | PMF | PM _{2.5} : 30.1% vehicular emissions; 28.9% industrial mixed dust; 24.7% soil/earth crust ; 16.3% fossil fuels/oil combustion. |
| (Nayebare et al., 2016) | Rabigh, Saudi Arabia (small town close to heavily industrialized areas) | Low volume air sampling pump, ambient samples collected on Whatman PTFE, 46.2 mm filters | PM _{2.5} | PMF | PM _{2.5} : 13.4% vehicular emissions; 14.7% industrial mixed dust ; 12.1% sea spray ; 39.9% soil/earth crust , 19.9% heavy oil combustion. |
| (Kholdebarin et al., 2015) | Tehran, Iran (four sites in Tehran metropolitan city) | High volume sampler. ambient samples collected on Whatman quartz microfiber filters | PM ₁₀ | CMB | PM ₁₀ : 95.4% road dust (wear and friction of car tires) , 4.1% transport, 0.4% Industries. |
| (Sowlat et al., 2013) | Ahfaz, Iran (city in southwestern Iran, high gas and oil rich region and in close proximity to the southern deserts of Iraq) | Anderson high volume air sampler, ambient samples collected on 20cm x 25cm glass-fibre filters | PM ₁₀ | PMF | PM ₁₀ : 41.5% crustal dust , 5.5% road dust , 11.5% motor vehicles, 8% marine aerosols , 9.5% secondary aerosols, 6% metallurgical plants, 13% petrochemical and fossil fuel combustion. |
| (Engelbrecht and Jayanty, 2013) | Tikrit/Balad/Taji/Baghdad/Tallil/Al Asad, Iraq (six monitoring sites along or close to the river valleys of Tigris and Euphrates rivers) | Air metrics MiniVol sampler, ambient samples collected on Teflon and quartz fibre filters | TSP, PM _{2.5} , PM ₁₀ | PMF | 5 factors (sources), four were ascribed to saline soils, dust-gypsum, dust-calcite, dust-siliceous and one factor attributes to exhaust emissions from gasoline vehicles. |

| | | | | | |
|----------------------------|--|---|--------------------------------------|--|---|
| (Khodeir et al., 2012) | Jeddah, Saudi Arabia (coastal city surrounded by mountains in the NE-E-SE) | Automated Cartridge Collector Unit (ACCU) sampler, ambient samples collected on Teflon filters | PM _{2.5} , PM ₁₀ | SPlus Factor Analysis model with Varimax rotations | PM _{2.5} : 69% heavy oil combustion, 8.2% resuspended soil , 8.6% industrial mix, 3.7% traffic. PM ₁₀ : 64% soil resuspension , 18% heavy oil combustion, 18% industrial sources, 9.3 marine aerosols . |
| (Massoud et al., 2011) | Beirut, Lebanon (three urban sites within 100 m distance from busy roads, and one of them is close to the commercial centre of the city) | Direct impaction using Partisol 2300 (R&P) sampler, and Virtual impaction using Sierra–Anderson Dichotomous SA246B sampler, ambient samples collected on Teflon laminated filters | PM _{2.5} , PM ₁₀ | PMF | PM ₁₀ : markers of tires and brakes, dust resuspension and biogenic crustal emission predominated . PM _{2.5} : secondary aerosols determined by the high concentration of nitrated and sulphated compounds prevailed. |
| (Abu Allaban et al., 2007) | Cairo, Egypt (six sites representing: area with significant agricultural activities, area close to busy road, residential areas close to industrial sources and residential areas with minimal surrounding sources) | Medium volume sampler, using Sierra-Andersen 254 PM ₁₀ inlet or Bendix PM _{2.5} cyclone (flow rate=113 l/min). samples collected on Teflon filters. | PM _{2.5} , PM ₁₀ | CMB | PM ₁₀ : major contributors are geological material , mobile sources and open burning. PM _{2.5} : major contributors are mobile sources, open burning and secondary species. |

Climate and meteorology play a major role in the generation and behaviour of fPM. Studies in the developing arid and semi-arid regions have shown distinct seasonal variations in fPM levels, mainly influenced by the frequently occurring dust storms (Abdeen et al., 2014; Nayebare et al., 2018). According to MODIS (Moderate Resolution Imaging Spectroradiometer) satellite images by NASA, 60 dust storms have occurred over the Middle East in the 8 years from 2003 to 2011, in which some has reached the eastern parts of Iran (data available at: <https://earthobservatory.nasa.gov/topic/natural-event>). The region contains the world's largest dust reservoir (the Sahara Desert), that emits hundreds of tetra grams of dust every year (Laurent et al., 2008). Active dust areas were also identified in south and southwest of Iran, Iraq, and the coastal areas of Oman, UAE, Kuwait and Saudi Arabia (Prakash et al., 2015). PM levels were reportedly the highest during summer and spring and the lowest during fall and winter (Kouyoumdjian and Saliba, 2006). The summer months are marked by the north-westerly (also called "Shamal"; means *north* in Arabic) winds that lift up dust from the Tigris and Euphrates basin in Iraq and blows it south-eastward it over most of the countries along the Arabian Gulf such as Iraq, Saudi Arabia, Kuwait, Qatar, Bahrain and UAE (Engelbrecht and Jayanty, 2013). A typical Shamal season starts on 30 May \pm 16 days and ends on 16 August \pm 16 days, with the highest frequency observed in June and July (Yu et al., 2016). The Shamal phenomenon occurs due to the convergence of two synoptic atmospheric systems: (i) the high-pressure system formed by the anticyclones over the north of Africa to eastern and central Europe and (ii) the low-pressure system represented by the Monsoon trough over Iraq, southern Iran, Pakistan, and India subcontinent (Hamidi et al., 2014). Hamidi et al. (2013) identified that the high-pressure systems responsible for 68% of the Shamal events extend from north of Egypt to east of Spain and south of France, and from centre of Libya to north of Italy, while the low-pressure systems associated with 67% of

the Shamal extend from centre of Pakistan to north-west of Arabian Gulf, and from north-east of Oman to north-east of Iran and south-east of Turkmenistan. The pressure gradient caused by aforementioned systems produces strong north-western winds, creating the perfect conditions for a Shamal event to occur. Al Senafi and Anis (2015) defined a Shamal day as a WNW-N winds with an hourly average wind speed $\geq 9.85 \text{ m s}^{-1}$ blowing during at least 3 hours day⁻¹, and it takes two consecutive Shamal days to call an event.

Ambient PM concentrations can reach substantial levels during dust events, and may remain high for extended periods of time (Goudie, 2014). For examples, a recent simulation of natural dust over central Middle East region estimated the minimum emissions during a Shamal episode (occurred between 18 and 26 June, 2015) to be $20 \mu\text{g m}^{-2} \text{ s}^{-1}$, and reaching several hundreds in some areas (Kontos et al., 2018). In Ahfaz (Iran), Shahsavani et al. (2012) reported 72 dusty days between April and September 2010, with the longest dust event occurring in July, lasted for five days and recorded a peak PM₁₀ concentration of $2028 \mu\text{g m}^{-3}$, and the most intense event recorded in June, lasted for two days with a peak concentration of $5337.6 \mu\text{g m}^{-3}$. Dust events don't only affect local surroundings, but transport dust for long distances across continents (Farahat, 2016). Simulations of one of the major dust storms that occurred over the Arabian Peninsula from 18 to 22 March 2012 showed that 78% of the generated dust was deposited locally while 22% was transported outside the modelling domain (Prakash et al., 2015). Episodes of the Saharan dust were indeed observed in several East Mediterranean cities (Athanasopoulou et al., 2016; Diapouli et al., 2017). Although the abundance of fPM in arid regions has traditionally been attributed to distal sources, their chemistry bears signatures of local soils and anthropogenic activities (Engelbrecht et al., 2009b). Hussein et al. (2018) reported a seasonal variation of PNC of coarse and PM_{1.0} ($\leq 1.0 \mu\text{m}$ diameter) particles in Amman which, when compared to the observed dust episodes,

indicated a significant contribution from local dust resuspensions during non-dusty seasons. Another study conducted in Bahrain (Coskuner et al., 2018) showed that $PM_{2.5}/PM_{10}$ ratio over a 7 years period presented a fluctuating - but mostly decreasing - trend from a mean value of 0.47 in 2006 to 0.31 in 2012 (total mean 0.31). This ratio decrease was ascribed to the increasing contribution of coarse particles from regional deserts, local construction activities and the presence of large unbuild and unprotected reclaimed lands. Similar ratios observed in Beirut (0.27-0.37; (Massoud et al., 2011)), and Makkah (0.001-0.99; (Munir et al., 2017)) were also attributed to domestic construction and demolition activities. On the contrary, these ratios increase in indoor environments during high dust periods (Krasnov et al., 2015), due to the better infiltration of smaller particles (Hamdan et al., 2015), and the higher deposition of larger ones (Argyropoulos et al., 2019). All of the above suggest that while regional dust can be challenging to control, a considerable amount of locally emitted fPM can be mitigated with proper regulatory measures (Wu et al., 2016).

The aim of this chapter is to explain the sources, generation mechanisms, and routes of entrainment for fPM. The methods for quantifying PM emissions including laboratory experiments, field measurements and dispersion modelling are also described. Finally, the health impacts of PM based on their target area within the body and their composition are discussed, followed by a section on the control methods that can be adopted to limit PM emissions. These principles are fundamental for the studies conducted in the coming chapters.

2.2 Sources and Mechanisms

The estimation of fPM emissions calls for an in-depth understanding of the factors associated with their initiation and behaviour (Schaap et al., 2009). The primary mechanisms used to understand the emissions of fPM have been broadly categorised into (i) wind/aeolian erosion from

natural sources such as desert sand as well as storage areas within mining and quarrying sites, and (ii) the mechanical attrition of materials due to movement and collision (USEPA, 2008). Natural fPM may also arise from sea salt aerosols formed by bursting air bubbles on the sea surface (Schaap et al., 2009). The mechanism of fPM emissions not only depends on the source but also the size of the particle (Alfaro and Gomes, 2001). These are further studied by measuring PM using a variety of experimental, laboratory and field-based methods, as described in the sections below.

The erodibility of dust particles from a surface is governed by a series of processes that depend on the meteorology and the properties of the exposed surface (Bagnold, 1973). Particles dislodge from a surface when the exerted wind speed exceeds a certain threshold value (u_{th}^* ; threshold friction velocity) causing the particles to migrate from the surface (Shao, 2009). In addition, the surface must have a significant proportion of roughness to provide friction for wind erosion (Gillette et al., 1982). The uplift of the particles from a surface is controlled by three main factors: the cohesive forces between the soil particles, the gravitational force and the wind shear stress. Depending on to the size of the soil particle, Bagnold (1941) defined three modes of particle's transport that occur when wind stress is applied to a surface. Larger soil particles ($>500 \mu\text{m}$) are hindered by the gravitational force, hence they drag along the surface rather than suspend in the air in the so called "creep" mode. Medium sized particles ($50-500 \mu\text{m}$) will overcome the gravitational force if the wind speed exceeds a certain threshold, but they can only reach a maximum height before they fall back to the ground. The latter creates a hopping behaviour which is called "saltation". The former two modes of traction and saltation then result in sandblasting causing smaller particles ($< 20 \mu\text{m}$) to escape into the air in what's called the "suspension" mode (Figure 2.2). The dispersing capacity of such particles once in the atmosphere depend on the initial

trajectory height, the settling velocity of the particle and the amount of atmospheric turbulence; the latter being the main factor for the later deposition of smaller particles apart from their low settling velocities (USEPA, 1995).

Based on the earlier wind tunnel studies, the vertical (suspension) flux was consistently found to be proportional to the horizontal (saltation) flux of particles, and they are both proportional to a power law of wind velocity (u) or wind friction velocity (u^*) (Neuman et al., 2009). Moreover, the number of particles entrained to the air is dependent on the ratio of the loss of kinetic energy to the binding energy (Shao et al., 1993).

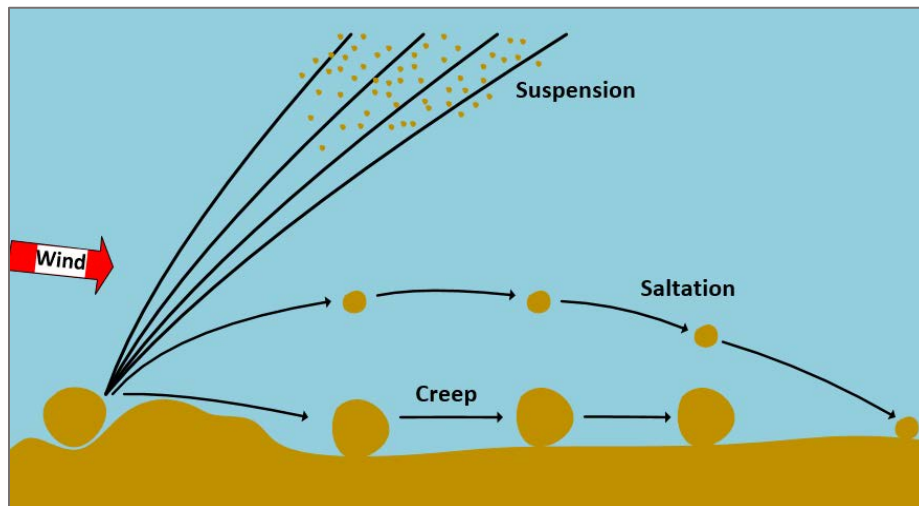


Figure 2.2 Schematic figure showing the movement of particles during wind erosion as taken from Schaap et al. (2009). As seen in the figure, the smaller particles engage in direct suspension while the larger fractions tend to saltate and creep.

Marticorena and Bergametti (1995) has developed one of the first dust models for the prediction of dust production rate (emission flux) which was later used in many regional modelling studies. Their model proposed a formulation of u_{th}^* that depends on the size and density of the soil particle, the fluid (air) density and viscosity, and the surface roughness length (z_0 ; measures the roughness of a certain terrain through the heights of its obstacles). The consideration of surface characteristics in the dust model proved to provide better predictions of dust intensities, compared

to the models that solely depend on wind speed variability, even when applied on a larger scale Marticorena et al. (1997)

Factors such as moisture properties of the material and size distribution are key parameters that affect the amount of fPM emitted through mechanical attrition of materials (NPI, 2005). A common scenario for mechanical processes is the friction between tire threads and road surface leading to the release of nanoparticles and PM₁₀ (Tsiouri et al., 2015). When the vehicle is forced to decelerate, the contact between brake components causes the brake lining to scarp and accumulate on the road surface (Thorpe and Harrison, 2008). The physical and chemical composition of the abraded brake wear varies depending on the material type. As the vehicles move on the road, the wheels cause pulverisation of road material and also leave the road exposed to air currents that further disperse particles (USEPA, 1995). Studies have shown that levels and composition of road dust is affected by the surrounding environment, such the intense traffic of uncovered heavy duty vehicles and proximity to construction works (Amato et al., 2009). Similarly, mechanical attrition between building materials during crushing and drilling releases nanoparticles as seen in Figure 2.3.

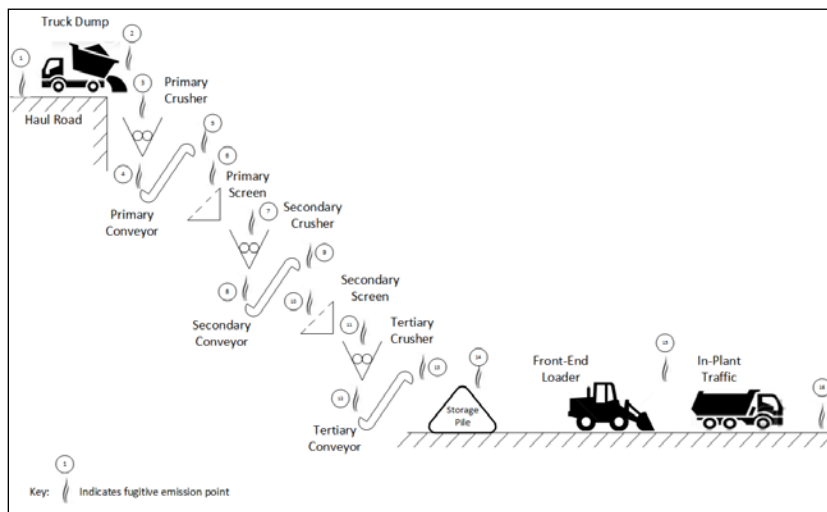


Figure 2.3 Process of rock crushing showing the potential sources of fPM emissions, as taken from Cowherd Jr. and Kinsey (1986)

2.3 Quantification of Emissions

Quantification of emissions is a critical aspect for every atmospheric pollutant and it is most of the times part of a larger exercise which starts with mapping and characterization of each source – a process which results in an emission inventory.

2.3.1 Experimental

Wind tunnel experiments were among the first techniques used to understand the saltation mechanism through simulating the meteorological conditions of the atmospheric boundary layer (Shao, 2009). Wind tunnels are straight-line suction tunnels, used to study a particular surface of chosen material, with a wind blower and instruments to measure parameters such as free stream velocity, horizontal saltation flux and vertical velocity of the particles (Roney and White, 2006). The selection of tunnel dimensions is critical to stimulate the turbulent boundary layer's characteristics of the studied surfaces (Neuman, 2003). In the case of Neuman et al. (2009), the tunnel surface used to calculate emissions from mine tailing was prepared by pulverising, wetting and oven baking to replicate the field conditions. Experiments can be modified by adding features such as pebbles to simulate the turbulent boundary layer as commonly seen in the desert sand (Roney and White, 2006). These experiments test the advection properties of the wind and how far the particles can be entrained. The suspended dust from the experiment can either be collected at the end of the tunnel or redirected back.

2.3.2 Field Measurements

Direct field-based measurements are probably the single “absolute” method to quantify emissions of an atmospheric pollutant. Especially in the case of a point stationary or mobile source like shipping (Eyring et al., 2005), optical remote sensing seems to provide very accurate results and high flexibility (Du et al., 2011). This is rarely the case for fPM where most of the times it is

released from a larger area. Integrated mass samplers are the most common methods for measuring fPM through the collection of ambient samples on filters (usually Teflon or glass microfiber) and later prepared to undergo gravimetric analysis (Lee et al., 2005). The collected samples usually undergo further analysis to identify their composition (Brown et al., 2008; Kouyoumdjian and Saliba, 2006; Rashki et al., 2013). The composition analysis is extremely useful in order to identify fPM sources from any other PM source (Engelbrecht and Jayanty, 2013). Samplers have different types and operating flow rates, and measurements can be taken using different averaging period and frequencies. Shaltout et al. (2018), for example, conducted an elemental analysis of PM_{2.5} in the Greater Cairo area, where he collected 24h PM_{2.5} samples (on polycarbonate filters) from two sites (residential and industrial) using a Dewel-Higgins type cyclone operated at flow of 3 l/min. He analysed the samples using multi-secondary XRF spectrometer for elemental analysis. When the composition of both the collected samples and the neighbouring sources are known, source apportionment methodologies, like PCA (Principal Component Analysis; (Thurston and Spengler, 1985)) and CMB (Chemical Mass Balance; (USEPA, 2004)), can be applied for an accurate determination of the released amounts (Pérez et al., 2016).

Real-time continuous mass monitors are another common way of measuring PNCs and PMCs due to their ability to capture even the small spatial and temporal variations. Widely used instruments for on-site PM measurements include spectrometers that work on light scattering technology. Such measurements are usually performed by air quality monitoring stations set up within or close to the emitting site and can cover even the very fine particles (Al-Dabbous and Kumar, 2014). For instance, Azarmi et al. (2015) measured PM particles from indoor refurbishment activities using a Grimm 1.107 particle spectrometers and a fast response differential mobility spectrometer (Cambustion DMS50), where instruments were placed just ~ 2

m from the nearest source. Other studies used smaller low-cost instruments such as in Pope et al. (2018), where (AlphaSense, OPCN2, firmware version 18) Optical Particle Sensors were used to measure PM levels in urban and rural sites in Nairobi, Kenya. The device measures PNCs in the range of 0.38-17 μm in 16 size bins, and converts data to PMCs following the European Standard (EN481). It was also equipped with a 37 mm diameter cascade to collect samples on Teflon filters for gravimetric analysis. These combined measurements were followed by a number of other studies. For example, Bu-Olayan and Thomas (2012) collected $\text{PM}_{2.5}$ 24h samples from different sites in Kuwait using EPAM-5000 particle impactor that uses both gravimetric and nephelometric techniques (the latter uses near-forward light scattering of infrared radiation to promptly provide PM concentrations in mg m^{-3}).

Quantification of fPM from mobile sources is rather difficult. The most common methods for ambient measurements are through monitoring equipment installed on vehicles (Pirjola et al., 2010), optical remote sensing (Yuen et al., 2015), and passive sampling on the side of the road and a background location, or through an upwind/downwind approach (Etyemezian et al., 2004). Measuring PM at road tunnels is another method that provides the advantage of recording traffic emissions within known boundary conditions (Lawrence et al., 2016). Road dust is usually collected by sweeping or vacuuming for further laboratory analysis. The former requires further sieving in the laboratory or inducing resuspension to collect PM through size selective inlets. Vacuuming is usually performed using designed instruments that pumps air at a controlled air flow rate and into collecting filters where only the sizes small enough to resuspend are collected (Amato et al., 2009; Padoan et al., 2018). For example, Amato et al. (2011) collected road dust from pavements at three different European cities using a rotative pump that pumps road dust into a PVC deposition chamber where particles begin to resuspend and only particles $< 10 \mu\text{m}$ can get

through a stainless-steel barrier and get collected on membrane filters. Some studies combine real time measurements and source apportionment techniques to develop EFs based on source, vehicle class and elemental components (Abu-Allaban et al., 2003; Bukowiecki et al., 2010).

2.3.3 Dispersion Modelling

Dispersion models are usually used to quantify emissions from larger geographical areas (Menut et al., 2013; Prakash et al., 2015). Often, an atmospheric dispersion model (ADM) is employed to facilitate calculation of the EF. Then the ADM results are used to back or inverse calculate the released amounts. The use of the ADM is necessary when the monitoring location is not “close enough” to the source of concern and only a portion of the emitted fPM reach the measuring equipment (e.g., due to dilution and deposition). For a more accurate estimation of the emissions, a second monitoring location is needed, which measurements will be subtracted from the first station’s measurements in order to account only for the source of concern. The exact location of the second monitoring equipment is critical and it has to take into consideration the local meteorology and the other sources in the vicinity. For example, Ketznel et al. (2007) applied the widely used street pollution model OSPM (Kakosimos et al., 2010) to estimate fPM from vehicles. Ono et al. (2011) applied AERMOD (American Meteorological Society/United States Environmental Agency (USEPA) model) to model windblown fPM from an exposed desert area at Mono Lake, California. Beegum et al. (2016) conducted a study to model aerosols over the Arabian Peninsula using a three-dimensional chemistry transport model (CHIMERE) with an offline coupling of the Weather Research and Forecasting (WRF) model.

Finally, either type of measurements, field or laboratory, can be used to develop an emission model or factor as a good approximation of the actual emission rate. The simplest expression to quantify fPM emissions is seen in Eq. (2.1) below (Cowherd Jr. and Kinsey, 1986) :

$$ER = A \cdot EF \cdot (1 - R) \quad (2.1)$$

where ER [mass × time⁻¹] is the estimated mass emission rate, A [activity × time⁻¹] is the source activity or extent, EF [mass × activity⁻¹] is the uncontrolled emission factor and R [-] is the fractional efficiency of any available air pollution control. For example, if we wish for the calculation of the fPM emission rate from vehicles, A is usually defined as [total travelled km per hour] and EF is given as [g km⁻¹]. This notation is followed by most guidelines and handbooks related to fPM (NPI, 2005) .

2.3.4 Emission Inventories

Since fugitive emissions are those that are not released from confined areas, it is quite cumbersome to track all of the emissions and hence multiple EFs are used to quantify emissions from every potential source – in other words to form an emission inventory. Chatzimichailidis et al. (2014) demonstrated a similar approach for an area of (25 × 25 km²) in Thessaloniki, Greece, covering both controlled PM emissions (Kakosimos et al., 2011) and fPM from vehicles, agricultural activities, and residential combustion. Multiple examples exist in literature where industrial fPM emissions were quantified using segregated EFs such as from mining activities (Trivedi et al., 2009), a slag smelter (Sanderson et al., 2014), and stone crushing (Sivacoumar et al., 2009).

In air quality management, emission inventories are the tools used to identify emission sources (often in a specific geographical area) and the amount of pollutants released into the atmosphere. They act as the key element for setting air quality guidelines, designing effective control measures and providing background data for air quality modelling (Winiwarter et al., 2009). Developing a sound emission inventory requires reliable data; often obtained from real-time measurements, literature, national authorities/databases, and international inventories.

Guidelines for compiling national emission inventories are provided by environmental organizations such as the European Environment Agency (EEA, 2016), New Zealand Ministry for the Environment (Ministry for the Environment, 2001), and USEPA (USEPA, 1995).

For many regions, these inventories have been developed and are available for direct use, such as the National Emissions Inventory (NEI) by USEPA (USEPA, 2014), and the European Monitoring and Evaluation Programme (EMEP) by EEA (EEA, 2016). Either inventory describes the emission quantification process for multiple types of sources and pollutants while it is also updated in a timely manner. Concerning fPM, neither inventory is complete nor exhaustive (Pouliot et al., 2012; Winiwarter et al., 2009). For example, the EMEP includes the fPM resulting from industrial activities but lacks most of the other sources. The NEI includes more sources under the “Emissions Factors & AP 42, Compilation of Air Pollutant Emission Factors” (USEPA, 1995), which covers multiple fPM emitting activities such as soil handling and cement production. On the other hand, the majority of these emissions have been estimated based on measurements collected at a specific coal-mining region (WRAP, 2006). Comprehensive emission inventories for the developing arid regions are virtually non-existent.

Nordic countries developed the NORTRIP model, to compute PM pollution from non-exhaust traffic sources (Denby and Sundvor, 2012). HBEFA (Handbook Emission Factor for Road Transport; (HBEFA, 2014)) includes fPM factors and it is used mainly in central Europe (Germany and Austria). MOVES (Motor Vehicle Emission Simulator; (USEPA, 2015)), the official emission modelling system by USEPA, provides as well some estimates for fPM. On the contrary, such sources are missing completely in COPERT, the corresponding EU emission modelling system. Furthermore, there are studies focusing on specific types of vehicular fPM such as wear of brakes (Grigoratos and Martini, 2015), studded tires (Denby et al., 2013), and road dust (Berger and

Denby, 2011). Some emission inventories provide models for the quantification of road dust that are too dependent on empirical parameters such as the one developed by the USEPA for calculating road dust resuspensions from unpaved roads depending of the road silt loading (USEPA, 2006). Venkatram (2000) tested the applicability of USEPA model and found that the road silt load cannot be accurately measured and thus the model cannot provide accurate estimates of the PM₁₀ emissions. Others provide constant EFs that were derived using local measurements and under certain conditions (Omstedt et al., 2005). EFs developed for Europe or North America may pose certain errors if applied to arid environments. Therefore, there is a pressing need for more measurements that cover different climatic conditions (such as the arid environments), and better models for the quantification of dust resuspension that consider the overlooked effects of meteorology, type of road, vehicle speed, and more (Amato et al., 2014).

2.4 Health Impacts

There are no epidemiological studies that focus specifically on the health effects of fPM emissions, probably due to the challenges facing their quantification. Therefore, we gather here some information about the risks, known so far, associated with the exposure to individual PM sources (in which some are of fugitive nature). We also provide an overview of some of the health effects observed in several areas across the developing arid regions.

The nature and magnitude of the health effects caused by PM pollution vary depending on the particle size, composition, dosimetry and length of exposure. The smaller the particles, the easier they can enter into the human body; the most common pathway being through the respiratory passage and into the lungs as seen and described in Figure 2.4 (Pope III and Dockery, 2006). Fine and ultrafine particles can easily pass to the systematic circulation (direct effect) (Nemmar et al., 2002), or interfere with the autonomic nervous system (indirect effect) that controls the heart beat

rhythm, potentially leading to heart attacks (Nelin et al., 2012). Long-term exposure to PM_{2.5} associates with adults (>30 years) mortality from ischemic heart disease (IHD), stroke, chronic pulmonary disease (COPD) and lung cancer (LC) (Burnett et al., 2014). Pope et al. (2002) conducted one of the largest studies in the United States to estimate the burden of disease by linking the risk factors of 500,000 adults with air pollution data from 151 metropolitan areas. His results confirmed a strong association between PM_{2.5} exposure and mortality showing that an increase of 10 µg m⁻³ in the long-term average of PM_{2.5} was associated with 4%, 6% and 8% increase in all cause, COPD and LC mortality, respectively. A recent study by Cohen et al. (2017) showed that the global mortality from PM_{2.5} exposure has increased from 3.5 to 4.2 million deaths between 1990 and 2015, ranking it the fifth mortality risk factor in 2015. Although the majority of the epidemiological studies focus on PM_{2.5} as a typical indicator of the PM-related health risks, some studies have examined the effects of coarse particles. According to a review by Brunekreef and Forsberg (2005), short-term exposure to PM_{2.5-10} seem to have a stronger connection with COPD and respiratory morbidity rather than mortality.

Particles from brake and tire wear lead to volatilization of organic compounds that are potentially oxidative (Kumar et al., 2014). Tire wear particles can induce Reactive Organic Species (ORS) leading to inflammatory response in the human lungs (Gualtieri et al., 2008). Road dust contains carcinogenic metals such as arsenic (As), chromium (Cr), and lead (Pb); the latter comes from the use of gasoline vehicles where it gets deposited on road surface and can continue to resuspend for long time (Engelbrecht et al., 2009a; García-Rico et al., 2016). UFPs that arise mainly from cooking not only persist for long periods but also have a large surface area absorbing pollutants like PAHs (polycyclic aromatic hydrocarbons) causing respiratory and cardiovascular illnesses (Valavanidis et al., 2008). PM from natural sources like desert sand are usually composed

of quartz and calcite but may differ based on the underlying geology of the studied region (Rashki et al., 2013). Inhalation of silica, sometimes found in desert sand and other industrial operations (e.g., mining and road construction), can lead to fatal lung diseases (Abdul-Wahab, 2006; Bang et al., 2015). Soleimani et al. (2015) found species of *Staphylococcus*, *Streptomyces* and *Bacillus* predominantly from desert sand in Iran present amongst the indoor bacterial composition causing pulmonary and skin infections. Already vulnerable patients such as those with COPD may be further affected by the dust storms as revealed in a study by Vodonos et al. (2014) and Heal et al. (2012).. Recent studies suggests an association between PM_{2.5} elements found in soil and road dust (Al, Ni) and Metabolic syndrome (a group of health problems that includes hypertension, high blood sugar and abdominal obesity) (Shamy et al., 2018); although further research is needed in this area. It is also important to note that sensitive groups such as children and elderly are more likely to develop health symptoms when exposed to high levels of particles. An exposure study on a group of infants to traffic-related air pollutants (including PM_{2.5}) have found a 6% and 12% increase in asthmatic cases by the first and second years of age (Brauer, 2002).

The greatest burden of disease from PM pollution is observed in the developing countries across the arid region (Cohen et al., 2005). PM₁₀ and PM_{2.5} levels reported in Ahvaz, Iran during April-June 2010 were responsible for 1153 and 285 mortalities and 6599 and 1558 morbidity cases, respectively (Shahsavani et al., 2012). Faridi et al. (2018) estimated a 132% increase in COPD mortalities in Tehran between 2006 and 2015 from chronic exposure to PM_{2.5}. Another study conducted in Jeddah during 2011-2012 showed excess levels of carcinogenic metals (Cd, Cr, As and Ni) in ambient PM₁₀, putting 0.01% out of each 1 million people in risk of getting the disease (Alghamdi, 2016). Overall, health studies assessing the impact of PM in the developing arid

countries are scant, and most of them use monitoring data rather than examining individual exposures (Anderson et al., 2012).

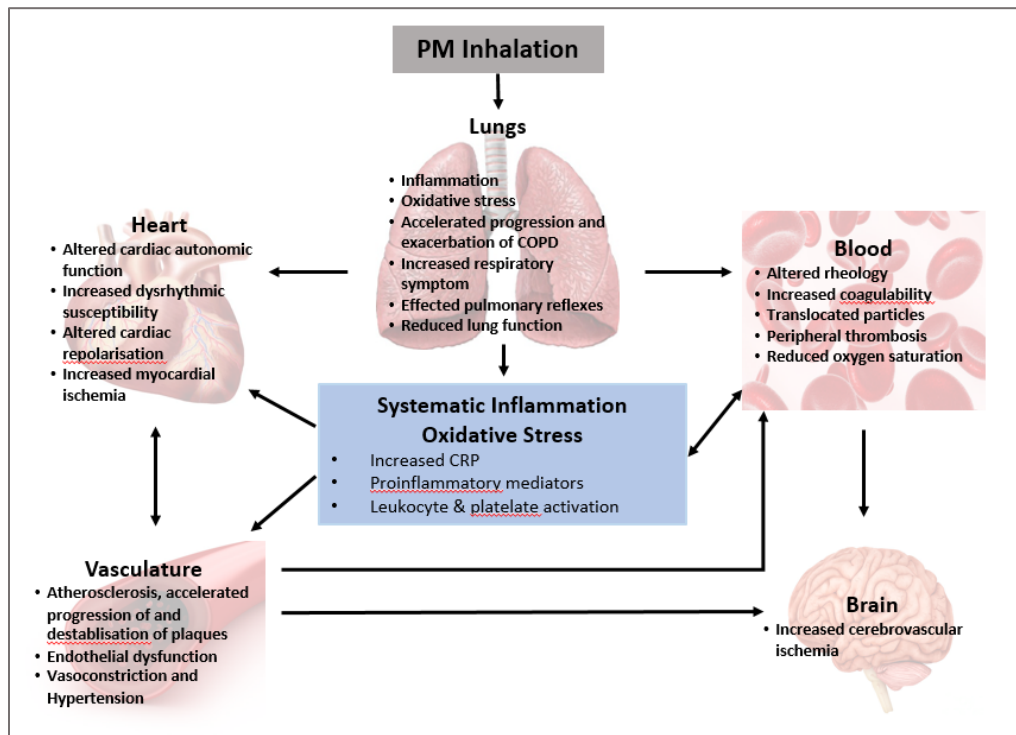


Figure 2.4. Potential pathways for PM within the human body as taken from Pope III and Dockery (2006)

2.5 Environmental Impacts and Control

In addition to its reported health risks, atmospheric PM affects visibility, vegetation growth, ecosystem functions, built infrastructure and climate change (Grantz et al., 2003; Kalenderski et al., 2013; Kumar and Imam, 2013). Hamza et al. (2011) conducted a study to investigate the effect of dust storms pre- and during 2009 in the Arabian Peninsula. They found that the increase in iron production during dust storms increases Dimethyl Sulphide (DMS) in the atmosphere which scatters solar radiation by oxidation and lead to decrease in global temperature. Furthermore, long range transported dust affects climate through the alteration of ice cloud nucleation properties (Huang et al., 2006; Sassen et al., 2003). Such findings have led to the inclusion of dust as a

component in climate change models (AQEG, 2007). On the positive side, dust deposition in the red sea keeps the balance of the marine ecosystems through the cooling of the seas surface and delivering nutrients (Kalenderski et al., 2013).

Although it is quite difficult to eradicate fPM emissions, there are various control mechanisms that can be used to suppress fPM and these are usually source specific. USEPA have described such control methods by dividing them for open and process-based sources of fPM (Cowherd Jr. and Kinsey, 1986). For instance, wind erosion of building materials in a quarrying or mining site can be limited through covered enclosures for storage, watering of surfaces, and construction of windbreaks by vegetation or a greenbelt (Neuman et al., 2009; NPI, 2005; Trivedi et al., 2009). The covering of enclosures and the use of windscreens can either be partial or complete depending on the source and the required amount of control. Watering of surfaces with water or a solution of chemicals helps to reduce the friction by wind drag and the water droplets act as a cohesive force among the particles binding them together thus decreasing emissions. However, control by water is only temporary and requires subsequent additions regularly. An alternative for emissions suppression using water alone is the use of foam made by vigorously mixing surfactants and water; foam not only has a greater wetting capacity but also uses lower amounts of water. Vegetation has proven effective in reducing air pollutants. Plants can remove fPM by intercepting the air carrying the particles (Al-Dabbous and Kumar, 2014). In addition to the above, Driussi and Jansz (2006) suggested control methods to minimize waste in mining industry, including gravity settling chambers, centrifugal cyclones and electrostatic precipitators for the removal of finer particles.

Vehicular emissions of PM can be reduced by using non-studded tires (which are uncommon in the arid regions), using chemical suppressants like magnesium chloride on roads, regular

cleaning using gutter brooms, reducing vehicle speed limits and limiting the number of vehicles on roads by encouraging walking, cycling and mass transportations (Denby et al., 2013). The chemical suppressants work similar to water that is they bind the particles together such that the emissions are reduced and are usually applied to the roads using a pressurised spray truck. Using chemical suppressants, however, is not only costly but may also lead to contamination of materials and are toxic to plants and animals. Combined sweeping and water washing showed positive reduction in PM levels in some areas, however it's still unknown how long it can last (Amato et al., 2010). Improving the quality of pavements and tires is another measure to reduce resuspension at road sites (Kholdebarin et al., 2015). Some preventive techniques, such as using masks and dust respirators as mentioned in (Kumar and Morawska, 2014), can reduce human exposure to PM. Unfortunately, most of the air pollution mitigation measures taken in the developing areas were towards reducing industrial and energy emissions (e.g., the use of lead-free fuels and low-sulphur diesel) rather than fPM (Chaaban, 2008).

2.6 Chapter Summary

fPM are those particles that are not released from vents or ducts and usually vary in diameter from 2.5-30 μm . They may be released from open sources through wind or from industrial processes. One of the main mechanisms is the wind/Aeolian erosion of fPM usually transporting desert sand material but also particles from open stockpiles. Pulverisation and mechanical attrition are the other processes that are most commonly associated with anthropogenic sources of fPM such as drilling, quarrying and crushing within construction sites. Resuspension of dust also occurs through heavy traffic flow within cities. In order to quantify fPM, methods used can be categorised into models and EFs, laboratory experiments and direct field measurements. Models that are specific to a particular source are used along with EFs in calculations to quantify emissions from

potential sources. Most common laboratory experiments to simulate the mechanisms of fPM emissions is the wind tunnel approach. Direct field measurements are usually conducted by air quality monitoring stations that consist of air filters used to capture ambient PM mass and then undergo gravimetric analysis to measure the concentrations. Such PM has been found to cause various health diseases especially pulmonary and cardiovascular illnesses due to their composition. Toxic elements are often found adsorbed to their surfaces and may have significant effects on entering the human body. Similarly, PM from desert sand was found to carry microbes causing respiratory illnesses. Hence, it is important to control fPM emissions through various methods such as wetting of surfaces, enclosing storage sites and constructing wind breaks. The appropriate control methods must be chosen in accordance with what is most efficient based on the source of fPM; for instance, reducing vehicle speeds and using non-studded tires were effective to curtail fPM from vehicular emissions.

This chapter indicates that further research is needed to understand the dispersion of fPM in areas with arid climates and poor monitoring systems, and the necessity to have accurate models for quantifying fPM. Further literature reviews are provided in the following chapters that relate to each of the objectives listed in section (1.2) of Chapter 1.

Chapter 3 Materials and Methods

This chapter provides a general description of the instruments and models used in this project. These include: (i) particle counters and particle samplers used for the field measurements of PM, (ii) the method used for gravimetric analysis of PM samples, (iii) the PMF model used for PM source apportionment, and finally (iv) the FDM and CALPUFF models used for dispersion modelling.

3.1 Introduction

The experimental part of this project included the continuous measurements of particle concentrations and the collection of ambient PM mass samples from two types of sources: construction sites (barren) and road traffic. PNCs and PMCs were measured using Grimm Enviro Check 365, an air quality monitoring station manufactured by Grimm Aerosol Technik GmbH & Co. KG, Germany (Section 3.2.1; (Grimm, 2009)). The ambient PM samples were collected using the microprocessor-controlled sampling system (MicroPNS) with size-selective inlets manufactured by Umwelttechnik MCZ GmbH, Germany (Section 3.2.2). This chapter also includes a description of the preparation and gravimetric analysis performed for the ambient samples which included the use of a high precision weigh balance (Section 3.3). Source characterization was performed using the PMF model (Section 3.4.1). Dispersion modelling was performed using FDM model (Section 3.4.2) and California Puff Model (known as CALPUFF; Section 3.4.3). Almost all maps in this project (excepts the ones created by the dispersion models) were prepared with the use of Quantum Geographic Information System (QGIS v2.18). Other software tools such as Origin2017 and R-3.5.1 (including the Openair package for analysing air

pollution data) were used for data analysis and visualization. Table 3.1 below summarises the instruments and models used in the various chapters of the thesis.

Table 3.1 Instruments and models used in chapters (4-6) of the thesis

| | Grimm EDM365 | MicroPNS | Gravimetric Analysis | PMF | FDM | CALPUFF |
|---|--------------|----------|----------------------|-----|-----|---------|
| Chapter 4 Flux Estimation of wind-blown fPM | x | | | | x | |
| Chapter 5 Vehicle-induced fPM | x | x | x | x | | x |
| Chapter 6 Environmental and Health Impact Assessment of fPM | | | | | | x |

3.2 Instrumentation

3.2.1 Grimm Enviro Check 365 – Environmental Dust Monitor

The Grimm Enviro Check 365 is a laser aerosol spectrometer placed in a stainless-steel housing that has a sampling tube and head on the top. The sampled air enters the unit through the head, passes through the sampling tube and enters the spectrometer to a measuring cell where the particles in the sampled air are detected by light scattering. The unit uses light scattering technology to measure hourly averages of PNCs [particles liter⁻¹] over a size range of 0.25 µm up to 32 µm in 31 size channels using a sampling rate of 1.2 litre min⁻¹. It also produces PMCs [µg m⁻³] using a proprietary algorithm calibrated to the National Institute of Standards and Technology (NIST, USA) Arizona test dust. According to vendor’s certificate, measurements are equivalent to the European Standards EN12341 and EN14907. Meteorological parameters were recorded by the climate sensor (WS600-UMB by G. Lufft Mess- und Regeltechnik GmbH, Germany) attached to the top of the monitoring station. The accuracies of the meteorological measurements were ±0.3 m s⁻¹ or ±3% (range 0-35m s⁻¹) and ±5% (>35 m s⁻¹) for wind speed, ±0.2 °C for temperature (range

-20-50 °C), $\pm 2\%$ for relative humidity (RH; range 0-100%) and $< 3^\circ$ (RMSE $> 1 \text{ m s}^{-1}$; range 0-359.9°) for wind direction.

3.2.2 Grimm MicroPNS – Microprocessor Controlled Sampling System

The MicroPNS is a low volume air sampler designed to measure PM mass following the EN12341:2014 standard (NSAI, 2014). The sampler sucks in the particulate-laden ambient air stream with a continuously regulated flow through a size-selective inlet and retains the PM on a 47 mm diameter filter. A built-in pump provides the vacuum required to pull the airflow at a 38.4 litre min^{-1} through to the sampling filter. The sampler contains two filter magazines, one for inserting the new filters and the other to collect the sampled filters. All these parts are included in a stainless-steel housing intended for outdoor sampling. Prior to operating the sampler, the new filters are placed in filter holders and placed in the unsampled filter's magazine. In this project we used two samplers with $\text{PM}_{2.5}$ and PM_{10} inlets to collect samples over 24h period. The filter media used in this project is Tissue Quartz filters manufactured by Pall.

3.3 Gravimetric Analysis of PM Samples

The gravimetric analysis is used to determine the mass concentrations of the PM samples collected on filters. A number of international institutions provide specific standards for the preparation and testing of sampling media (i.e., filters) for fitness of purpose in order to optimize the results of PM mass concentration measurements (e.g., the European Standard EN 12341:2014). Prior to each sampling, the tissue quartz filters were conditioned in an environmental chamber for at least 24-48 hours at a controlled temperature of 20-23 °C and RH of 30-35% (USEPA, 1987). The filters were weighed using (Sartorius WZA26-CW by Sartorius Lab Instruments GmbH & Co, Germany), a high precision weigh cell with 1 μg readability and $\leq \pm 1 \mu\text{g}$ repeatability. Filters were only handled with tweezers and placed in sealed petri dishes before and after each weighing.

The weighed unsampled filters are then removed from their petri dishes and inserted into the filter holders and placed in a sealed container to transport to the measuring site. Filters were changed every 7 days during the campaign period. The sampled filters were transported back to the laboratory, conditioned and weighed following the same above procedure. The PM mass is calculated as the weight difference of the sampled and unsampled filters, and divided by the sample volume (recorded by the sampler) to calculate the daily concentration ($\mu\text{g m}^{-3}$). Field blanks were obtained for each filter batch (each 7 days) for quality control purposes.

3.4 Models

3.4.1 Positive Matrix Factorisation (EPA PMF 5.0) Model

Receptor models are mathematical tools used to quantify source contributions to samples through the composition/tracers of the source. Compositions of the measured samples are obtained through the chemical analysis prior to entering to the receptor model. PMF is one of the most successfully applied receptor models (Belis et al., 2015), developed by the USEPA and is based on the principles described in Paatero et al. (1997). The latest version of PMF (EPA PMF v5.0) is used in this project, and it implements a multivariate factor analysis technique to solve the chemical mass balance between the measured species and the source profiles using Eq. (3.1) below (Norris et al., 2014):

$$x_{ij} = \sum_{k=1}^p g_{ik} f_{kj} + e_{ij} \quad (3.1)$$

where x_{ij} is the concentration of the measured species j in sample i , g_{ik} is the contribution of factor (source) k to sample i , f_{kj} is the concentration of species j in factor profile k , and e_{ij} is the residual (error) for each sample-species; represents the difference between the measurements x and the modelled g and f . PMF solves the above equation using least-squares and uses error estimates to provide weights in the fitting process. The model has the capability of handling missing data and

data below detection limits. Moreover, it implements a non-negative constraint to reduce ambiguity of the factors. The source types can be identified through the interpretation of factor profiles. The best fit solution is the solution that achieves the minimum object function Q , which is:

$$Q = \sum_{i=1}^n \sum_{j=1}^m \left[\frac{x_{ij} - \sum_{k=1}^p g_{ik} f_{kj}}{u_{ij}} \right]^2 \quad (3.2)$$

Where u_{ij} is the uncertainty of species j in sample i . The uncertainties are provided to the model by the user in the form of file, and are either observation-based (i.e., provides uncertainty for each species in a sample), or equation-based (i.e., provides species-specific parameters to calculate the uncertainty for each sample). The equation-based uncertainties file has one delimited row of species with species names, a second row with species-specific method detection limit (MDL), followed by a third row of species-specific uncertainty. For concentrations less than or equal to the provided MDL, the uncertainty is calculated using a fixed fraction of the MDL (Polissar et al., 1998). If the concentration is greater than the MDL, the calculation is based on a user provided fraction of the concentration and MDL (Norris et al., 2014):

$$\text{Uncertainty} = \sqrt{(\text{Error fraction} \times \text{concentration})^2 + (0.5 \times \text{MDL})^2} \quad (3.3)$$

The MDL and error fractions are instrument and/or analytical procedure-specific.

The PMF model provides two types of Q for the runs. Q_{true} is the goodness of fit calculated using all points, and Q_{robust} is the goodness of fit excluding the points not fit by the model (i.e., points where uncertainty-scaled residual is >4).

3.4.2 Fugitive Dust Model (FDM)

FDM is a USEPA developed air quality model designed specifically to compute emissions and deposition impacts of fugitive dust sources (Winges, 1991). FDM is based on the Gaussian plume formulation but specifically adapted to incorporate an improved gradient-transfer deposition algorithm. Emissions of each source are split into a number of particle size classes, where a gravitational settling velocity and a deposition velocity are computed by the model for each class. The pollutant transport is ruled by the general atmospheric advection-diffusion equation. After a number of simplifying assumptions, the pollutant concentration is computed using Eq. (3.4) below:

$$\chi = \frac{Q}{2\pi\sigma_y\sigma_z u} e^{-\frac{y^2}{2\sigma_y^2}} e^{-\frac{-v_g(z-h) - v_g^2\sigma_z^2}{2K} - \frac{v_g^2\sigma_z^2}{8K^2}} \left[e^{-\frac{(z-h)^2}{2\sigma_z^2}} + e^{-\frac{(z+h)^2}{2\sigma_z^2}} - \sqrt{2\pi} \frac{v_1\sigma_z}{K} e^{-\left[\frac{v_1(z+h)}{K} + \frac{v_1^2\sigma_z^2}{2K^2}\right]} \operatorname{erfc}\left[\frac{v_1\sigma_z}{\sqrt{2K}} + \frac{z+h}{\sqrt{2}\sigma_z}\right] \right] \quad (3.4)$$

where χ is the pollutant concentration [g m^{-3}], K is the eddy diffusivity [$\text{m}^2 \text{s}^{-1}$], Q is the emission rate [g s^{-1}], u is the wind speed [m s^{-1}], σ_y , σ_z are the standard deviation of the concentration in the y and z directions [m], v_g is the gravitational settling velocity [m s^{-1}], h is the plume centreline height [m], x , y and z (height) are the coordinates of the receptor [m]. The v_1 is $(u_d - v_g/2)$ where u_d is the deposition velocity [m s^{-1}], and erfc denotes the error function. The FDM model is used in this project to estimate the dispersion of fPM from bare construction sites (Chapter 4).

3.4.3 CALPUFF Model

The latest CALPUFF model (v7.2.1), coupled with the interface from Lakes Environmental (CALPUFF View v8.4.0) software, was used to calculate the atmospheric dispersion of fPM. CALPUFF is a non-steady state Lagrangian Gaussian puff model, developed since 1990, that advects ‘puffs’ of material emitted from modelled sources, simulating dispersion and transformation processes along the way. The CALPUFF modelling system includes CALMET

model for the post-processing and downscaling of mesoscale meteorological data, and CALPOST for post-processing of the results. CALMET generates hourly wind and temperature fields on a 3D gridded domain using observational or prognostic meteorological data, terrain elevations and land use/ land cover (LULC) information. CALPOST calculates averages, summarises concentrations and wet/dry deposition fluxes, and creates plot files from two or more source groups from different CALPUFF runs. CALPUFF View is an integrated graphical user interface for the CALPUFF modelling system and their related pre- and post-processors. In this thesis, the CALMET domain consisted of a 100x100 grid with a resolution of 2 km. The meteorological input was provided in the form of MM5 (Fifth-Generation Penn State/NCAR Mesoscale Model) weather data based on a parameterisation described at an earlier work (Gopaldaswami et al., 2015). Additional post processors of the model were utilized in this work such as: PRTMET; that lists selected meteorological data from CALMET and creates plot files, APPEND; that can append two or more CALPUFF concentration, wet flux, dry flux or relative humidity (visibility) files, and CALSUM; that sums and/or scales concentrations or wet/dry fluxes from two or more sources or source groups from different CALPUFF runs. Due to the large amount of data and number of runs needed to be performed, the sources data were uploaded to CALPUFF using the external file option that allows the specification of sources using variable emission files. Further details of the modelling are described in Chapters 5 and 6 of this thesis. Finally, all simulations were executed using the high-performance computing (RAAD2) facilities at Texas A&M University at Qatar.

3.5 Chapter Summary

This chapter provides a description of the instruments and materials used to measure PNCs and PMCs, and methods of collecting meteorological data. Further information about the results of the field campaigns are presented Chapters 4 and 5. The chapter also provides the principals of

the source apportionment model (PMF) used in Chapter 5. Finally, it provides a description of the models (FDM and CALPUFF) used to simulate the dispersion of fPM in Chapters 4,5, and 6.

Chapter 4 Flux Estimation of fPM Emissions from Loose Soils (Calcisols)

The aim of this chapter is to estimate fPM emissions from a common soil – the Calcisols – in dry and semi-dry regions. We consider the wind erosion of loose Calcisols owed to human activities i.e., construction earthworks. We employ both, the field measurements and dispersion modelling, to correlate meteorological variables, fPM concentrations, and emission fluxes. The overall objective is to understand the Aeolian erosion mechanisms and obtain the EFs of fPM produced by a specific type of soil and surface conditions. Therefore, we chose a construction site at rest as a study area, located within the city of Doha, State of Qatar. This work appeared in (Hassan et al., 2016).

4.1 Introduction

A major source of airborne pollution in dry arid lands is fPM, which is a frequent product of soil erosion from winds (Tsiouri et al., 2015). The meteorology and low vegetation cover of arid regions make them highly susceptible to wind-blown particles (Namdari et al., 2018). On the other hand, many such regions, like the Middle East Area, are experiencing rapid rates of urbanization, industrialization and construction, resulting in increased human exposure to the airborne PM. Although chemically “inert” and just a portion of airborne particles, windblown fPM cannot be ignored as they comprise the majority of PM in many arid and semi-arid environments (Marticorena et al., 1997) and need to be studied and regulated (USEPA, 2011).

According to the Food and Agriculture Organization (FAO, 2014), one of the most common reference soil groups of arid and semi-arid environments are the Calcisols, formerly been called

“Desert Soils”. These soils cover big areas of the Middle-East, North Africa, Central Asia and Australia (see Figure 4.1). As discussed earlier, emission inventories for dust particles and PM are available for European (EEA, 2016) and North American (USEPA, 1995) domains. These inventories cover information on fugitive emissions from some sources such as agricultural (Pouliot et al., 2012), while non-exhaust vehicle emissions and emissions produced by wind shear and material transfer processes remain poorly attended (Kumar et al., 2013; Winiwarter et al., 2009) and limited to the regional scale (Schaap et al., 2009).

fPM emissions introduce the largest complexity and uncertainty in air quality assessment, which affects their quantification, modelling and control efforts (Sanfelix et al. 2017). Different approaches such as field measurements (Brown et al., 2008; Kouyoumdjian and Saliba, 2006; Shahsavani et al., 2012), laboratory scale testing (Neuman et al., 2009; Roney and White, 2006) and dispersion modelling (Ono et al., 2011) have been used in the past. In the work of Ono (2006), sand flux measurements from four areas at Owens Lake, California (USA) were measured using low-cost Cox Sand Catchers (CSC) and electronic sensors. These measurements were used to empirically determine the surface erosion potential, followed by an application of Gillette Model to estimate the sand flux. The latter provided good predictions (R^2 ranging from 0.72 to 0.87) when compared to the measured hourly sand flux rates. More recently, Ono et al. (2011) quantified the windblown PM_{10} from Mono Lake in California (USA), using the Dust Identification (Dust ID) method. In this method, PM_{10} emissions are calculated using the proportionality ratio (presented as K-factor) between the vertical and horizontal flux of PM_{10} ; these fluxes are estimated using the mass of saltating particles measured by CSCs. Hourly emissions were then entered into a dispersion model (AERMOD) to predict hourly PM_{10} concentrations. The model predictions were compared to the concentrations measured on-site in order to calculate hourly K-factors, and use

them to re-calculate hourly PM₁₀ emissions. This method, which accounts for the change in surface conditions, provided good results (factor of two, FAC2 = 60.2%, R² = 0.77 between modelled and observed data) compared to the wind tunnel-based emissions measured for the same surface. Kinsey et al. (2004) used time-integrated and continuous exposure profiling to evaluate the EFs of PM₁₀ and PM_{2.5} for mud carry out from a major construction site in metropolitan Kansas City in Missouri (USA). Time-integrated air sampling was conducted using high-volume air samplers to collect PM₁₀ and PM_{2.5} samples from the site. In addition, vacuum sweeping was used to collect surface samples for the analysis of roadway material, and pneumatic traffic counters and visual recordings for the vehicle loads. EFs (expressed in mass emitted per vehicle distance travelled, µg km⁻¹) were calculated by normalizing the spatially integrated exposure (total particle mass collected) against traffic volume (total distance traveled from all vehicles). The resulted PM₁₀ EF was found to be within the range reported earlier (USEPA, 1995) but PM_{2.5} factor was far lower. Another work was presented by Abdul-Wahab (2006) to assess the impact of fPM emissions from cement plant activities using the FDM model. Her work made estimates of the emission rates using the empirical EFs reported in the Australian National Pollutant Inventory (NPI, 1999), and entered them along with the meteorological and receptor data into the FDM to compute the dust emission concentrations. Model predictions were compared to the actual concentrations measured at residential areas adjacent to a cement plant. These measurements were measured using high volume samplers that collect total suspended particulates (TSP) and calculate their concentrations using the sample volume. Although the model showed an under-prediction of the measured concentrations, a correlation coefficient of (R² = 0.92) was obtained when comparing predicted and measured values.

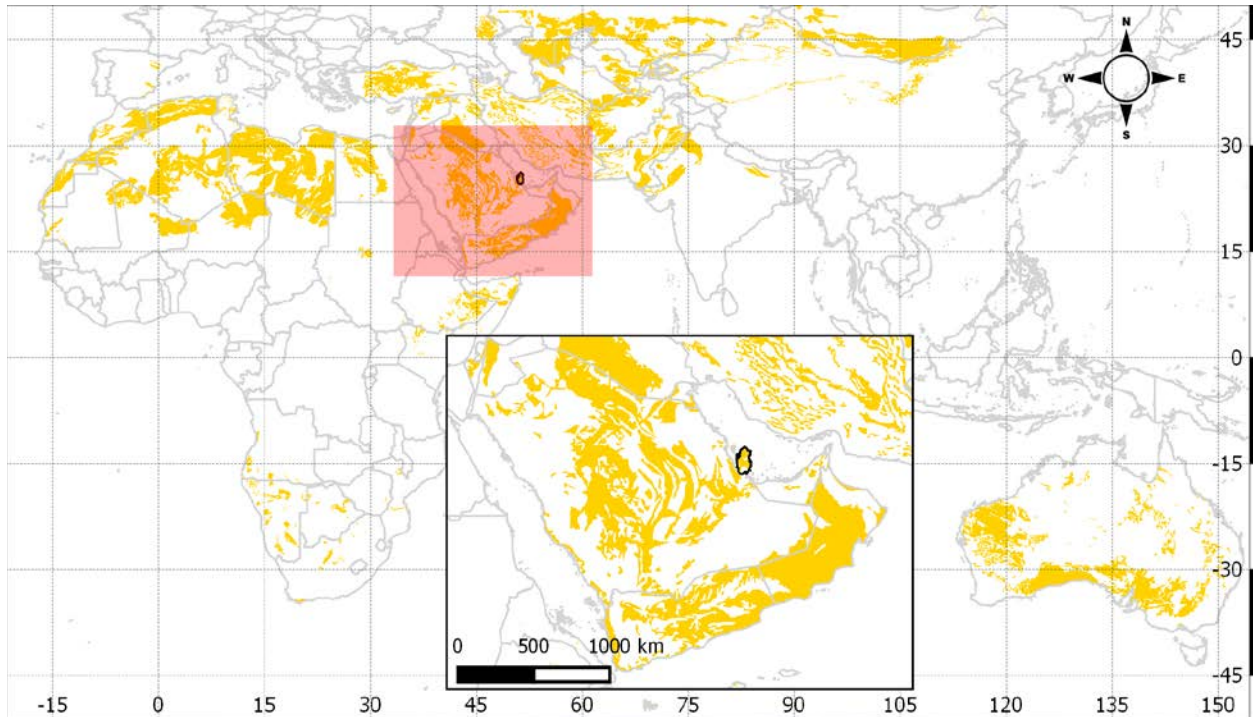


Figure 4.1 Map showing main worldwide areas and the Middle East (inset) covered by Calcisols (FAO, 2014)

Other studies followed the wind-tunnel approach, such as the work presented by Roney and White (2006), to determine fPM emissions from Owen’s (dry) Lake in California (USA) using an environmental boundary layer wind tunnel (Saltation Wind Tunnel - SWT). The tunnel was used to measure PM_{10} concentrations and vertical velocity for multiple soil samples and different surface conditions. The emission rates were then obtained through a material balance of the control volume and the inlet/outlet mass fluxes. The ratios of vertical flux/horizontal flux and horizontal flux/total soil flux were calculated and plotted using the wind tunnel results and were found to agree with other field studies (Gillette et al., 1997; Niemeyer et al., 1999) of Owen’s Lake. A similar wind-tunnel approach was followed by Neuman et al. (2009) to obtain the relationship between fPM emissions, wind velocity and water content of mine tailings. Recently, Sanderson et al. (2014) also found good agreement between wind tunnel and field measurements when applied to fugitive emission rates from a large nickel smelter in Sudbury, Ontario (Canada). In their work,

mass emission rate was measured through a wind tunnel experiment using the control volume method while vertical dust flux was determined using finite difference approximation. A comparison showed a strong agreement between the measured rate and flux ($R^2 = 0.99$), and that both vary with u^* with a strong correlation ($R^2 = 0.80-0.95$). In the work of Yuwono et al. (2014), wind speed and soil moisture dependent EFs were developed to calculate dustfall and suspended particles from two different types of soil (Oxisol and Ultisol). Dustfall and suspended particles were measured for a number of collected soil samples using a lab scale wind tunnel, followed by a statistical analysis to obtain the Pearson correlations and the relative contribution of wind speed and soil moisture, and their exponential relation to the dust generation rate.

For the air quality management, emission estimates are necessary in order to evaluate the sources, design control strategies and develop suitable mitigation techniques. One way to quantify emissions is using the empirical factors developed by well-established environmental institutions. However, information on fPM emissions in the currently available inventories is limited compared to a large number of different sources that can produce fPM emissions. Furthermore, using analogs factors may result in inaccuracies when applied to certain surfaces of interest (Sanderson et al., 2014). It is worth noting here that the existing factors were developed for certain geographical regions (e.g., geology) and weather conditions, which may lead to inaccuracies when applied to other conditions. Up to date, the vast majority of studies on fPM emissions modelling focus on the wind erosion of typical soils and bare lands of North America and Europe.

In this chapter, we focus on the fPM emissions modelling from a common soil – the Calcisols – in dry and semi-dry regions of North-Africa, Middle East, Central Asia and Australia (Figure 4.1). In addition, we consider the wind erosion of loose soil owes to human activities i.e., construction earthworks. We employ both, the field measurements and dispersion modeling, to

correlate meteorological variables, fPM concentrations, and emission fluxes. The overall objective is to understand the Aeolian erosion mechanisms and obtain the EFs of fPM produced by a specific type of soil and surface conditions. Therefore, we chose a construction site at rest as a study area, located within the City of Doha, State of Qatar. To the best of our knowledge, this is a unique study focusing on fPM from construction areas, which are usually very close to, or within residential areas and has a direct impact on the local air quality.

4.2 Methodology

An experimental field campaign and dispersion modelling were combined in order to examine the relationship between the meteorological variables and fPM emissions, and develop the specific functions for the emission fluxes (i.e., emission rates per area). The field campaign was conducted for measuring PNCs at two locations – a construction site and a background location. Thereafter we used a dispersion model – FDM (Winges, 1991) – in an iterative manner to estimate the source-receptor relationship. The modelling and experimental results were post-processed for the calculation of the emission fluxes and the development of their new functions. Finally, these functions were compared with the functions reported in USEPA’s AP-42 (USEPA, 1995), and also applied for the calculation of ground level PM concentrations, as a step of evaluation.

4.2.1 Site Description

The experimental field campaign was conducted for a period of two months between April and May 2014 (Hassan, 2015). PNCs and meteorological parameters (i.e., wind speed, wind direction, relative humidity, ambient pressure and temperature) were measured at two locations: a construction site (which is also the studied source) and a background location (Figure 4.2a). The background station was placed on the rooftop of a building (height = 10 m) located ~1.5 km away

(northeast) from the construction site station which was located at the southern boundary of the construction site (Figure 4.2b). Both sites are located within the Education City of Doha, (State of Qatar); the Education city is a complex that hosts branch campuses of seven international universities, a number of research centres, industry-related offices and student recreational activities (Figure 4.2a). In this complex, most buildings are of low height (1-2 floors; <10m). Although there are some buildings with 3-4 floors, none of them is directly in between the two monitoring sites. On the other hand, there is a wide road in between the two sites with considerable traffic (both light and heavy-duty vehicles), but still equivalent to all other surrounding roads. The specific construction site (~0.15 km²; Figure 4.2b) was selected because it was at rest during the campaign, so we consider that Aeolian erosion of the loose soil was the only source of fPM. The site was also chosen as it represents a typical open bare land covered by the carbonates-based soil of the region, highly susceptible to wind activity and close to residential areas (Figure 4.2a). According to the wind roses diagrams for the monitoring stations, no significant impact was observed from nearby buildings and obstacles on their wind velocity and direction (Figure 4.3). We also studied a number of polar plots (Figure 4.3b and c: mean PM₁₀ concentrations and Figure A1 in Appendix A: weighted mean PM₁₀ concentrations by wind speed/directions) and observed negligible influence by other major sources for the selected wind directions (i.e., WNW (West-northwest) to ENE (East-northeast)).

4.2.2 Data Collection

PM number concentrations and meteorological data were collected using Enviro Check 365 air quality monitoring station (see Section 3.2.1). Prior to the field campaign, a side-by-side intercomparison was conducted between the two monitoring stations for two weeks, which resulted in standardized differences of less than 7% (i.e., the maximum of the distribution of the differences

was in all cases within the uncertainty limits of the calibration standards $\pm 3\%$). The main input data required to run the FDM model include meteorological data, sources information, receptors information and particles characteristics. Meteorological measurements on a minute basis were recorded by the climate sensor attached to the monitoring station

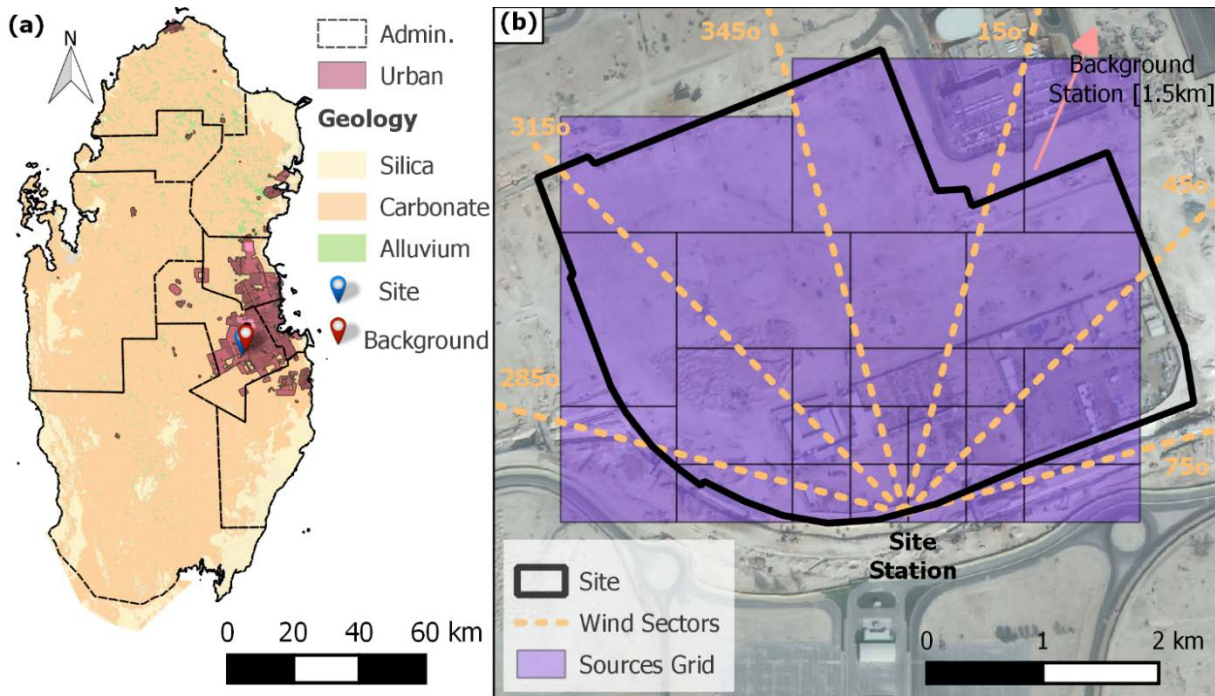
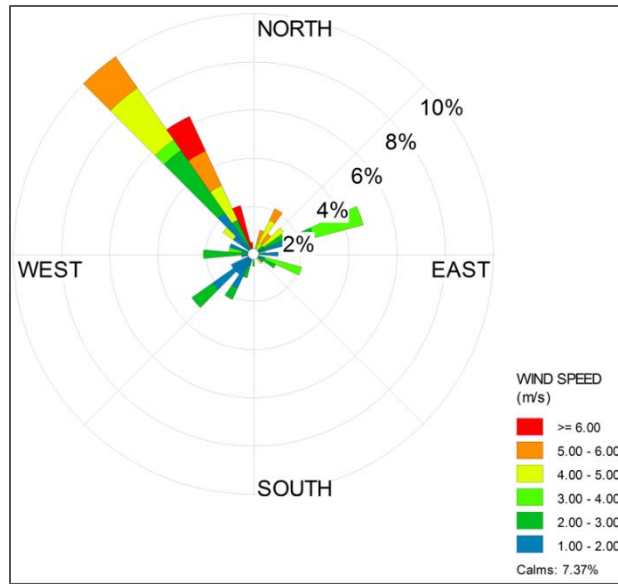


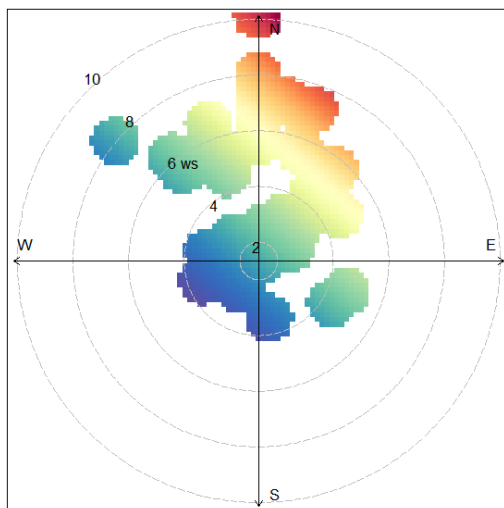
Figure 4.2 The study area showing: (a) Qatar geological map and sites locations, (b) outline of the construction site and the formed 23 area sources (Section 4.2.3).

. Averaging of wind direction was computed by the Mitsuta method (Mori, 1986). In the absence of atmospheric stability measurements or output from the local meteorological agency, we obtained it using the turbulence-based (σ_A) method (USEPA, 2000). This method employs the standard deviation of wind direction and the scalar mean wind speed for the calculation of the hourly atmospheric stability. Mixing heights were also required by the model as part of the meteorological inputs. General values of the mixing height (from 400 m to 1800 m) were assigned for each time period following a stability class based approach (Winges, 1991). This assumption

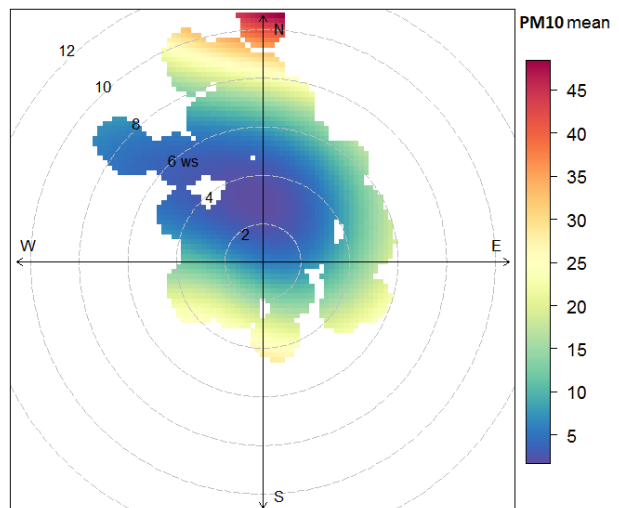
was considered adequate because of the small size of the site and the vicinity of the monitoring station to the emission sources. Finally, a roughness length of around 0.06 cm was selected following the textbook guidelines, which corresponds to a flat desert terrain. This assumption is considered valid for the internal boundary layer where both the source and monitoring station are located (Barlow, 2014).



(a)



(b)



(c)

Figure 4.3. (a) Wind rose for the construction site station during the studied period. Polar plots of PM_{10} mean concentration ($\mu g m^{-3}$) by wind speed ($m s^{-1}$), (b) for the construction site station during the study period, and (c) for the background station during the study period.

4.2.3 Atmospheric Dispersion Modelling

The USEPA has approved a wide range of well-validated atmospheric dispersion models that can predict concentrations of various air pollutants on both local and regional scales (USEPA, 2005). Most of these models are either limited to gaseous pollutants or designed for large spatial domains. In addition, lack of specific modules to treat different particle sizes may induce deviations on the estimation of concentrations from fugitive dust emission sources (Abdul-Wahab, 2006). In this study, we aimed to choose a simpler model in order to facilitate inverse calculations.

The FDM, which is selected in this study, is a USEPA developed air quality model designed specifically to compute emissions and deposition impacts of fugitive dust sources (see Section 3.4.2). Although this model is no longer available on the USEPA's website (last version 1993), it has been used in the latter years by researchers and showed satisfactory results in predicting fPM from different industrial (e.g., cement and coal mines) sources (Abdul-Wahab, 2006; Trivedi et al., 2009). A study by Prabha (2006) showed a comparison between FDM and the Industrial Source Complex Short Term Model (ISCST3) for the short-term simulated emissions from mining activities. The FDM model showed a high accuracy ($d = 82\%$; index of agreement) in predicting emissions compared ISCST3 model ($d = 44\%$). Another comparison is presented in Scott (2008), verifying the significance of vehicle traffic and wind-eroded TSP (from chromite ore processing residue affected soils) and their associated inhalation risks. Using three different dispersion models (FDM, ISCST3, and AERMOD), emission estimates within a FAC2 were achieved by both (FDM) and (ISCST3) while the values predicted by AERMOD were as much as 5-folds of the measured.

FDM incorporates point, line and area sources; the latter is used in this study. Area sources in FDM have to be rectangular up to a width to length ratio of 1 to 5 (Winges, 1991). In order to obtain the source input information required by the model (i.e., area sources dimensions,

coordinates of the area source centre point and release height of emissions), the total area of the construction site has been divided into 23 smaller area sources (Figure 4.2b), formed on a grid of 50×50 m squares. FDM requires strictly rectangular area sources. Therefore, these squares were grouped in a way to form rectangular area sources, with different dimensions (see Figure 4.2b), and to be aligned with the wind sectors. In other words, we aimed to keep each of these area sources as much as possible within the respective wind sector (Figure 4.2b). Although this was not possible in all cases, it later facilitated post-processing of results and inverse calculations.

FDM expresses PM emission fluxes, owing to wind erosion, as a power function which is also supported by a large number of emission modelling studies (Sanderson et al., 2014):

$$E = Q_0 u^w \quad (4.1)$$

where E is the emission flux [$\text{g m}^{-2} \text{s}^{-1}$], Q_0 is the proportionality constant [$\text{g m}^{w+2} \text{s}^{1-w}$], u is the wind speed [m s^{-1}], and w is the wind speed dependence factor [-]. Q_0 and w are site and soil specific parameters, respectively.

4.2.4 Source Characterization

For the characterization of each area source, and in order to collect additional information that is necessary for FDM, we collected five soil samples (hereafter referred as SS#) from different areas of the site and conducted four different types of analysis that included bulk density calculation, PSA, XRD and XRF. Three samples (referred to as SS1 to SS3) were collected from the construction site area (Figure 4.2b) and further two samples (i.e., SS4 and SS5) from the surrounding area, following the (USEPA, 1995) guideline for soil loading estimation. The same guideline was followed for the bulk density calculation.

The average density of the tested soil was found to be around 2340 kgm^{-3} . The crystallographic analysis showed that the soil consists mainly of 55% Dolomite ($\text{CaMg}(\text{CO}_3)_2$),

30% Calcite (CaCO_3), 3% Gypsum ($\text{CaSO}_4 \cdot 2(\text{H}_2\text{O})$) and the remaining 12% is mostly Silica (SiO_2). This is expected since the majority of the surface soil in the State of Qatar (Figure 4.2a) is based on carbonates. Particle size analysis showed (Figure 4.4) that most samples (SS1 to SS3) from the construction site include two modes at $\sim 20 \mu\text{m}$ and $900 \mu\text{m}$ (particles greater than $2,000 \mu\text{m}$ had been sieved out). Although the chemical and morphological compositions were similar for all samples, the samples from the surrounding area (SS4 and SS5) showed only one mode at around $900 \mu\text{m}$. This difference is attributed to the different earthworks in the two areas. Thus, the soil of the construction site appears to have smaller particles, which would be more susceptible to Aeolian erosion. Following the above characterization and according to the Food and Agriculture Organization (FAO, 2014), this soil belongs to “Calcisols”. Calcisols accommodates soils with a substantial accumulation of secondary carbonates, widespread in arid and semi-arid environments, and often associated with highly calcareous parent materials.

4.2.5 Evaluation of EFs

The dispersion model, FDM, was used in an iterative manner to develop the source-receptor relationship and to calculate the best-fitted emission flux for two averaging periods (15-minute and 60-minute intervals). Two to ten iterations were performed until achieving a 3 decimals accuracy (of the values reported in Table 4.1). The iterative calculation was performed for five particle size classes (<2.5 , 2.5-6, 6-10, 10-20 and $20-30 \mu\text{m}$) in order to match the $\text{PM}_{2.5}$ and PM_{10} fractions, and the PM fractions discussed in the AP-42; the compilation of air pollutant EFs by USEPA (USEPA, 1995). To perform the first run of the model, the initial value for the emission flux was assumed to be equal to unity and constant during the whole period. After the first iteration, the emission flux was still considered equal for all 23 rectangular shaped sources but not anymore constant for the whole modelling period. This assumption was based on the fact that the

construction site surface material has uniform chemical and morphological compositions (see Section 4.2.4) and is exposed to the same conditions (i.e., meteorology). The model (FDM) predicted concentrations and the measured concentrations were used to correct the emission flux for each time period and size class, based on the linear relationship between the emission flux and the concentration:

$$E = E' \frac{C_M}{C_P} \quad (4.2)$$

where E' is the emission flux [$\text{g m}^{-2} \text{s}^{-1}$] entered to the model, E [$\text{g m}^{-2} \text{s}^{-1}$] is the corrected emission flux, C_p [$\mu\text{g m}^{-3}$] is the predicted concentration by the model, and C_M [$\mu\text{g m}^{-3}$] is the net measured concentration. The latter was calculated by subtracting the concentration measured by the background station from the concentration measured by the construction site station (also called receptor point as per the FDM). For the first run of FDM, E' refers to the unit emission flux (i.e., $E' = 1 \text{ g m}^{-2} \text{s}^{-1}$).

The calculated emission fluxes (E'), for each particle size class, were classified based on the cardinal wind direction into twelve wind sectors of 30° each. The background station is positioned NNE (North-northeast; $\sim 23^\circ$) of the construction site monitoring station, so we filtered the data and used those within the WNW to ENE (285° to 75°) sectors, as shown in Figure 4.2b. This wind direction range is large enough to account for all the fPM emitted from the construction site, that could reach to the receptor, and to include a representative fraction of the collected QA/QC (Quality Assured/Quality Controlled) data, in this case, $\sim 50\%$. It is also small enough to consider the measurements at the background site representative of the background PM levels. Due to permission constraints, there were no other better alternative locations for the two stations. To support our assumption of the selected wind directions (WNW to ENE or 285° to 75°), we examined a number of polar plots (Figure 4.3b and c) for both sites. Figure 4.3c shows balanced

mean PM₁₀ concentration levels from all wind directions for the background station, which means that no significant source affects the measurements there. For the construction site measurements (Figure 4.3b), we observe mainly the impact of the construction site itself (at 285° to 75°). The contribution of each wind direction and speed to the overall mean PM₁₀ concentration value supports the above findings (presented in Appendix A, Figure A1). The correlations between the calculated emission fluxes and each of the meteorological parameters were examined in order to identify, qualitatively, the confidence in the results.

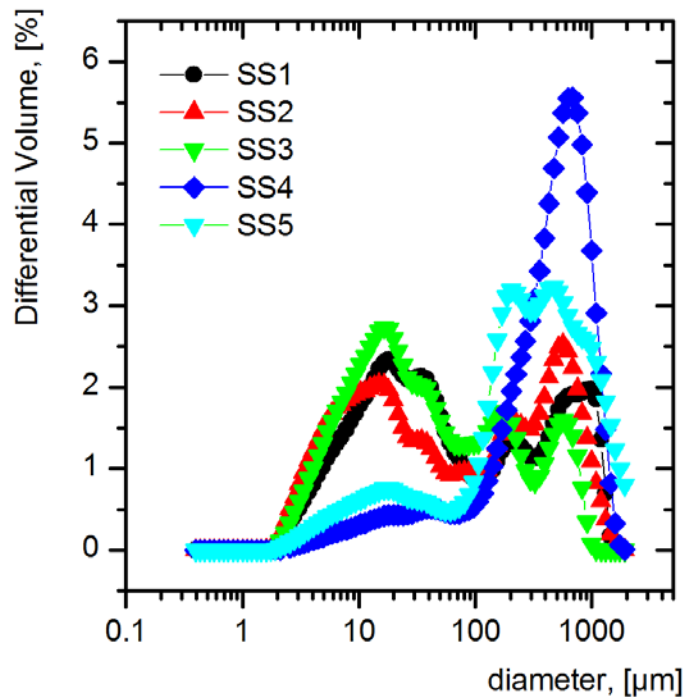


Figure 4.4 Particle size analysis of the five collected soil samples (SS). Soil SS1 to SS3 are from within the construction site and SS4 and SS5 are from the nearby area.

4.3 Results and Discussion

This section presents the results related to the fugitive emissions from the selected source. Initially, we present and discuss the actual PM measurements. Then, we discuss the correlations between the meteorology related measurements and various PM fractions. Furthermore, we present

the calculated emission fluxes for each size class and compare them with literature values for similar sources (e.g., the USEPA's AP-42). Finally, we use the estimated emission fluxes to calculate the impact of the construction site, as expressed by the ground level concentrations. These concentrations are then compared with the measured data.

4.3.1 Measurements

The weather during the study was typical for the period, with an average temperature of 31 ± 5 °C; there was no rainfall and average relative humidity was found to be in the range of 32 ± 22 %. Prevailing wind direction was NNW (Figure 4.3), which is also the annual prevailing wind direction for the region. In this work, all the measurements were averaged to 15-minutes and 60-minutes. All the data were checked manually for the purpose of quality assurance and quality control (QA/QC). For steady-state Gaussian plume models, such as FDM, periods of calm wind (i.e., wind speed < 1 m s⁻¹) must be treated before entering to the model (USEPA, 2005). Data with wind speed less than 1 m s⁻¹ (7.4% of the valid data) but greater than the threshold of monitoring station (i.e., 0.3 m s⁻¹) were set equal to 1 m s⁻¹, and wind speed data below the threshold of the instrument were disregarded (USEPA, 2005). We also disregarded the data for the periods when the monitoring stations were non-operational due to issues such as overheating, clogging, dust storms, and power cuts. It is worth mentioning here that there were periods where the cooling of the background station was not adequate because it was directly exposed to the sun (internal temperatures greater than 60 °C). Eventually, we used around 40% of the total data collected for the analysis and modelling purposes.

During the study period (40% QA/QC data), very high concentrations were observed at both, the construction site and background location, for all size classes. Figure 4.5 presents the time series plot of the measured particulate matter (PM₁₀ and PM_{2.5} mass concentrations) and the wind

(velocity and direction) at the site station. PM_{10} mass concentrations varied from $50 \mu\text{g m}^{-3}$ to over $600 \mu\text{g m}^{-3}$, while $PM_{2.5}$ from $10 \mu\text{g m}^{-3}$ to $200 \mu\text{g m}^{-3}$. Mass concentration peaks followed the high-velocity occurrences, which in turn were demonstrated mainly from northerly winds. In fact, even low wind velocities ($\sim 2 \text{ m s}^{-1}$) were also able to demonstrate PM_{10} concentrations of around $200 \mu\text{g m}^{-3}$. Note that the construction site during the whole period was at rest, there were no other similar construction sites in the vicinity, and the background mass concentrations in most cases were about an order of magnitude lower than those from the construction site during the sampling period. Hence, background mass concentrations were omitted from Figure 4.5.

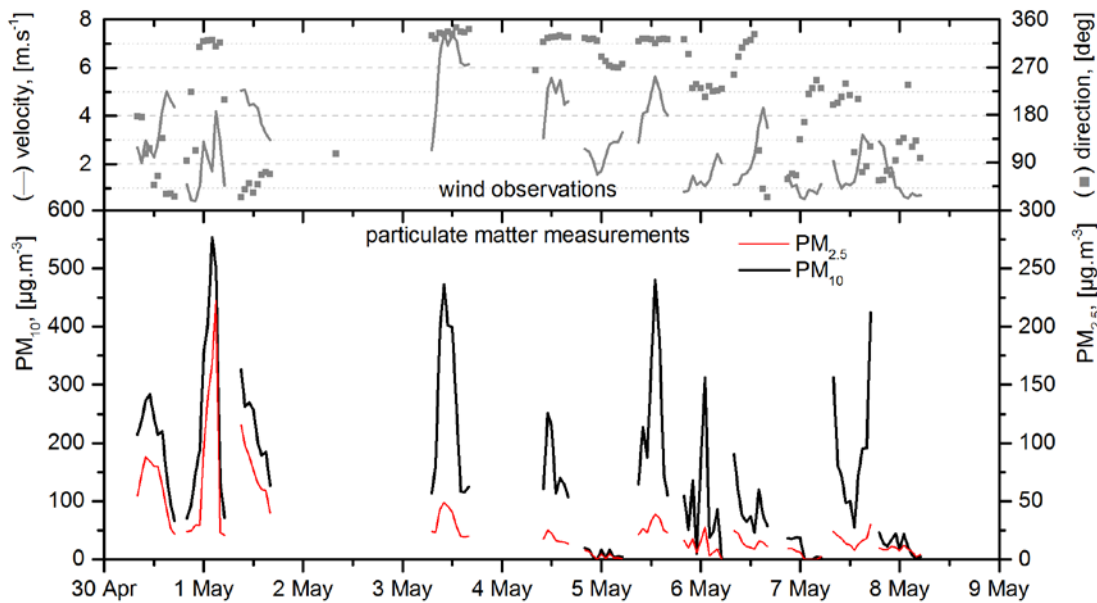


Figure 4.5 A time series showing the change of mass concentration and the wind (at the construction site station) for an indicative period (~ 1 week) and after the exclusion of invalid data as described in Section 4.3.1.

On the other hand, during severe dust events (not included in Figure 4.5) as reported by Qatar Meteorology Department (QMD), the background station demonstrated concentrations of both PM_{10} and $PM_{2.5}$ about an order of magnitude higher than those at the construction site station (values were eliminated QA/QC). We could not locate a specific explanation for this trend.

4.3.2 Correlations between the Measured Concentrations and Wind Speeds

The correlations between all the measured data (meteorology and concentrations) for both locations and time periods were computed and investigated. The meteorological and concentration measurements at the construction site and the background location were compared in order to examine the correlation between all the variables. Concerning the 15-minute averaged data, a high correlation (R^2 between 0.74 and 0.99) was observed between the concentrations of the different size classes at both locations. This indicates that all particle size classes are strongly related and their largest fraction is affected by the same sources. We also consider a safe assumption that the construction site produces the majority of the measured particles, based on the high difference between the concentrations at the two locations (Section 4.3.1). Calculation of emission fluxes was made for 15-minutes and hourly averages. For the 15-minutes averages, a correlation (R^2 between 0.32 and 0.76) was calculated between the emission fluxes and measured wind speeds at the site; the higher correlations were observed for the smaller particles' size classes (i.e., diameter $\leq 10 \mu\text{m}$). This is an expected result since wind speed is the main cause of particles entrainment and favours smaller particles. It is also an indication that the origin of the majority of the smaller particles is common for the construction and background sites.

The time resolution of 15-minutes was initially chosen based on a rough estimate of the particles transfer time-scale from the background location to the monitoring station at the construction site. This way, it was possible to increase the number of available data points for the emission flux calculations. However, observed correlations were too low, so we used the 60-minutes averages (usually a standard time scale in air quality work). The obtained correlations were quite higher (i.e., R^2 between 0.34 and 0.91) and deemed satisfactory. This result can be interpreted as an effect of the distance between the two monitoring stations.

4.3.3 Estimation of the Emission Fluxes

Following the methodology described in Section 4.2.5, we calculated the parameters of the emission flux function (see Eq. 4.1). Table 4.1 presents these parameters (for the hourly averages dataset) and the goodness of fit results for four particle size classes (i.e., ≤ 2.5 , 2.5–6, 6–10 and ≤ 10 μm). Each function provides the developed emission flux for the corresponding particle size class and expresses the wind dependence of particles entrainment. Validation metrics (FAC2, FB, and NMSE) for the predicted emission fluxes are also provided (Table 4.1). Please note that PM_{10} emission flux was evaluated twice: (i) once using the predicted emission flux function, and (ii) once as a summation of the emission fluxes of the first three classes. However, as shown in Table 4.1, the latter case gave better results compared to the predicted function.

Table 4.1 Parameters of emission flux function ($E = Q_0 u^w$; $\text{g m}^{-2} \text{s}^{-1}$) for four particle size class and the goodness of fit results (for hourly averages dataset)

| Particle Size Class (μm) | Q_0 | w | R^2 | adjusted R^2 | RMSE | FAC2 | FB | NMSE |
|---|-------------------------|-------|-------|----------------|------------------------|-------|-------|--------|
| ≤ 2.5 ($\text{PM}_{2.5}$) | 4.405×10^{-07} | 1.867 | 0.132 | 0.121 | 0.014×10^{-5} | 0.508 | 0.382 | 1.563 |
| 2.5-6 | 1.534×10^{-06} | 1.654 | 0.444 | 0.435 | 1.064×10^{-5} | 0.523 | 0.165 | 0.510 |
| 6-10 | 3.547×10^{-07} | 2.691 | 0.693 | 0.688 | 1.272×10^{-5} | 0.587 | 0.064 | 0.435 |
| ≤ 10 (PM_{10}) | 2.475×10^{-06} | 2.061 | 0.582 | 0.575 | 2.668×10^{-5} | 0.015 | 1.636 | 14.951 |
| PM_{10} (as sum of <2.5 , 2.5-6, 6-10)** | | | | | | 0.569 | 0.151 | 0.414 |

- RMSE, Root Mean Square Error
- FAC2, Factor of Two
- FB, Fractional Bias
- NMSE, Normalized Mean Square Error

* Quality acceptance: $\text{FAC2} > 0.5$ (50%); $|\text{FB}| < 0.3$ ($\pm 30\%$); $\text{NMSE} < 0.4$

** Predicted emission flux based on the summation of the first three particle size classes

The goodness of fit results (Table 4.1) shows a better performance for larger particles, which is expected and already demonstrated by the correlations discussed in the text above. Other

empirical studies have developed similar relations for the dust flux, as a power function of the wind (or friction) velocity, with parameter values of the same range as in this study. Sanderson et al. (2014) review a good number of these studies, but only a couple of them cover similar land use and soil composition. For example, Neuman et al. (2009) developed flux equations with a power factor in the range of 1.3 to 4 for PM₁₀ for various mine tailings. Emission flux equations for total suspended particles (TSP) from different sources, including construction, were also developed by Nickling and Gillies (1989) with a power factor in the range of 1.3 to 3 for PM₁₀ and up to 6 for TSP.

Among these studies, we selected the widely used emission inventory AP-42 (USEPA, 1995) for comparison since it is partially included in the European, Australian and other inventories. According to AP-42 the erosion potential for a dry exposed surface is calculated using the below equation:

$$P = 58(u^* - u_{th}^*)^2 + 25(u^* - u_{th}^*) \quad (4.3)$$

where P is the erosion potential [g m^{-2}], u^* and u_{th}^* are in [m s^{-1}]. The wind-generated particulate emissions from a surface consisting of both erodible and non-erodible material can be estimated using the below emission factor equation:

$$E = k \sum_{i=1}^N P_i \quad (4.4)$$

where E is the emission flux [$\text{g m}^{-2} \text{year}^{-1}$], k is the particle size multiplier, P_i is the erosion potential corresponding to the observed fastest mile of wind for the i^{th} period between disturbances [g m^{-2}], N is the number of disturbances per year (used to adapt the Potential for the selected time scale).

AP-42 provides u_{th}^* (from 0.43 to 1 m s^{-1}) for the selected particle sizes in the 250 to 4,000 μm range, but not for the typical airborne particles (e.g., PM₁₀ and PM_{2.5}). The calculated AP-42

emission rates showed very low sensitivity for u_{th}^* less than 0.4 m s^{-1} . For simplicity, we selected a threshold value of 0 m s^{-1} . Figure 4.6 presents a detailed comparison of this work and the AP-42 emission fluxes. A good level of agreement is observed between this work and the AP-42. Note that the AP-42 emission fluxes were developed for open coal mines, which might demonstrate an equivalent behaviour to the fine carbonated loose soil (Calcisols) of this study owing to earthworks. If one applies an apparent fitting, which is a method applied by default in many tools like Microsoft Excel, using the logarithmic expression of the power function then the resulted emission flux has a remarkably good agreement with the AP-42 ones (adjusted $R^2 > 0.90$). On the other hand, 90% prediction bands highlight the significant uncertainty of these calculations and that more studies are necessary to reduce the uncertainty and improve the accuracy (Figure 4.6).

We applied the new emission fluxes to FDM for the calculation of the concentration at the receptor (construction site station) and compared them to the measured data (Figure 4.7). Note that this is a plausible result because all measurements have been used for the calculation of these emission fluxes. Nevertheless, we have performed this exercise to demonstrate the overall impact of the “high” uncertainty (i.e., the 90% confidence bound in Figure 4.6, indicate a high uncertainty on the estimates). As shown in Figure 4.7, modelled values (concentrations) indicate an overestimation of the net measured concentrations (note that background levels are omitted). Values are filtered in two groups based on the wind direction: (i) values within the wind sectors where emitted particles are transferred from the construction site towards the monitoring station (285° to 75°), and (ii) values from the wind sectors where no emitted particles reach the monitoring station (75° to 285°) from the construction site. The estimated FDM concentrations (shown in Figure 4.7) are acceptable, and for PM_{10} mainly fall within the FAC2 statistical metric, which is a common metric in evaluating the performance of dispersion models.

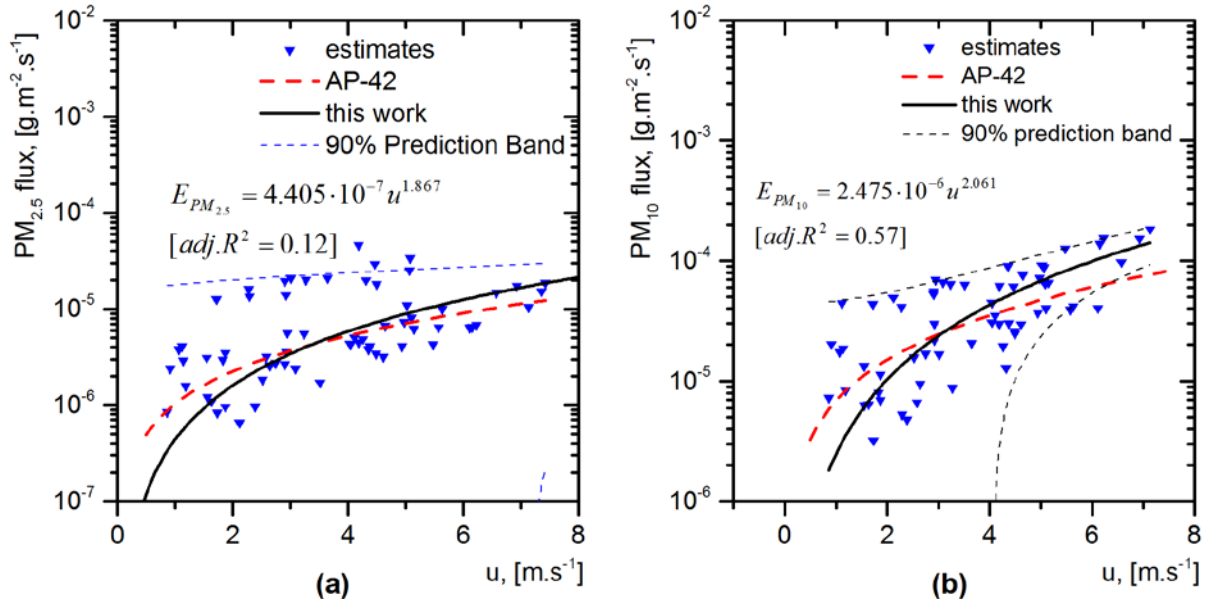


Figure 4.6. Comparison between this study (estimated emission fluxes), the proposed function and AP-42 emission fluxes for (a) PM_{2.5}, and (b) PM₁₀. Dashed lines show the 90% confidence and prediction bands

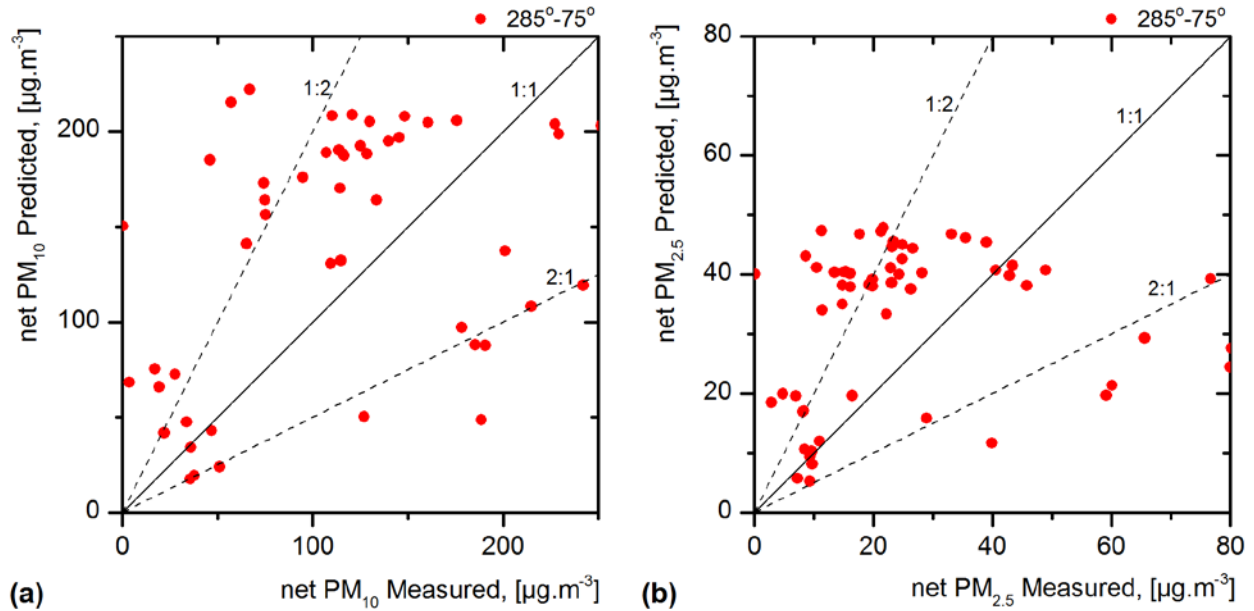


Figure 4.7. Scatter plot of modelled versus measured (net) mass concentrations for: (a) PM₁₀, and (b) PM_{2.5}. Plots also indicate the data filtered according to wind sectors. Solid line indicates perfect agreement and dashed lines show a difference of a factor of two (FAC2)

4.4 Chapter Summary and Conclusions

The release of PM from loose soils is poorly characterized in the widely used emission inventories and published literature. In this study, we focused on the fPM emissions from loose Calcisols (soils with a substantial accumulation of secondary carbonates) that is widely spread in arid and semi-arid environments (i.e., North Africa, Middle East, Central Asia, and Australia).

A ‘two months field campaign was conducted at a construction site within the city of Doha (Qatar) to measure PM concentrations over a size range of 0.25 to 32 μm . The time period of the campaign was chosen deliberately when the construction site was at rest and the only source of particles was wind erosion of the loose soil. FDM was implemented to calculate PM concentrations and obtain their emission fluxes in an iterative procedure. The model results were fitted to a power function, which expresses the wind velocity dependence. Power factors were estimated as 1.87, 1.65, 2.70 and 2.06 for the particles ≤ 2.5 , 2.5–6, 6–10 and ≤ 10 μm size ranges, respectively. Power factors fitted to the data were found to show an adjusted R^2 that varied from 0.13 for the smaller particles up to 0.69 for the larger ones. These power factors are in the same range of those reported in the literature for similar sources. Other validation metrics (FAC2, FB, and NMSE) were estimated. The FAC2 results, for example, show values between 0.508 and 0.587 for almost all particle size classes. Nevertheless, and to the best of our knowledge, this is the first study focusing on construction sites (loose soil) of carbonates-based soil. The loose Calcisols is potentially one of the main fPM emission sources in the Middle-East and other dry arid regions.

On the other hand, the large uncertainty on the calculated fluxes is demonstrated by the wide 90% prediction bands, which indicates that more studies are necessary to reduce the uncertainty in estimating the fugitive emissions from similar sources. Moreover, fPM is released from a large number of other related sources (i.e., earthworks and vehicles), which are also poorly

characterized. Lacking information on fPM sources is critical, given that many of these sources can be seen close to residential areas and could have a direct impact on sensitive groups such as the elderly and children. For this purpose, another dominant source of fPM in the subject areas (non-exhaust traffic PM) is investigated in Chapter 5.

Chapter 5 Vehicle-Induced fPM Emissions

The aim of this chapter is to combine measurements and modelling techniques to derive EFs and models for exhaust and non-exhaust fPM, representative of an arid urban environment (i.e., city of Doha, Qatar). Linear and non-linear models have been derived by utilizing field measurements taken nearby major roads, source apportionment to estimate source contributions, dispersion modelling and regression analysis. The results presented in this chapter aim to contribute to a more comprehensive emission inventory for fPM in desert arid and semi-arid areas. This work appeared in (Hassan et al. 2020a; revised version under review).

5.1 Introduction

Road traffic is an indisputable source of particulate matter (PM) pollution in urban areas (Pant and Harrison, 2013). Exposure to vehicular PM can cause acute respiratory and cardiopulmonary conditions, especially to sensitive groups such as children and elders (Brauer, 2002; Fan et al., 2009). Therefore, exhaust particles that come out of a vehicle's tailpipe have been extensively studied and widely regulated in many European and North American countries (Thorpe and Harrison, 2008). Over the years, implementation of emissions control strategies has led to successful reduction in exhaust PM. In contrast, little has been done to address the impact of the non-exhaust (i.e., fugitive) sources (Shirmohammadi et al., 2017).

Vehicle-induced fugitive Particulate Matter (VfPM) is generated from the abrasion of brake, tire and road components as well as resuspension of dust by the passing vehicles (Kumar et al., 2013). The latter being of greater importance in areas and urban environments with desert arid climate (Tsiouri et al., 2015). Studies in North Carolina, USA suggested that VfPM is the main

source of PM₁₀ in urban roads (Abu-Allaban et al., 2003). Measurements collected from two different types of roads in Switzerland found that brake wear and road dust contributed 59% of the total PM₁₀, compared to 41% from exhaust sources (Bukowiecki et al., 2010). Furthermore, abrasion of brake and tire components can produce enormous amounts of sub-micron sized particles (<300 nm in diameter), which pose a higher risk on human health (Kumar et al., 2013). Despite their significance in urban roads, the current knowledge on VfPM and their behaviour is far from comprehensive (Pant and Harrison, 2013).

Various techniques have been developed to measure and characterize VfPM. The conventional techniques include quantifying VfPM under real-time conditions through simultaneous measurements at a road-side and a background location (Harrison et al., 2012; Krecl et al., 2018), measuring concentrations at the ends of a road tunnel with known boundary conditions (Lawrence et al., 2016; Riccio et al., 2016) or collecting direct measurements using mobile vehicles (Hussein et al., 2008; Kwak et al., 2014). In reality, estimating individual contributions from non-exhaust (VfPM) traffic sources is difficult because of the interactions between the different sources (e.g., differentiating between the wear directly emitted by the road surface and the pre-deposited material on the road) (Thorpe and Harrison, 2008). Chemical characterization and source apportionment methods are often combined to determine source-specific contributions through the fingerprints of their tracer elements (Amato et al., 2016a). For instance, Bukowiecki et al. (2010) carried out an elemental size-segregated measuring campaign at two different roads in Switzerland, where the USEPA PMF model was employed to identify source contributions and estimate PM₁₀ emission factors (EFs) for brake wear and resuspension using pre-estimated NO_x EFs for Switzerland (INFRAS, 2007). Other studies aimed to examine a particular mechanism under a controlled environment, such as the use of laboratory scale models

to simulate road-tire interactions (Grigoratos et al., 2018). Laboratory set ups are advantageous in maximizing the collection of particles, but they tend to underestimate emissions, probably due to the elimination of real world dilution effects (Aatmeeyata et al., 2009; Dahl et al., 2006).

The amount and characteristics of emitted VfPM are highly dependent on meteorology, surface characteristics, and driving conditions. For example, the use of studded tires during the winter season in Nordic countries can dramatically increase the amount of VfPM (Ketznel et al., 2007). In the study of Hussein et al. (2008), mobile measurements were collected from different roads and pavements in Stockholm using a modified version of the TRAKER (Testing Re-entrained Aerosol Kinetic Emissions from Roads) test vehicle (described in Etyemezian et al., 2003b). The results showed that studded tires increase road dust emissions between 2.0 to 6.4 times compared to friction tires and 4.4 to 17 times compared to summer tires. In contrast, a recent study by Lawrence et al. (2016) estimated non-exhaust PM₁₀ EFs from a busy tunnel in London to be just slightly higher (i.e., 16.7-19.3 mg VKT⁻¹ – vehicle kilometre travelled) compared to exhaust emissions (i.e., 11.1-12.8 mg VKT⁻¹). In a similar way, resuspension of road dust during wet conditions (e.g., rain or snowfall) is low, compared to dry periods when evaporation rates increase with temperature (Omstedt et al., 2005).

Surely, there is a large number of specific EFs available in the literature to calculate VfPM emissions based on road type, vehicle class, and driving conditions (some are summarised in Table 5.1), mostly developed for the typical fleets and climate conditions of Europe and North America. It is obvious, however, that these are so specialized that they might be restricted to specific regions, and hence, non-applicable in areas where fPM tend to be a bigger challenge like arid or semi-arid desert climates (Hassan et al., 2016). For this reason, the overall aim is to generate EFs for VfPM appropriate for urban environments with desert arid climates.

In this chapter, EFs and models for such an urban environment (i.e., city of Doha, Qatar) and representative of the wider Middle East Area, have been derived by utilizing field measurements taken nearby major roads, source apportionment to estimate source contributions, dispersion modelling and regression analysis. The results presented in this chapter aim to contribute to a more comprehensive emission inventory for fPM in desert arid and semi-arid areas.

5.2 Methodology

5.2.1 Derivation of the VfPM Emissions

Traffic induces PM emissions directly and indirectly. The former, referred to as vehicle exhaust (VEX) emissions, depend mainly on the vehicle numbers, type, technology and the driving conditions factors. The estimation of VEX emissions has been thoroughly studied with well-established literature, EFs and models like the European COPERT (Gkatzoflias et al., 2006) and the US MOVES (USEPA, 2016). The indirect traffic emissions (non-exhaust or VfPM) are the topic of this study. They are more complex and, in addition to the above factors, depend on the meteorology and road conditions (e.g., material, deposited dust). As noted in Section 5.1, one of the approaches to estimate the EFs is to combine source apportionment studies, based on field campaigns, with dispersion modelling tools, based on accurate traffic data. The source apportionment tool calculates the contribution of VEX emissions to the measured values of PM or gaseous pollutants by taking advantage of their very characteristic elemental profile. The dispersion modelling relates the vehicle numbers (traffic intensities) and the aforementioned factors with these contributions and provides the means to estimate the EFs. Including more factors into the calculations increases the accuracy of the EFs and decreases the uncertainty. The use of gaseous pollutants (e.g., using NO_x EFs to estimate dilution rate; (Pant and Harrison, 2013)), when available, is preferred for PM.

On the other hand, barren lands, construction sites, and other natural sources of PM are expected to have a similar elemental profile to the road dust resuspension (Amato et al., 2011) - in other words to the VfPM. This prohibits direct estimation of the VfPM without further assumptions and calculations. One option to estimate the VfPM is to calculate the individual contributions of all non-traffic sources with similar elemental profiles using emissions and dispersion modelling and subtract them from the total measured contribution in order to obtain the VfPM portion. Usually, this total measured contribution is referred to as resuspension or crustal material in source apportionment studies. This option has been followed herein with the additional hypothesis that transboundary contributions to the airborne crustal material (i.e., resuspension) are strongly correlated with wind (speed and direction) or negligible under normal dust levels, i.e., excluding regional dust events. The latter is a critical hypothesis that will be investigated prior to the calculations, and was based on a recent study by Kontos et al. (2018) that focused on the natural dust emissions in the wider area of interest and a previous own study on the sensitivity of fPM emissions to land use and land cover data (Hassan et al., 2017b; Hassan et al., 2016). A regression analysis with all the related factors (traffic intensities, vehicle class, and meteorology) will result in an appropriate EFs for VfPM with acceptable correlation to the measurements.

Figure 5.1 describes the above methodology and the interconnections between the employed methods, while each method is described in detail in the following sections.

Table 5.1 Literature Emission Factors (EFs) for Traffic PM [mg VKT⁻¹]

| Location | Road Characteristics | Methodology | Exhaust | Non-exhaust | Reference |
|---|---|---|--|--|----------------------------|
| Nevada and North Carolina, USA | Different roads with high speed, low speed and exits. | Roadside continuous measurements were used to derive total fleet emission factors, and integrated PM samples were used to attribute EFs to exhaust, resuspended road dust and brake wear emissions using Chemical Mass Balance (CMB) modelling. | PM _{2.5, LDV} : 7-52 PM _{2.5, HDV} : 57-480 PM _{10, LDV} : 7-65 PM _{10, HDV} : 57-570 | Brake Wear: PM _{2.5, LDV} : 0-4 PM _{2.5, HDV} : 0-13 PM _{10, LDV} : 0-79 PM _{10, HDV} : 0-610 Resuspension: PM _{2.5, LDV} : 2-26 PM _{2.5, HDV} : 17-300 PM _{10, LDV} : 41-780 PM _{10, HDV} : 230-7800 | (Abu-Allaban et al., 2003) |
| Treasure Valley (TV), Idaho, USA | Arteria, Collector, Interstate, Local/Residential | Concentrations were linked to variables such as vehicle speed and downwind flux using regression analysis to estimated emission potential. | - | Resuspension: PM ₁₀ : 1700-8000 | (Etyemezian et al., 2003a) |
| Copenhagen, Denmark Stockholm, Sweden Leipzig & Berlin, Germany Helsinki, Finland Klagenfurt, Austria | Urban/Asphalt | Swedish Model; calculates EF for non-exhaust traffic emissions by accounting for the variability of dust load and surface moisture. (Omstedt et al., 2005) | PM: 28-50 | PM ₁₀ : 46-198 | (Ketznel et al., 2007) |
| Copenhagen, Denmark | Urban (main road, traffic lights and slow traffic) | German Method; uses the procedure in INFRAS (2007) emission factor handbook to calculate exhaust emissions, and the | PM: 19-32 | PM _{10, fleet} : 29-118 PM _{10, LDV} : 10-90 PM _{10, HDV} : 200-800 | |

| | | | | | |
|---------------------|-------------------------------|--|--------|---|-----------------------|
| | | procedure of Gehrig et al. (2004) to calculate non-exhaust traffic emissions using PM concentration difference upwind/downwind and NO _x (dilution tracer). | | | |
| Copenhagen, Denmark | Urban/Asphalt | Danish Method; EFs follow the structure of COPERT 4 model (Gkatzoflias et al., 2006), and depend on vehicle class (e.g., car/van/truck) | PM: 50 | PM _{10,fleet} : 59 PM _{10,LDV} : 50/70 PM _{10,HDV} : 230 | |
| London, UK | Urban/Roadside, Street Canyon | Measurements. Estimating PM ₁₀ using NO _x as exhaust tracer. Non-exhaust=coarse fraction PM _{2.5-10} . Resuspension=Coarse-Abrasion | - | Resuspension: PM _{10,LDV} : 0-48 PM _{10,HDV} : 139-432 | (Thorpe et al., 2007) |
| Barcelona, Spain | Urban | PM vertical profiles were estimated using an array of samplers arranged in a vertical set up next to a road. The deposition and emission flux were estimated using the terminal concentration (calculated from the square fit of all samplers concentrations). | - | Resuspension: PM ₁₀ : 12-47 | (Amato et al., 2012) |

5.2.2 Field Campaign

Measurements were carried out during a three-month field campaign in the city of Doha in Qatar. Qatar [11,571 km²] is a coastal state with ~ 2,750,000 inhabitants, where the majority live in or around its capital city, Doha. Doha represents 1.1% of Qatar's total area and accommodates ~ 40% of its total population (2015 Report of the Qatar Planning and Statistics Authority). Qatar has witnessed substantial growth in its transportation sector in the recent years, as part of Qatar's vision 2030. According to Qatar's ministry of development planning and statistics, the total number of registered vehicles (including motorcycles) have increased by 34% between the years 2011 and 2015 (MDPS, 2015).

The field campaign was conducted from April to June 2015 at a sampling site adjacent to a trafficked road. The monitoring site was set up just outside a high-rise office building, located at Al Rumaila West area at the city centre of Doha (Figure 5.2), characterized by sparse high-rise buildings (around 3-7 floors). The building overlooks Al Istiqlal Road (~ 50 m), a busy urban road with an average fleet of 77,300 vehicles per day during weekdays and 54,400 vehicles per day on weekends with ~ 95% of the vehicles being light duty. The road has 6 lanes, 3 in each direction, and intersects with Mohammed Bin Thani road (NW) and Al Rayyan road (SW), which are two major roads of the city's road network.

Particle number (PNC) and mass (PMC) concentrations were measured using Grimm Enviro Check 365 monitoring station (Section 3.2.1; station's inlet was at ~ 1.7 m height). Integrated 24h ambient samples of PM_{2.5} and PM₁₀ were collected using two separate MicroPNS air samplers (Section 3.2.2; sampling height ~ 1.7 m). A total of 90 (24h) samples of PM_{2.5} and PM₁₀ were collected. Prior and after each sampling, filters were conditioned and gravimetrically weighed following the methodology described in Section 3.3. The filters were placed in petri-dishes after

weighing and transported to and from the sampling site in sealed containers to avoid contamination. Samples were then chemically analysed for carbon, ionic and elemental characterization. More details on the chemical characterization methods have been published in a past study (Saraga et al., 2017) and the elements/species employed herein are reported in Section 5.2.3.



Figure 5.2 A map of Doha’s major roads network showing the sampling site and the adjacent roads

5.2.3 Source Apportionment

Source Apportionment is the identification of ambient air pollution sources and the quantification of their contribution to air pollution levels. Receptor modelling comprises a source apportionment approach, aiming to re-construct the contribution of emissions from different sources of atmospheric pollutants based on ambient measurement data (i.e., PM chemical

composition) observed at monitoring sites. The latest PMF model by USEPA (PMF v.5.0) has been used in the present study (described earlier in Section 3.4.1).

In this study, the elemental analysis of the measured samples as described in (Saraga et al., 2017) yielded 17 trace elements (Al, As, Ba, Cd, Co, Cr, Cs, Cu, Fe, Ga, Mn, Ni, Pb, Rb, Sr, V, Zn), 8 water-soluble ions (Cl^- , NO_3^- , SO_4^{2-} , Na^+ , NH_4^+ , K^+ , Mg^{2+} , Ca^{2+}), elemental and organic carbon (EC, OC). To avoid double mass counting (K and K^+ , Ca and Ca^{2+}), the ionic forms were excluded from the analysis. A combined $\text{PM}_{2.5}$ and PM_{10} dataset was used as input to the PMF model. Eleven samples were initially excluded from the model: nine samples were excluded for too many missing species and two samples (one of each fraction) were treated as outliers and excluded from the analysis due to extremely high concentrations attributed to a single dust event recorded on May 4th, 2015. Co, As, Cd, Pb, Ga, Rb, Sr, Cs and Ba were set as ‘bad’ species and excluded from the analysis due to the high percentage of missing values. Ni, Zn, Cu, and Ca were set as ‘weak’ species due to their low signal/noise (S/N) ratio and/or bad scaled residuals (d-matrix). PM concentration was set as total variable. Concentration data below the MDL were substituted with half of the MDL and missing concentration data were substituted with the median value for the specific specie (Polissar et al., 2001). Equation-based uncertainties were used (estimated based on analytical errors; refer to section 3.4.1), and the modelling extra uncertainty was adjusted to 12%.

Constraints were applied in order to reduce rotational ambiguity and obtain more physically meaningful factors (Paatero et al., 2002). Bootstrap runs (BS), in addition to the advanced tools of the PMF (v.5), the displacement (DISP) and the bootstrap-displacement (BS-DISP) methods, were used to evaluate rotational ambiguity.

5.2.4 Estimation of Traffic Intensities

The principal road network of Doha city is comprised of 230 road segments, across the whole Doha Metropolitan Area, spanning an area of around 25 km diameter, according to the Doha's Public Work Authority (DPWA personal communication). Traffic intensities are measured regularly throughout the years using automatic and manual means, but not consistently in terms of frequency and location. For example, the DPWA carried out three major studies to measure traffic intensities at multiple roads in 2010, 2011, and 2015 for most of the road segments in Doha but not always the same. Their campaigns took place once or twice a year for a week (7 days) and collected hourly traffic counts per segment, lane, and type of vehicle (heavy duty and light duty). At the same time, the road network is changing drastically with new layouts and transitions from roundabouts to intersections and interchanges, while the total number of vehicles increased by 34% from 2011 to 2015. In addition, most of the main roads consist of multiple lanes per direction and with vehicle numbers approaching 100k per day. All these factors considered, a reference traffic counts dataset was synthesized using the available data with traffic counts per hour, day of the week, and type of vehicle (heavy and light duty). Although important, more details on the derivation of this dataset are beyond the scope of this study.

5.2.5 fPM Emissions from Barren Lands and Construction Sites

Emissions modelling of the fPM from barren lands and construction sites was based on two different approaches. The former is calculated based on the well-established and validated model of Schaap et al. (2009) for the regional modelling of particulate matter. This model was developed on the principles of the proposed atmospheric dust cycle by Marticorena and Begametti (1995). Later, others (e.g., (Liora et al., 2015)) elaborated on the parameters of these models and proposed improvements. For this study, we selected the original regional modelling scheme as a baseline

with no later modifications. Calculation of fPM emissions from construction sites is based on a simpler approach but its parameters were developed and validated in our own field studies that characterized emissions from the local surface soil (i.e., Calcisols) (Hassan et al., 2016); more details can be found in the previous chapter.

For both approaches, detailed land use and land cover (LULC) information are required. For the current study area, i.e., State of Qatar, there were two relevant LULC databases. The first is the Harmonized World Soil Database (HWSD) (FAO, 2014) which provides surface soil (0-100 cm depth) data. The second is based on a recent local geological study (West and Al-Mulla, 2013). For this study, we combined information from these two databases with recent satellite photos (Google Earth) and site-visits to develop one LULC map and database that incorporates, as well, the exposed (barren) lands within the metropolitan area. The final map had a resolution of 0.5×0.5 km² and includes the clay-sand-silt compositions for each relevant LULC category.

5.2.6 Dispersion Modelling of PM

The latest CALPUFF model (v7.2.1), coupled with the interface from Lakes Environmental Software was chosen to calculate the atmospheric dispersion of PM (Section 3.4.3). Meteorological input was provided in the form of MM5 weather data based on a parameterisation described at an earlier work (Gopaldaswami et al., 2015). The modelling domain was 200×200 km² centred on the city of Doha with a nested resolution following the LULC map resolution. An additional discrete receptor was added at the field campaign site.

Eventually, dispersion modelling resulted in four discrete contributions to the PM concentration levels: (i) the contribution of barren lands and constructions sites, later referred to as (AR10), estimated using the fPM emissions described in Section 5.2.5, (ii) the contribution of light-duty vehicles and (iii) the contribution of heavy-duty vehicles estimated using a unity

emission factor (1 mg VKT^{-1} ; referred to later as (c_{ldv}) and (c_{hdv}), respectively), and (iv) the contribution of the road surface – Aeolian resuspension using again a unity emission factor (1 mg km^{-1} ; referred to later as c_{road}). A fifth dispersion contribution was estimated indirectly combining results from the PMF analysis and the AR10 contribution (VfPM) and further discussed in Section 5.3.2.

5.3 Results and Discussion

5.3.1 Measurements

During the campaign period, hourly air temperatures ranged from 17.36 to 45.13 °C, relative humidity from 5.94% to 34.04%, and wind speeds from 0.02 to 8.59 m s^{-1} (Table 5.2). Calmer winds were observed between midnight and early mornings (mostly $<3 \text{ m/s}$) while higher averages up to 4.1 m s^{-1} were reported between 12:00h and 18:00h (local time). Obviously, the measured wind direction is biased by the nearby building, as this is reflected in the wind rose diagram (Figure 5.3). Therefore, mesoscale modelling results have been employed after validation with airport wind data (~6 km SE). Thus, prevailing winds blew from North and East.

Table 5.3 presents the ambient mass concentrations as reported by the particle counter and estimated with the weighted filters. Due to the high variability of the PM measurements we categorized the PMC measurements into typical days ($<200 \mu\text{g m}^{-3}$), minor dust events (200-1000 $\mu\text{g m}^{-3}$), and major dust events ($>1000 \mu\text{g m}^{-3}$) following recommendations from past studies (Al-Dabbous and Kumar, 2015; Draxler, 2001; Saraga et al., 2017). Noteworthy, the majority of the herein reported major dust events coincides with the respective warnings issued by the Qatar Civil Aviation Authority, and were excluded from further analysis, following the QA/QC criteria presented in Section 5.2.3.

Figure 5.4 presents the hourly time series of the measured PMCs and wind speeds. Missing data are due to technical issues or maintenance of the instruments. The pollution roses (Figure 5.5) present the measured PMCs partitioned by wind speed and wind direction (major events excluded). It appears that PM₁₀ levels were mainly affected by sources to the East, which is consistent with the major road next to the building and also the coastline. In contrast, PM_{2.5} levels appear to be affected by a “point” source to the Northeast that coincides with a large nearby road intersection. We believe that this difference between the PM_{2.5} and PM₁₀ pollution roses is attributed to the different driving conditions at the road intersection compared to the free flow, also reported in similar studies (Goel and Kumar (2015)), and the sea salt and shipping emissions coming from the coastline (see Section 5.3.2 on the source apportionment results)

Table 5.2 Statistical results of the measured meteorological parameters

| | Min. | Max. | Mean | SD |
|---------------------------------|-------|-------|-------|-------|
| Temperature [°C] | 17.36 | 45.13 | 33.59 | 5.94 |
| Humidity [%] | 5.94 | 91.02 | 34.04 | 17.12 |
| Wind Speed [m s ⁻¹] | 0.02 | 8.59 | 3.39 | 1.49 |

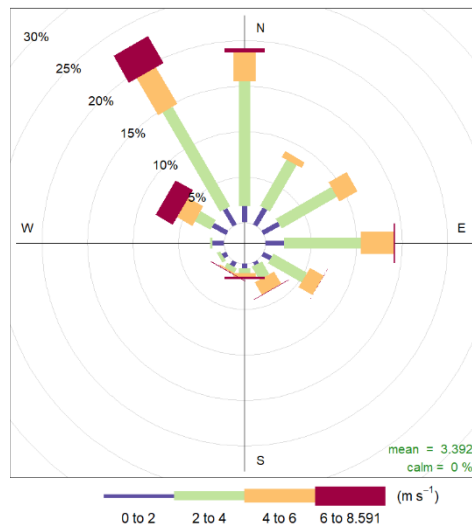


Figure 5.3 Windrose diagram at the sampling site during the campaign period

Table 5.3 Statistical analysis of the daily measured PMC data

| Instrument | Category* | # days | PM _{2.5} [$\mu\text{g m}^{-3}$] | | | | | PM ₁₀ [$\mu\text{g m}^{-3}$] | | | | |
|--------------|--------------|--------|--|------|--------|----------------------------|-----------------------------|---|------|--------|----------------------------|-----------------------------|
| | | | SD | Mean | Median | 5 th percentile | 95 th percentile | SD | Mean | Median | 5 th percentile | 95 th percentile |
| Grimm EDM365 | Typical Days | 38 | 29 | 79 | 71 | 40 | 130 | 29 | 163 | 168 | 102 | 198 |
| | Minor Event | 45 | 207 | 135 | 92 | 63 | 165 | 1129 | 478 | 241 | 206 | 919 |
| | Major Event | 2 | 794 | 899 | 899 | 394 | 1404 | 4328 | 4649 | 4649 | 1895 | 7403 |
| | Total | 83 | 156 | 109 | 85 | 50 | 154 | 842 | 334 | 207 | 131 | 439 |
| PM Sampler | Typical Days | 23 | 58 | 123 | 125 | 38 | 218 | 26 | 166 | 172 | 119 | 195 |
| | Minor Event | 23 | 325 | 279 | 181 | 106 | 753 | 322 | 363 | 278 | 218 | 602 |
| | Major Event | 1 | - | 1569 | 1569 | 1569 | 1569 | - | 1781 | 1781 | 1781 | 1781 |
| | Total | 46 | 241 | 201 | 144 | 59 | 409 | 249 | 267 | 214 | 123 | 402 |

* minor dust events with PM₁₀>200 $\mu\text{g.m}^{-3}$ and major dust storms with PM₁₀>1000 $\mu\text{g.m}^{-3}$ (Al-Dabbous and Kumar, 2015; Draxler, 2001; Saraga et al., 2017)

A more detailed analysis of the diurnal and weekday patterns is shown in Figure 5.6, using a threshold of $PM_{10} < 200 \mu\text{g m}^{-3}$ (the suggested daily mean for non-dusty days). On average, PM_{10} followed the traffic patterns, it peaked in the late morning on weekdays (1000h-1200h) and again in the afternoon (at 1400h-1500h & 1800h), corresponding to the usual rush hours due to schools and offices activity. PM_{10} levels were slightly lower during weekends (Friday-Saturday), compared to weekdays (Sunday-Thursday) with the exception of Monday. It is probable that the patterns observed or not observed (e.g., the lowest levels should have been observed on Friday morning due to the close to zero traffic), were affected by low intense dust events. To explore this further, the threshold value for PM_{10} was lowered progressively to around $PM_{10} < 160 \mu\text{g m}^{-3}$, reaching to a PM_{10} weekday pattern closer to the one expected and without affecting the diurnal one. On the contrary, the $PM_{2.5}$ diurnal profile is “flat” with very small variations and the weekday profile counterintuitive with lowest values observed on Tuesdays and the highest ones on Thursdays-Saturdays. The corresponding weekday pollution roses (with $PM_{10} < 160$ or $200 \mu\text{g m}^{-3}$) also identified the road intersection, in the North-Northeast, as a major hot spot with a few more hot spots in other directions, where other road intersection lies (see Figure 5.2). On the other hand, the pollution rose of Tuesdays’ was the only one with the road intersection in the North-Northeast not being identified as a major hot spot (see Figure B1 in Appendix B). Based on the rather short available data it was not possible to extract a definite cause for these observations, even though the temporal variation of the meteorological parameters (e.g., wind speed, temperature and humidity) was investigated for the whole 12 weeks of the field campaign. In any case, the $PM_{2.5}$ weekday variations were rather small ($\pm 10 \mu\text{g m}^{-3}$) and the $PM_{2.5}$ diurnal profile so “flat” that both the assumptions of a) significant sources with non-temporal variation (e.g., industry, construction) and b) counterbalancing sources and formation/suppression mechanisms (e.g., boundary layer

height, humidity, secondary particles, normal traffic patterns, intense heavy-duty traffic during night) are equally plausible. Increasing the threshold value up to $PM_{10} < 1000 \mu g m^{-3}$ did not change the $PM_{2.5}$ patterns nor the PM_{10} diurnal variation, but flattened the PM_{10} weekday variation.

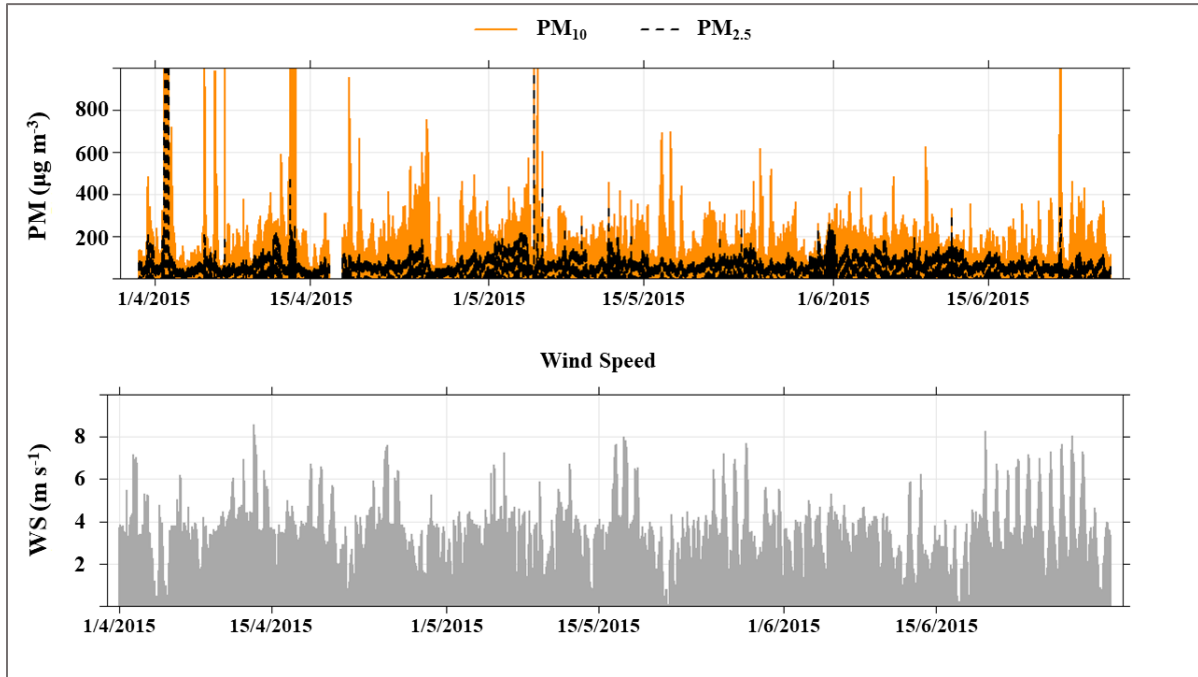


Figure 5.4 Time series of the hourly measured $PM_{2.5}$ and PM_{10} concentrations using the particle counter.

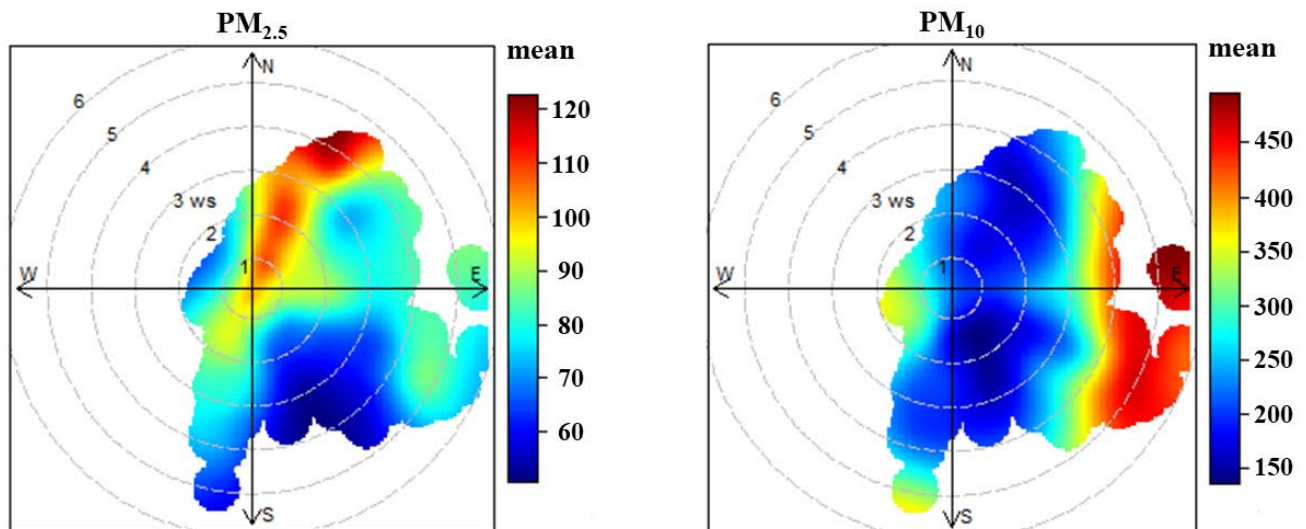
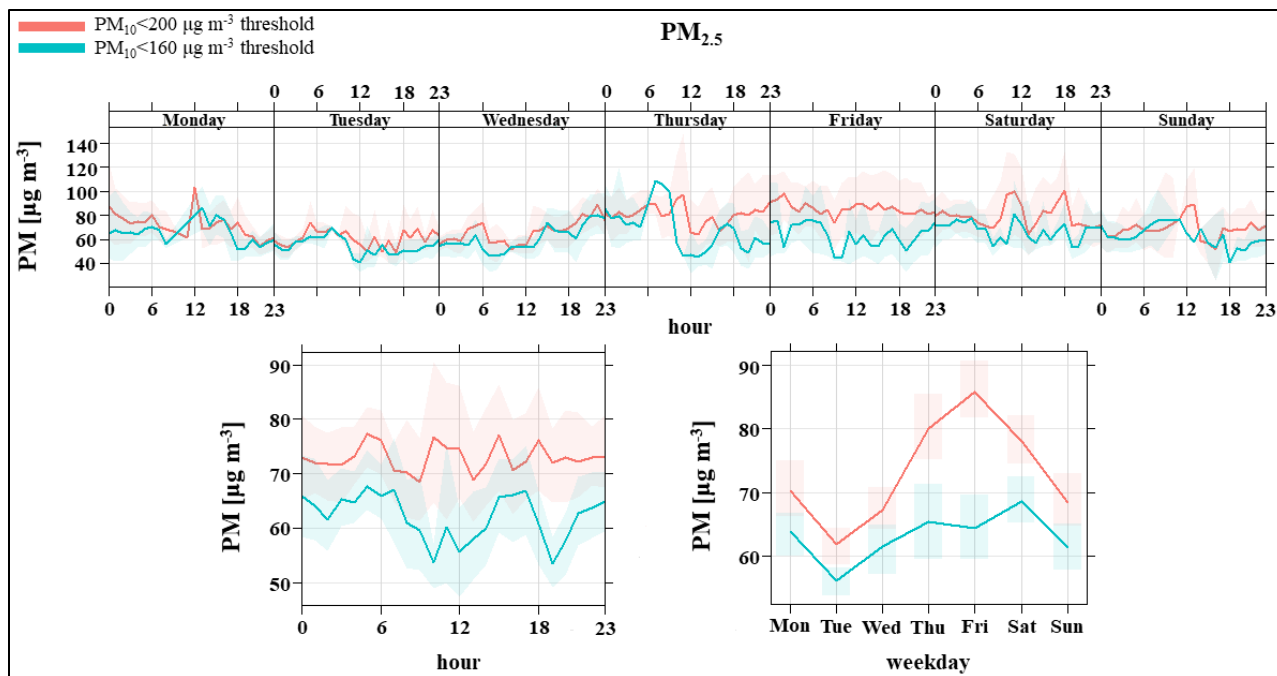
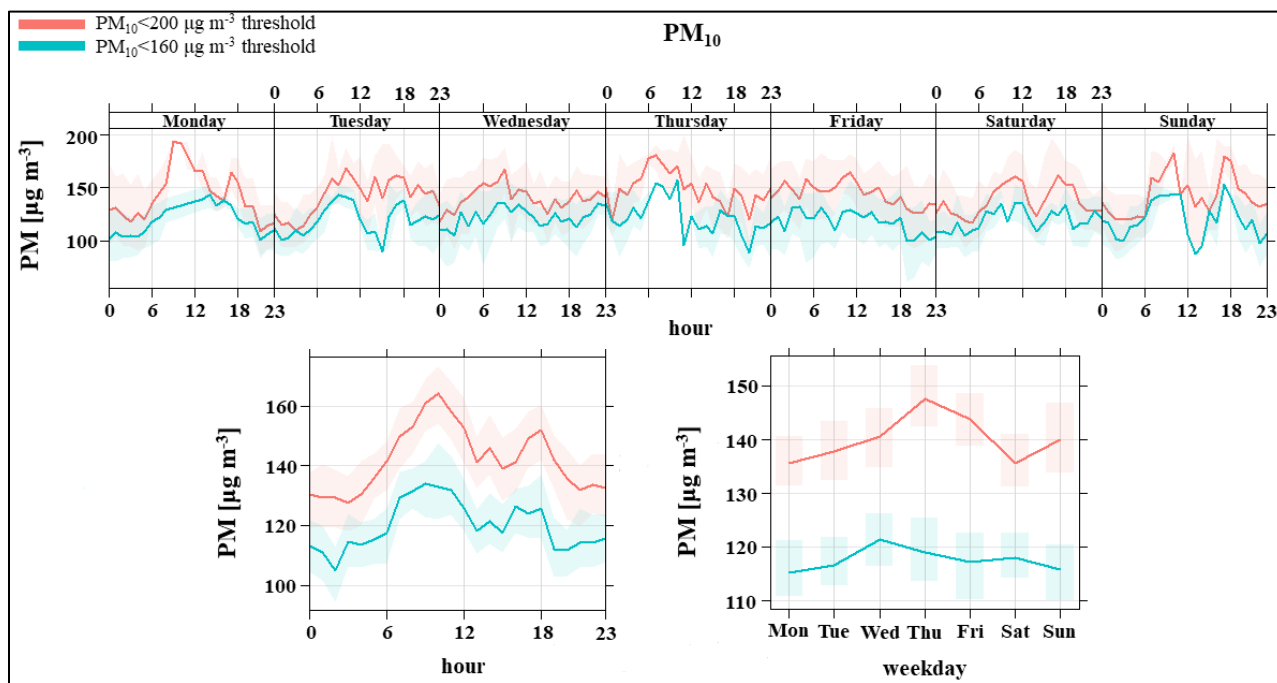


Figure 5.5 Pollution roses of the PMCs ($\mu g m^{-3}$) hourly measurements ($PM_{10} < 1000 \mu g m^{-3}$).



(a)



(b)

Figure 5.6 Mean diurnal and weekly variations of (a) $PM_{2.5}$ and (b) PM_{10} concentrations using two subsets of the data ($PM_{10} < 200 \mu g m^{-3}$ & $PM_{10} < 160 \mu g m^{-3}$). The shaded areas indicate the 95% confidence intervals.

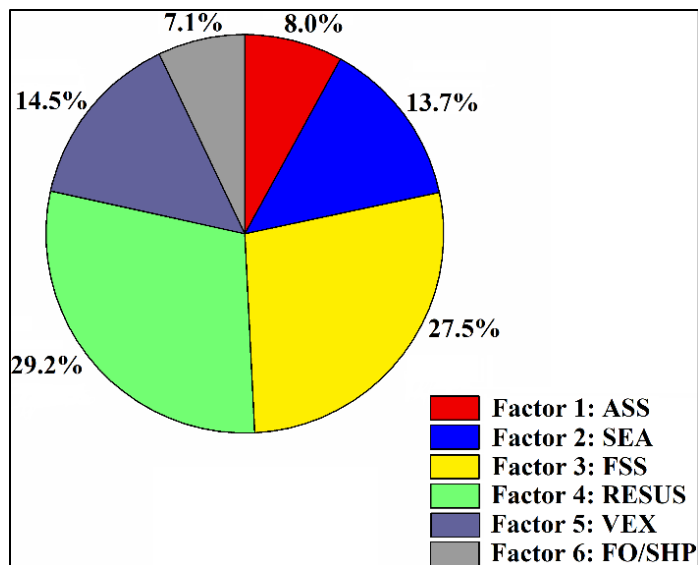
5.3.2 Source Apportionment

For each factor 20 runs were performed, in order to obtain Q-value stability. All runs converged and Q values ranged between $\pm 1.2\%$. Q-robust value was lower than 1.5 times the Q-true value, indicating that outliers are not significantly impacting the Q value. The optimal number of factors was determined by examining the Q values for PMF solutions resulting from a range of the -number of factors- values without excluding the solution's physical validity (Reff et al., 2007). A range of solutions were examined with different number of factors (3-12), but six was the maximum number of factors corresponding to meaningful sources.

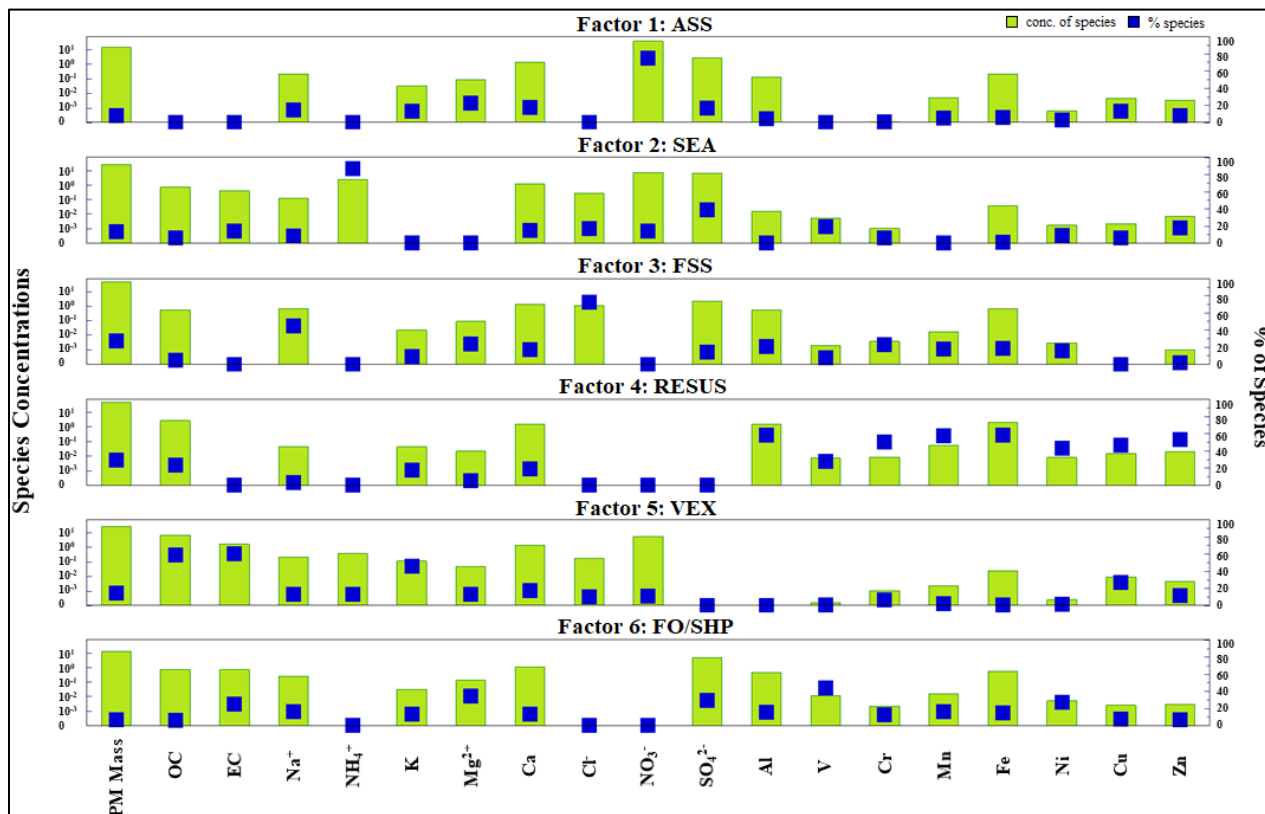
Factors 1 and 3 were both associated with Na^+ and Mg^{2+} , which are typical tracers of sea salt. This is an expected result as the measuring site is located at a distance of ~ 1.2 km from the eastern coastline of Doha. Factor 1, however, was characterized as “aged sea salt” (ASS) due to the absence of chlorine and the presence of high level of NO_3^- , indicating the formation of sodium nitrate (Pérez et al., 2016). Factor 3 was characterized as “fresh sea salt” (FSS) due to the high loadings of Cl^- , Na^+ and to a lesser extent Mg^{+2} (Amato et al., 2016a), and the Cl^-/Na^+ ratio of 1.63 (Pey et al., 2013). Due to the abundance of NH_4^+ and SO_4^{2-} , Factor 2 was characterized as “secondary aerosols” (SEA) which are typical components of regional and long-range transport emissions (Saraga et al., 2019). Factor 4 was the dominant factor with 29.2% contribution and showed mixed composition of crustal elements (Ca, Al, Fe and Mn) as well as brake wear markers (Zn and Cu). This mixture depicts a profile of dust source that possibly includes non-exhaust from traffic, due to the abrasion of vehicle wear and dust resuspension (RESUS) (Heo et al., 2017). Factor 5 was strongly associated with carbonaceous elements EC and OC, and to a lesser extent Cu and Zn, with an OC/EC ratio of 0.86, falling within the ranges previously reported for (VEX) emissions (Amato et al., 2016a). Factor 6 was identified as a combined combustion factor of “fuel

oil/shipping” (FO/SHP) emissions. The fuel oil combustion is owed to the presence of V, Ni, and SO_4^{2-} possibly from industrial processes (Sowlat et al., 2013), which would be a reasonable guess giving that an industrial area is located ~ 13.1 km away from the monitoring site. V and Ni are also tracers of shipping emissions. Although the estimated V/Ni ratio (1.58) in this study was less than the ranges previously reported for shipping emissions (Pandolfi et al., 2011), the V/Cu ratio (8.43) is $\gg 1$ which, according to Tolis et al. (2015), is a value of clear primary shipping emissions. The percentage contributions and profiles of the factors are shown in Figure 5.7.

In the present study, two constraints needed to be applied with the limitation of $dQ\%$ being kept at the lowest value of 0.5%: i) for the RESUS factor: Ca and Fe were pulled up maximally and ii) for the VEX factor: EC was pulled up maximally. Compared to the initial results, no substantial changes to either the constrained profiles or the constrained contributions were observed, amplifying the accuracy of the selected solution. A third constraint was applied to the FO/SHP as it showed no OC content, which should not be the case for fuel combustion. OC was pulled up maximally for FO/SHP and minimally for ASS. The constrained solution showed similar convergence as the base run and yielded a $dQ\%$ of 0.41, and improved the solution with OC content of 6.13% for the subject factor. After the constraint’s application, BS, DIS and BS-DIS runs were conducted for evaluating the model’s solutions. In particular, 100 bootstrap runs were performed (default value of minimum correlation 0.6), and the results were regarded reliable as $>90\%$ of the factors were mapped. DIS runs resulted in the validity of the final PMF solutions as no factor swaps (i.e., exchanges) were observed for the smallest $dQ_{\text{max}=4}$ while the decrement of Q was $<1\%$. Through BS-DISP analysis, the final solution was considered to be valid as $<0.5\%$ drop was associated with the Q value (Norris et al., 2014).



(a)



(b)

Figure 5.7 Factor contributions (constrained) to the total PM and the elemental profiles for each of the PMF factors as percentage contributions and absolute concentrations (ASS: aged sea salt, SEA: secondary aerosol, FSS: fresh sea salt, RESUS: resuspension, VEX: vehicle exhaust, FO/SHP: fuel oil/shipping)

5.3.3 Derived Emission Factors

Following the presented methodology (Section 5.2), three distinct sets of data have been created: (i) the six PMF factors (identified PM sources), (ii) four meteorological variables (including the estimated u^*), and (iii) five specific contributions including the light-duty, heavy-duty, road surface and PM area sources (barren land and construction sites) that have been derived employing dispersion modelling. The symbols and the correlation matrix for the 15 aforementioned daily datasets are presented in Figure 5.8. Although many interesting arguments could be extracted from this matrix, the focus of this study is the vehicle-induced PM (VEX and VfPM). PMF identified the VEX PM which is positively correlated with the vehicle (0.51-0.52) and road (0.53) dispersion contributions. On the other hand, the resuspension factor (RESUS) is poorly correlated with traffic-related contributions, and moderately correlated with the dispersion contributions (AR10) from barren lands and construction sites revealing that this factor includes airborne crustal material beyond the road dust. Removing this contribution from the resuspension factor (RESUS-AR10), the non-exhaust (VfPM) dispersion contribution is derived. The VfPM has no correlation with the traffic related contributions indicating no linear relation with the contributions. It is worth noting here that VEX is negatively correlated with the wind speed (ws) which implies that strong winds dilute the impact of exhaust traffic PM rather than increasing them. In fact, the very strong winds have not been included in the source apportionment analysis following the exclusion of the major dust events. Finally, both VEX and VfPM show a negative correlation with humidity, indicating the effect of moisture in suppressing traffic emissions.

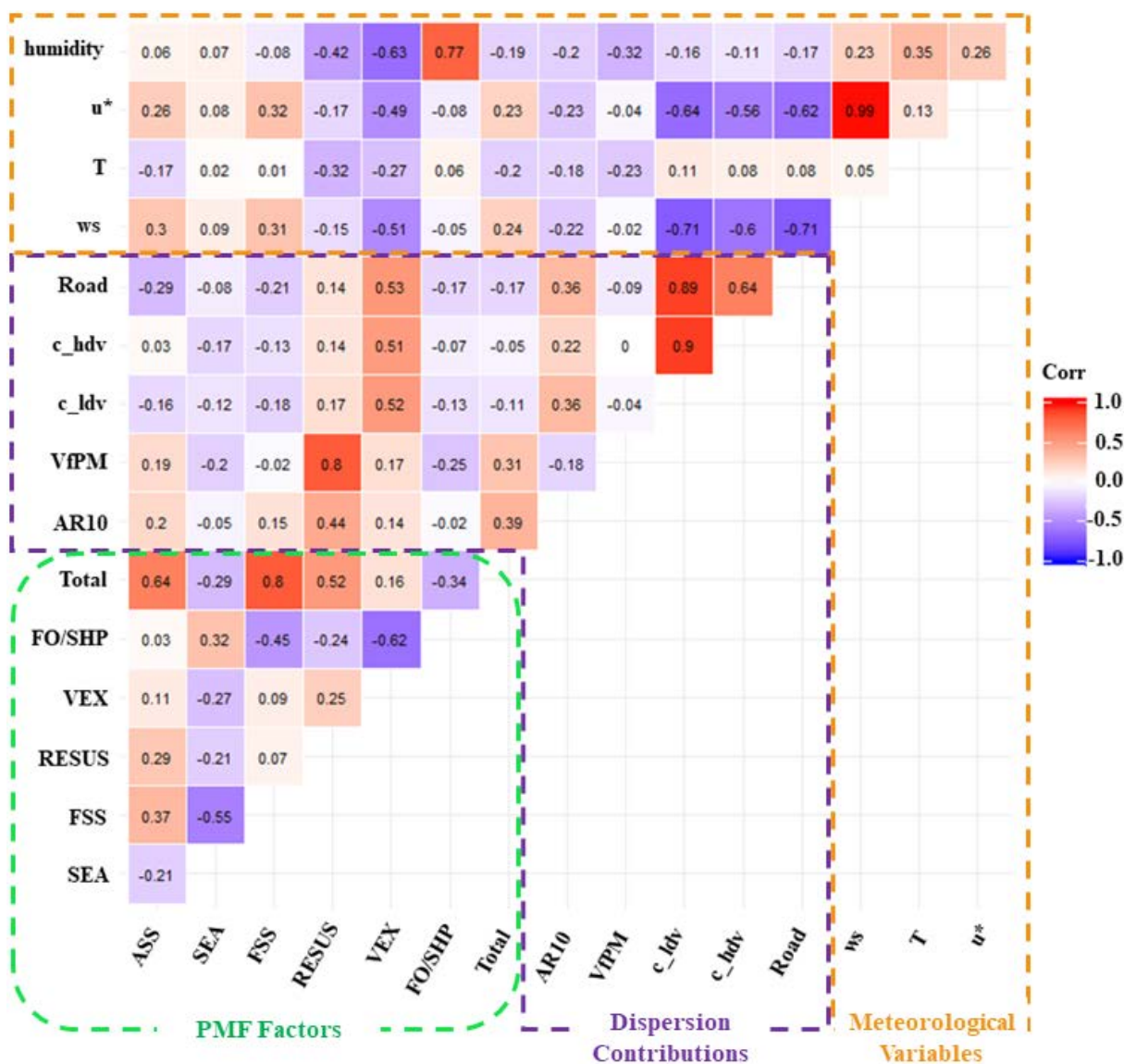


Figure 5.8 Correlation heatmap for the estimated PMF factors (ASS: aged sea salt, SEA: secondary aerosol, FSS: fresh sea salt, RESUS: resuspension, VEX: traffic, FO/SHP: fuel oil/shipping, and Total), meteorological quantities (ws: wind speed, T: temperature, u*: friction velocity, and humidity), and dispersion modelled quantities (AR10: barren lands and construction, VfPM: RESUS-AR10, c_ldv: contribution of light-duty vehicles, c_hdv: contribution of heavy-duty vehicles, and road: contribution of road surface).

The derivation of the EFs [mg VKT^{-1}] for the VEX and VfPM was achieved using linear and non-linear regression analysis (with single and multi-variables) offered by the Stats package (v3.5.2 “lm” and “nls”) in R software. In both cases (VEX and VfPM), it was not possible to derive

separate EFs for the heavy and light duty vehicle types. This was due to the low counts of heavy-duty vehicles for the roads close to the measurement's location, although all 230 road segments have been employed. Therefore, we decided to apply four different combinations of the traffic counts in the regression analysis and use the results to estimate the range of the proposed EFs: (i) total contributions of traffic ($c_{ldv}+c_{hdv}$), (ii) only the light-duty contributions (c_{ldv}), (iii) an arbitrary 50% increase in heavy-duty emission factor ($c_{ldv}+1.5 c_{hdv}$), and (iv) an arbitrary 100% increase in heavy-duty emission factor ($c_{ldv}+2 c_{hdv}$), compared to light duty.

As a result, the estimated EF (PM_{10}) for VEX, using linear regression, ranged from 620 to 730 $mg VKT^{-1}$ (Adjusted $R^2 \sim 0.84$; Figure 5.9a). Concerning the estimated EF(PM_{10}) for VfPM, they ranged from 1080 to 1410 $mg VKT^{-1}$ (Adjusted $R^2 \sim 0.70$; Figure 5.9b). All the estimated EFs up to this point secured a confidence level (p-value for the t-test) of 99% or better. Further to the above and following past literature suggestions, we performed a non-linear regression analysis to derive the VfPM EF using road and meteorological parameters. Among the many combinations tested, the below models for PM_{10} VfPM showed good agreement (i.e., adjusted $R^2 \sim 0.70-0.71$), but not better than the linear model:

$$EF = a \times u^b$$

$$EF = a \times u^b + cH$$

$$EF = (a + cH) \times u^b$$

where, EF [$mg VKT^{-1}$] is the emission factor, u is the wind speed [$m s^{-1}$], H is the humidity [%], and a , b and c are empirical parameters. At the same time, the significance of each new parameter was rather weak (p-value in the range of 60%-80%). Conversely, based on the data and analysis of this study, a linear model for the VfPM EF is proposed.

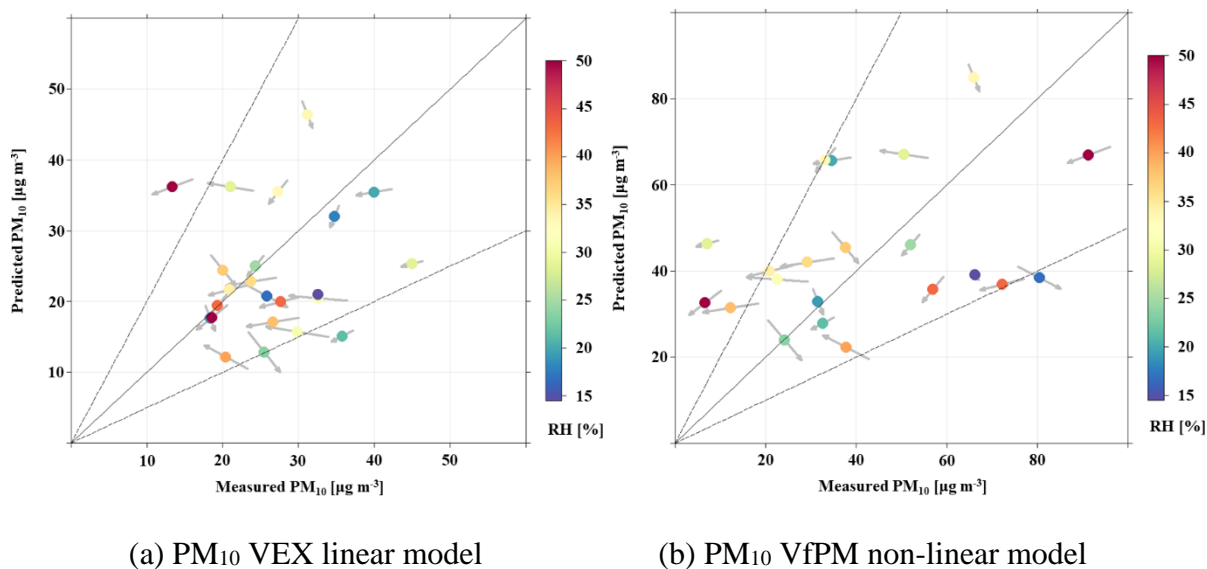


Figure 5.9 Scatter plot examples of the measured vs predicted (a) exhaust (VEX) and (b) non-exhaust (VfPM) PM₁₀ concentration levels with the proposed (linear) EFs. Vectors correspond to the daily wind speed and prevailing direction, and colors correspond to the average relative humidity [%].

For PM_{2.5}, the estimated EF for VEX using linear regression ranged from 170 to 260 mg VKT⁻¹ (Adjusted R² ~ 0.49), and for VfPM from 405 to 680 mg VKT⁻¹ (Adjusted R² ~ 0.39). The scatter plots are shown in Figure B2 in Appendix B

5.4 Chapter Summary and Conclusions

In this chapter we derived one of the first EFs and emission models to estimate VEX and VfPM in areas with arid desert climates. A combination of field measurements, chemical characterization, and dispersion modelling was used to calculate emission contributions at the measuring site. Following a linear regression analysis (using solely the traffic contributions), the fitted EF (PM₁₀) for VEX and VfPM ranged from 620 to 730 mg VKT⁻¹ (adjusted R² ~ 0.84), and 1080 to 1410 mg VKT⁻¹ (adjusted R² ~ 0.70), respectively. A non-linear regression analysis provided emission models for VfPM having similar performance to the linear model, but increased the p-value indicating a weak hypothesis. The EFs presented herein seem to be higher than the

ranges reported in Europe (Amato et al., 2016b; Ketzel et al., 2007) and within the ranges reported in USA (Abu-Allaban et al., 2003). Although the results are plausible, we recommend further investigations to improve emissions modelling for VfPM and build a diverse database for the arid desert climates. The developed models from this chapter and Chapter 4 can be incorporated into PM emission inventories (regional and local scale) in order to improve the assessment of fPM impact, and personal exposure. For this purpose, the developed EFs are used in Chapter 6 to assess the environmental and health impact of different emission inventories.

Chapter 6 The Impact of fPM on Air Quality and Health in Dry-Arid Areas

The aim of this chapter is to examine the environmental and health impacts of fPM through rigorous modelling activities and utilization of past field campaigns at a typical arid and dry area in the Middle East (i.e., State of Qatar). To achieve this, (i) relevant fPM sources will be mapped, (ii) appropriate emission models and input parameters will be selected, (iii) modelling results will be evaluated against measurements, and (iv) finally an assessment is conducted to determine the contribution of fPM and the impact of the emission models on the WHO's EBD estimates. This work appears in (Hassan et al. 2020b; ready to be submitted to Atmospheric Environment).

6.1 Introduction

As concluded, from the preceding chapters, the arid and semi-arid regions are facing a huge brunt of fPM pollution, usually ascribed to the natural dust generated at regional level >100km (Beegum et al., 2016). In fact, source attribution studies conducted in several Middle Eastern cities showed that crustal material accounts for more than 50% of the urban PM levels (Alolayan et al., 2013; Nayebare et al., 2016). Some of the richest and most active dust sources were identified at the river valley of Tigris and Euphrates in Iraq, Iran, Kuwait, Saudi Arabia and along the eastern coastline of the Arabian Peninsula (Prakash et al., 2015). A recent simulation of natural dust over Central Middle East estimated average emissions in the range of 20-70 $\mu\text{g m}^{-2} \text{s}^{-1}$, with daily emissions exceeding 1,000 $\text{mg m}^{-2} \text{day}^{-1}$ (Kontos et al., 2018). The broader region is also subjected to frequent dust storms, originating mostly from the world's largest desert (the Sahara) in North Africa which produces billions of tons of dust annually (Kalenderski et al., 2013; Saliba and

Massoud, 2011). The impact of such sources extends beyond the local domains with dust being carried for long distances across continents (Diapouli et al., 2017).

Recently, there has been a strong emphasis on the impact of fPM driven by local anthropogenic sources in the developing regions (Qiao et al., 2018; Tsiouri et al., 2015), because of the rapid urbanization and industrialization taking place and the inevitable increase in construction works and road transport. For example, in Middle Eastern cities, road traffic is commonly identified as a major source of PM (Abu Allaban et al., 2007; Heo et al., 2017). While it is commonly believed that exhaust emissions prevail on roads with intense traffic, several studies provided compelling evidence that non-exhaust particles from tire, brake and road dust contribute significantly to urban fPM (Amato et al., 2011). Construction activities, another source of anthropogenic fPM, can increase local PM concentrations to several times above background levels and pose a higher health risk due to the intense release of sub-micron sized particles (<300 nm in diameter) especially in the vicinity of populated areas (Kumar et al., 2012). A recent field study conducted in Israel, Jordan and Palestine estimated that construction fPM contributed 12% of the total PM_{2.5} (Heo et al., 2017). Another study in Bangalore, India, showed that people living in proximity of a construction site were exposed to PM concentrations at least seven times above the WHO's recommended limits (Chowdhuri and Gupta, 2017).

A number of developing countries in the arid regions have made serious efforts to control anthropogenic pollutants, including fPM, through the establishment of regulatory activities (Issa and Al Abbar, 2015). Foremost, effective strategic planning and decision making urge for consistent monitoring and modelling systems (Abbass et al., 2018). The former requires large capital investment and demanding operations, while the latter is easier to attain and mainly driven by detailed emission inventories; i.e., databases for determining the sources and emissions of

pollutants (Winiwarter et al., 2009). The most renowned emission inventories are the ones provided by national regulatory bodies such as the AP-42 by USEPA (USEPA, 1995), the EMEP by the EEA (EEA, 2016) and the NPI of Australia (NPI, 1999). Several literature studies also provide more localized, high-resolution and area-specific emission inventories (Kara et al., 2014; Markakis et al., 2012). As previously stated, most of the available inventories were developed with data from European and North American regions and thus focus on sources that are not representative of the arid environments, such as agriculture (Chatzimichailidis et al., 2014) or the use of studded tires (Omstedt et al., 2005) and omit important sources such as construction and barren lands (Hassan et al., 2016). Although some inventories incorporate fPM, they proved inadequate to handle the variability and complexity of fugitive sources (Sanf elix et al., 2017).

It is clear from the above discussion that locally induced fPM is a prominent environmental and health stressor in arid and dry areas while any control and regulatory activity lack the necessary planning tools (e.g., emission inventories) (Kuenen et al., 2011). At the same time, it is unknown how the locally produced fPM contributes to various health assessment criteria, e.g., WHO's EBD, and how sensitive is the latter to the available quantification methods. The aim of this chapter is to address the aforementioned challenges through rigorous modelling activities and utilization of past field campaigns at a typical arid and dry area in the Middle East (i.e., State of Qatar). To achieve this, the following objectives have been set: (i) map the relevant fPM sources, (ii) select appropriate emission models and the critical input parameters, (iii) evaluate these models and parameters against measurements, and (iv) assess the contribution of fPM and the impact of their emission models on the WHO's EBD method.

Table 6.1 Examples of emission inventory studies in areas with arid or semi-arid climates

| Study | City, Country (year) | Pollutants | Source type | Emission Factors | Dispersion Modelling |
|-------------------------|---|---|---|---|--|
| (Baayoun et al., 2019) | Beirut, Lebanon Year: 2009-2016 | NO _x , CO, SO ₂ , PM _{2.5} | Exhaust emissions from diesel generators and light-duty vehicles | EMEP/EEA Tier 2 (2016) | - |
| (Mokalled et al., 2018) | Beirut-Rafic Hariri International Airport, Lebanon (2012) | NO _x , VOCs | Emissions from aircrafts landing and take-off operations | Atmospheric Emissions Inventory Toolkit (EMIT) by Cambridge Environmental Research Consultants (CERC), UK | Model: ADMS by CERC |
| (Sindhwan et al., 2015) | Delhi, India (2010) | CO, NO _x , SO ₂ , PM ₁₀ | CO, NO _x , SO ₂ , PM ₁₀ | Literature | - |
| (Waked et al., 2012) | Beirut, Lebanon (2010) | CO, NO _x , SO ₂ , NMVOC, NH ₃ , PM ₁₀ and PM _{2.5} | Transport sector, power plants, industry and other combustion sources. Biogenic sources | EMEP/EEA Tier 2 | 5 km x 5 km over Lebanon and 1 km x 1 km over Beirut |
| (Ettouney et al., 2009) | Kuwait, Kuwait (2003) | SO ₂ , NO _x , CO | Motor vehicles, power plants, oil fields and oil refineries | USEPA | Model: ISCST model Domain: 160 km x 140 km |

6.2 Methodology

Here, we describe the core methods employed to achieve the aforementioned objectives and aims. Firstly, the study area is briefly described along with the identified fPM sources (Section 6.2.1). Section 6.2.2 presents a synopsis of similar efforts to develop emission inventories in the nearby regions of the study area and an analysis of the selected emission models for each source type. The latter reveals the strong dependence of the selected models on LULC information and characteristics. Subsequently, the available data of the study area is explained in detail in Section 6.2.3. Finally, Sections 6.2.4 and 6.2.5 specify the methods used for atmospheric dispersion modelling and health assessment, respectively. Given the various available approaches for each of the above steps, a number of different cases have been constructed and studied, which are outlined in Section 6.2.6. Note that, for each step, we employ two different approaches: one that follows the state-of-the-art and standard practices, and a second that is based on our own studies and localized approximations (refer to chapters 4 and 5).

6.2.1 Study Area and fPM Sources

The State of Qatar and its capital city, Doha, was selected as the study area due to its dry and arid climate, the intense fPM generation activities (construction, Aeolian erosion etc.), access to the required information (the reference year 2015), and the availability of comparable previous studies. Qatar is a small Peninsula on the north-eastern coast of the Arabian Peninsula, it has a population of around 2.7 million with more than 50% residing in and around the metropolitan area (2015 Report of the Qatar Planning and Statistics Authority). Average temperatures ranging from 15°C to 44°C, average relative humidity from 22% to 63%, and an annual rainfall of less than 120 mm usually accumulated in a few days per year (PSA, 2018). The climate of Qatar can be classified as hot and dry-desert (BWh) on the Köppen–Geiger climate classification. The emphasis of this

chapter is on how locally generated fPM affects local air quality in arid and dry regions, however, the term local does not explicitly define the scale, despite its wide use in the literature. Thus, the physical and administrative boundaries of the study area herein have been used to define the local character for the State of Qatar and the metropolitan area of the city of Doha.

Two types of fPM sources have been identified in the study area: (i) the bare lands within and outside the metropolitan area, and (ii) the non-exhaust traffic emissions, or as referred to in the previous chapter (VfPM). These sources were selected based on their enormous contribution to fPM according to our earlier PM characterization study (Saraga et al., 2017), and previous regional assessments conducted by others (Kontos et al., 2018; Menut et al., 2013). The characteristics of the sources are discussed in Section 6.2.2 and their locations are depicted in Figure 6.1 and Figure 6.2 (Section 6.2.3).

6.2.2 Emissions Modelling

Only a handful of studies have focused on assessing the spatial and temporal characteristics of atmospheric pollutants in the study area and creating local emission inventories; some examples are listed in Table 2.1. Nevertheless, most of them are based on the European or North American inventories due to the lack of dedicated emission models/factors for the local sources, and with the most inventories neglecting the fPM as it was mentioned earlier. In contrast, most of the regional scale studies, which included PM, employed specific emission models to account for fPM (Kontos et al., 2018) but did not account for the VfPM nor for the bare lands within the urban area. The reason is that this information is missing from the available global land-use/cover databases (e.g., USGS, 2000) and global emission inventories (Emissions Database for Global Atmospheric Research; EDGAR v4.3.2 in (Crippa et al., 2018)). The former aspect is further discussed in Section 6.2.3.

6.2.2.1 Barren Land - Aeolian erosion and resuspension

Emissions modelling of windblown dust (i.e., barren lands) was conducted using two different approaches. The first approach, reflects the state-of-the-art and standard practice, is based on the LOTOS-EUROS model (Schaap et al., 2009) which is the basis of the NEMO (natural emissions model; Liora et al. (2016)) that has been tested recently on the broader study area (Kontos et al., 2018). This model has been developed on the principles of the proposed atmospheric dust cycle by (Marticorena and Bergametti, 1995), where (u_{th}^*) is calculated using the soil particle size and the turbulent flow characteristics. The model then uses a drag partitioning scheme that considers the effect of surface roughness (z_o) and a soil moisture correction factor (f_w) that depends on the soil moisture to correct the u_{th}^* with the limitation of z_o not exceeding 0.5 cm. In this study, the drag partition scheme was modified according to the update of MacKinnon et al. (2004) that allows the extension of z_o up to 10 cm, and the soil moisture correction factor (f_w) was set to one, assuming a dry condition (Shaw et al., 2008). In addition, the u_{th}^* was multiplied by 0.9 to account for the soil erosion below the threshold during decreasing wind speeds driven by inertia (Nickovic et al., 2001). The model key formulations are presented in Appendix C.

The second modelling approach is based on a simpler model which was developed and validated in chapter 4 to characterize emissions from the local surface soil (i.e., Calcisols) (Hassan et al., 2016). This is not a generalized model but a specific one for barren land that has undergone some level of anthropogenic treatment but is still characterized as barren land, e.g., constructions sites before the superstructure works. In this model, the emissions flux is expressed as a power function of the wind speed (refer to Eq. 4.1 and Table 4.1 in Chapter 4):

6.2.2.2 Road Traffic fPM

Similar to the barren lands, the VfPM emitted by the major road network of Doha city was modelled using the standard practice (i.e., selected EFs from the literature; (Abu-Allaban et al., 2003)) and EFs developed specifically for dry and arid areas in our previous chapter. The former study developed mass EFs for road traffic emitted by typical fleets of urban US cities using multi-lag regression analysis. It was selected for this work due to the analogy between the Doha and US fleets (in terms of vehicle make and size) and driving conditions compared to Europe. In the latter study (Chapter 5), we developed EFs for vehicle induced PM using a combination of field measurements, source apportionment, dispersion modelling and linear regression, with the assumption that EFs for heavy-duty vehicles are 200% of the light-duty vehicles (refer to Section 5.3.3). The principal road network of Doha city is comprised of 230 road segments (Figure 6.2), as described earlier in chapter 5, and the hourly traffic intensities [vehicle hour⁻¹] for each road segment were obtained from Doha's Public Work Authority. In addition to VfPM, the VEX emissions were modelled for comparison (Section 6.3.3).

6.2.3 Land-use Characterization and Surface Properties

LULC data is a crucial component in calculating dust emissions. It provides the surface properties needed by the meteorological model for the estimation of (u^*). It also provides the soil properties for the estimation of soil texture and identifying the erodible surfaces. In this chapter, we explored two different LULC maps of Qatar (standard and own practice). The first is the default LULC map, downloaded automatically by CALPUFF View model (Section 6.2.4) based on the Global Land Cover Characterization (GLCC) version 2 by the United States Geological Survey (USGS) agency (USGS, 2000). The second LULC is our modified version of the GLCC map based on the surface soil classification from the Harmonized World Soil Database (HWSD) (FAO, 2014)

and an own mapping exercise of the exposed (barren) lands within Doha's metropolitan area. The modifications were made using Quantum Geographic Information System (QGIS v2.18). The modified LULC accounts for the variability of soil surfaces over the study area, for the accurate estimation of surface properties such as z_o and the clay-sand-silt compositions. The latter is necessary for emissions modelling (Section 6.2.4). The z_o values used in this study follow the ones recently estimated by Tan and Fang (2018) from GLCC data. Figure 6.1 shows both LULC maps and classifications, both scaled or obtained to a resolution of 0.5 km².

6.2.4 Dispersion Modelling

For the atmospheric dispersion, a single approach was adopted to model the transport of PM in a domain that covers 200 x 200 km² area over the state of Qatar (Doha city at the centre of the domain). The latest CALPUFF model (v7.2.1), coupled with the interface from Lakes Environmental Software was chosen to calculate the atmospheric dispersion of PM (described in Section 3.4.3). CALPUFF is a non-steady state Lagrangian Gaussian puff model that has been employed in many similar studies (e.g., (Chatzimichailidis et al., 2014)). The meteorological model (CALMET) was run twice for each LULC map (Section 6.2.3).

Due to the large source files and to reduce the processing time, the overall domain (200x200 km²) was modelled with a resolution of 2x2 km². To enhance the level of detail around the metropolitan area, a smaller nested domain (38.5x38.5 km²) was modelled with a resolution of 500x500 m². For the same reason, additional calculation points (called discrete receptors) were placed along each road segment, 100 m apart (a total 3277 receptors), when modelling the traffic PM. Also, four more discrete receptors were placed: three at the locations of the Ministry of Environment's monitoring stations (data are publicly available) and one at the monitoring location of our past field campaign (refer to Section 5.2.2). Figure 6.2 shows the major roads network of

Doha and all the discrete receptors. CALPUFF is not a parallelized model but the required clock time was reduced significantly (to 3-5 days per scenario) by running separately the area sources, across multiple time periods each with a restart of two days, and the road sources in groups of 10 roads per simulation. In the end, all results were combined using the “append” or “calsum”, postprocessing utilities. All simulations were executed using the high-performance computing (RAAD2) facilities at Texas A&M University at Qatar.

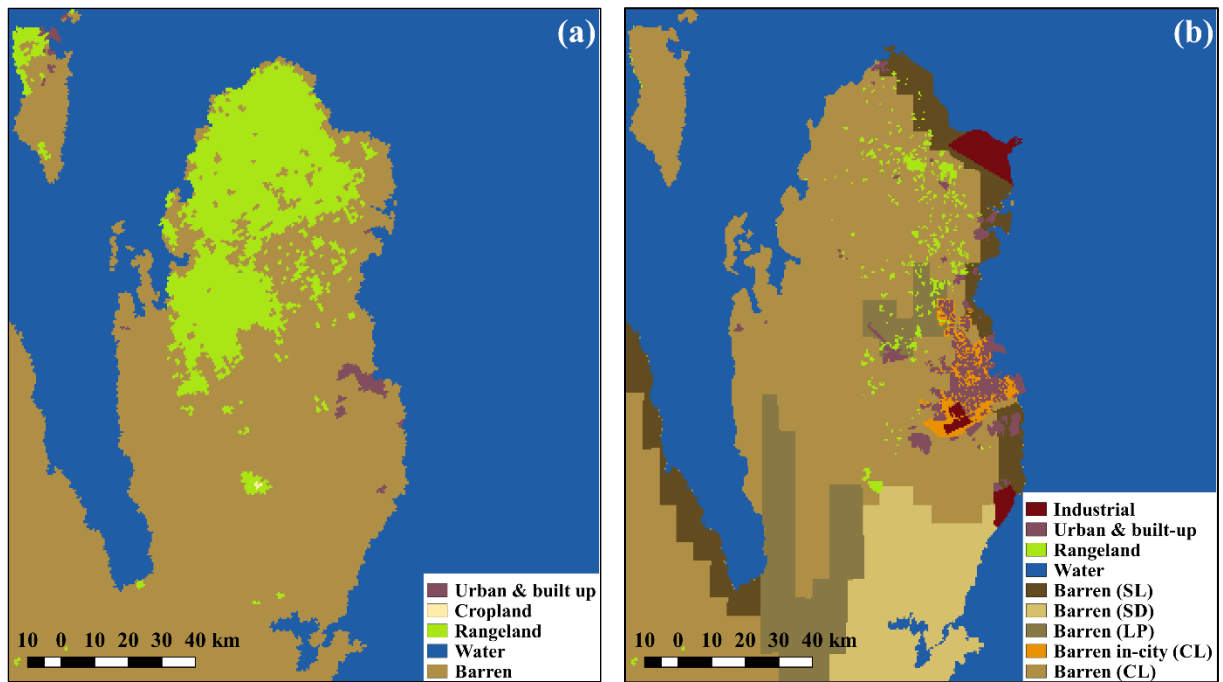


Figure 6.1 The LULC maps of the study area (a) GLCC (standard practice), (b) OWN (modified). The OWN land-use map shows the soil HWSD classifications of soils: SL= Solonchanks, SD = Sand Dunes, LP = Leptosols, CL= Calcisols.

6.2.5 Health Impact Assessment Criteria

The WHO provides one of the most widely applied methods, the environmental burden of disease (EBD) method, to estimate changes in mortality attributed to changes in pollutant concentrations (Ostro, 2004). The main components of the EBD are: (i) the ambient air pollution exposure data (e.g., the annual concentrations), (ii) the information of the exposed group including

population and annual death rates, and (iii) the concentration-response function (also known as the relative risk; RR) that relates the magnitude of the health outcome to the change in air pollutant concentration.

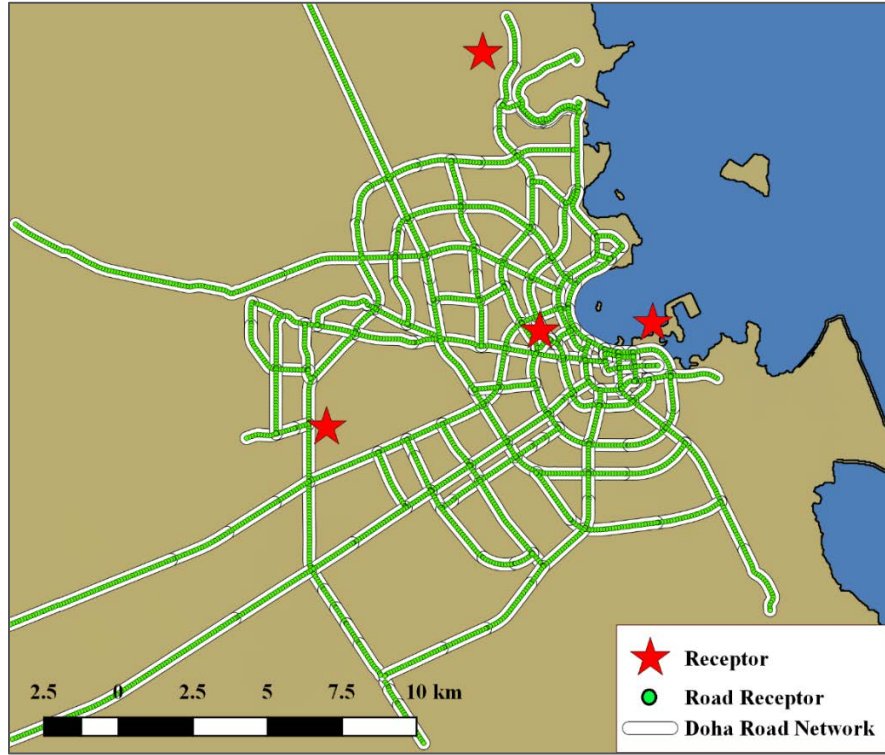


Figure 6.2. Map showing the major roads network (230 segments) in the Doha metropolitan area and the discrete receptors.

Due to the lack of long-term ambient data and cause specific mortality data, we calculate here the “all cause” mortality from short-term exposure to PM₁₀ for all ages. The RR function recommended by WHO for short-term exposure is represented by the below linear relationship (Ostro, 2004):

$$RR = \exp[\beta(X - X_o)] \tag{6.1}$$

where X is the annual mean concentration [$\mu\text{g m}^{-3}$], X_o is a reference exposure concentration [$\mu\text{g m}^{-3}$] that can be represented by a background level or the desired target (Arranz et al., 2014), and

β is an empirical coefficient that represents the increase rate of mortality per unit increase in PM (ranges 0.0006-0.001; recommended 0.0008). In this study, X_0 was set as the WHO's recommended annual guideline of $20 \mu\text{g m}^{-3}$, following similar approach followed by others (Andreão et al., 2018; Faridi et al., 2018). The health impacts of air pollutants should ideally be estimated using exposure data collected over several years (especially for the chronic effects) to prevent bias related to seasonal variations (Ostro, 2004). However, herein we employed data only for one year (2015) because the focus is on the parameter's sensitivity rather than the health impact assessment.

Next, the fraction of disease burden attributable to the risk factor (AF) is calculated using the below equation:

$$AF = \frac{RR - 1}{RR} \quad (6.2)$$

The AF fraction is then combined with mortality rate and population data to estimate the excess mortality attributable to the PM exposure:

$$\Delta M = AF \times R \times P \quad (6.3)$$

where, ΔM is the excess mortality, R is the mortality rate in deaths per 1000 people and P is the exposed population. The mortality rate for Qatar for the year 2015 was obtained from the annual births and deaths report released by Qatar's Planning and Statistics Authority (PSA), that is one death per thousand population for all age groups. The population data for Doha (per county) were obtained from the Ministry of Public Health (MoPH), and re-gridded as presented in Figure 6.3.

Typically, the EBD method is applied over a whole country or region. Herein, we applied the method over each simulation grid cell in order to assess the sensitivity of the above criteria to the selected modelling approaches. To achieve this, the available population data were distributed to the modelling grids (Section 6.2.4) with the appropriate GIS function. Finally, we estimated the

ΔM by applying Eq. (6.3) to each grid cell using the baseline mortality and corresponding population for each cell. Unfortunately, there are still no specific mortality data per cell although there are ongoing activities to collect such data along with other similar information (e.g., International Classification of Diseases-ICD10). The above method was verified by comparing the ΔM value reported for Qatar by the WHO's with the sum of the ΔM values at each grid cell.

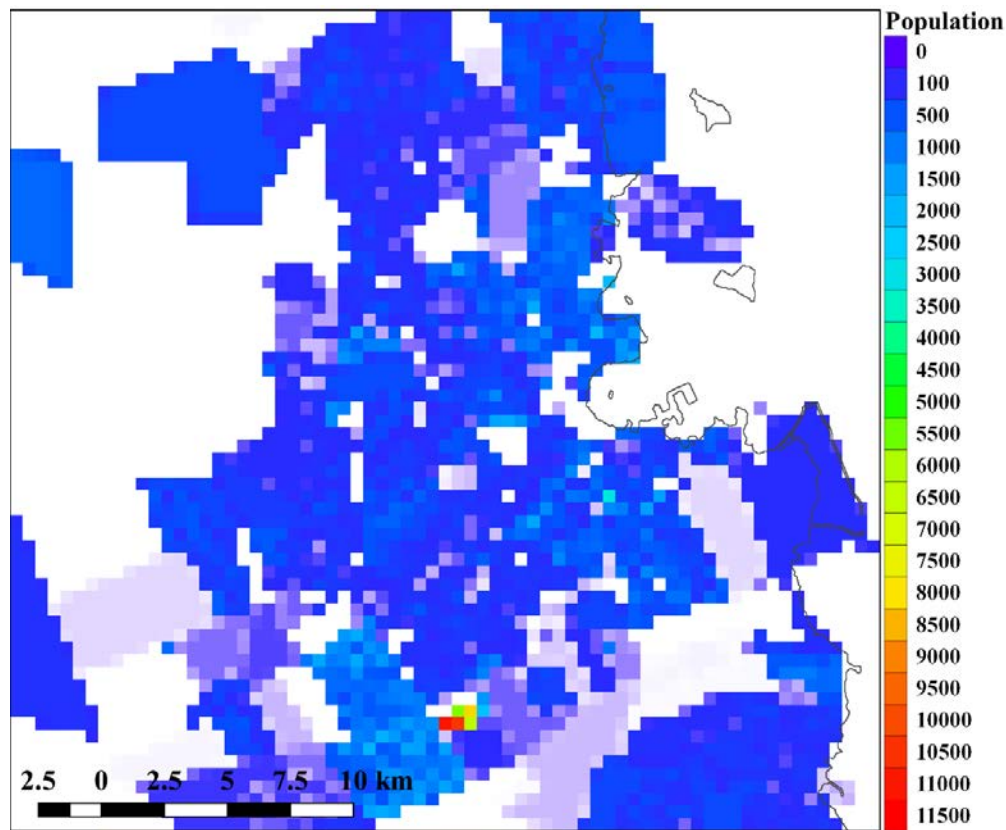


Figure 6.3 Gridded population of 2015 over Doha's metropolitan area

6.2.6 Modelling Cases

Following the above methods, four distinct modelling cases are formulated (see Table 6.2). The baseline case (Case 0) reflects the standard practice of the WHO with one health impact assessment criteria utilized for the whole population based on an annual average concentration

obtained from the local monitoring network or satellite data. The other three cases improve, in principle, the baseline method by assigning to the population location-specific average concentrations. More specifically, Case 1 reflects another standard practice with the emissions being estimated from regional models and inventories developed elsewhere, following global LULC databases (GLCC). Methods in Case 2 are the same as in the previous one but follow a LULC database developed locally (OWN). Finally, Case 3 incorporates improved – locally developed – methods in all aspects (i.e., LULC and emission models).

Table 6.2 The four modelling scenarios formulated to study the sensitivity of the health impact assessment criteria

| Case # | Description | | |
|--------|---|---|---|
| 0 | Whole population exposed to one annual average concentration based on monitoring or satellite data | | |
| 1-3 | Population exposed to location specific average concentration based on varying modelling approaches | | |
| | <i>Land Use/Cover</i> | <i>Emissions</i> | |
| | | <i>Barren Land</i> | <i>Traffic</i> |
| 1 | GLCC | | |
| 2 | OWN | All as in (Schaap et al., 2009) | Abu-Allaban et al. (2003) |
| 3 | OWN | Doha as in (Hassan et al., 2016) Rest of Qatar as in (Schaap et al., 2009) | All as in chapter 5 (Hassan et al., under review) |

6.3 Results and Discussion

6.3.1 Emission Fluxes

The mean spatial distribution of barren land emissions over Qatar are shown in Figure 6.4 and Figure 6.5 for PM₁₀ and PM_{2.5}, respectively, for Cases 1 to 3. Significant spatial differences are observed depending on the employed LULC (Case 1 vs 2) and the inclusion of the barren land inside the metropolitan area (Case 3). The PM₁₀ emission fluxes from the barren lands in the rest of Qatar which were predicted using the Schaap model show high spatial variability in all cases,

ranging from as low as $1 \times 10^{-3} \mu\text{g m}^{-2} \text{s}^{-1}$ and reaching up to $22.0 \mu\text{g m}^{-2} \text{s}^{-1}$ (1×10^{-5} to $1 \mu\text{g m}^{-2} \text{s}^{-1}$ for the $\text{PM}_{2.5}$) along the western coast of Qatar. This variability is attributed to the dependency of the Schaap model on the soil texture (i.e., particle size), and the appearance of high NW winds that promote the production of dust along the west coast. In terms of soil texture, the highest emissions are emanated from the Calcisols type of soils which are identified as medium texture (mass mean diameter of $D_{p,i}=520 \mu\text{m}$ according to Chatenet et al. (1996)), and the lowest are emitted by Sand Dunes which are coarse soils ($D_{p,i}=690 \mu\text{m}$). The estimated levels are somehow comparable to the results presented by Fountoukis et al. (2016) , who simulated the dust over the Arabian peninsula using the WRF-Chem model to compare two different dust schemes, but are lower compared to the ones estimated by Kontos et al. (2018), who uses the NEMO model that employs different set of surface parameters than the Schaap model.

For the greater metropolitan area of Doha, the predicted PM_{10} emission fluxes using our own model (Case 3) ranged from 0.05 to $42.0 \mu\text{g m}^{-2} \text{s}^{-1}$ (1×10^{-3} to $6.0 \mu\text{g m}^{-2} \text{s}^{-1}$ for the $\text{PM}_{2.5}$) which is considerably higher than the emissions predicted using just the Schaap model (Cases 1 and 2) by at least one order of magnitude; i.e., between 0.03 to $2.0 \mu\text{g m}^{-2} \text{s}^{-1}$ for Case 1 (7×10^{-4} to $0.05 \mu\text{g m}^{-2} \text{s}^{-1}$ for the $\text{PM}_{2.5}$) and 0.03 to $3.2 \mu\text{g m}^{-2} \text{s}^{-1}$ for Case 2 (5×10^{-4} to $0.09 \mu\text{g m}^{-2} \text{s}^{-1}$ for the $\text{PM}_{2.5}$). These predicted values for Case 3 are also considerably higher than the ones reported by Fountoukis et al. (2016) but of the same order as the ones presented in (Kontos et al., 2018).

The mean spatial distribution of PM_{10} and $\text{PM}_{2.5}$ emissions from exhaust (VEX) and non-exhaust (VfPM) road traffic are illustrated in Figure 6.6 and Figure 6.7, respectively. Similar to the barren land emissions, our approach (Case 3) predicted significantly higher VEX and VfPM emissions compared to the literature (Cases 1 and 2). As shown in Figure 6.6, our model (Case 3) predicted PM_{10} VEX emissions ranging from 2.2 to $30.7 \mu\text{g m}^{-2} \text{s}^{-1}$ (0.8 to $10.7 \mu\text{g m}^{-2} \text{s}^{-1}$ for the

PM_{2.5}) compared to 0.2 to 3.1 $\mu\text{g m}^{-2} \text{s}^{-1}$ (0.2 to 2.8 $\mu\text{g m}^{-2} \text{s}^{-1}$ for the PM_{2.5}) by the literature model. The VfPM emissions using our model ranged from 3.8 to 53.4 $\mu\text{g m}^{-2} \text{s}^{-1}$ for PM₁₀ (1.8 to 25.3 $\mu\text{g m}^{-2} \text{s}^{-1}$ for the PM_{2.5}) compared to 0.2 to 2.8 $\mu\text{g m}^{-2} \text{s}^{-1}$ (0.1 to 1.1 $\mu\text{g m}^{-2} \text{s}^{-1}$ for the PM_{2.5}) by the literature model. A higher variability between VEX and VfPM is observed for PM₁₀ and PM_{2.5} by our approach compared to literature model. The total annual emissions from all sources are reported in Table 6.3.

Noteworthy, the ratios of the emitted PM_{2.5}/PM₁₀, using our proposed approaches, show matching patterns with the ratios of measured airborne PM during the field campaign, reported in earlier works (Argyropoulos et al., 2019; Saraga et al., 2017). For the barren lands, the ratio is less than 0.13, indicating that the majority of wind-blown dust is in the coarse mode. It also matches the reported value during a severe dust event (Argyropoulos et al., 2019). For the traffic PM, the ratio is ~ 0.4 for VEX and 0.5 for VfPM.. In addition, the latter ratio for the emitted VfPM matches the measured ones, for the airborne PM, which were in the range of 0.2-0.7 for normal days (with no dust events) (Argyropoulos et al., 2019) and 0.62±0.18 for the whole period (Saraga et al., 2017); similar ranges (0.5-0.6) have been reported in other studies for similar regions and climate (Coskuner et al., 2018; Krasnov et al., 2014).

Table 6.3 Total Annual PM emission from barren lands, VEX, and VfPM road traffic

| Modelling Case | Annual PM Emissions (Tonnes) | | | | | |
|----------------|------------------------------|--------|--------|------------------|--------|--------|
| | PM _{2.5} | | | PM ₁₀ | | |
| | Barren | VEX | VfPM | Barren | VEX | VfPM |
| Case 1 | 6,338 | 428 | 173 | 199,993 | 480 | 410 |
| Case 2 | 9,365 | 428 | 173 | 282,773 | 480 | 410 |
| Case 3 | 36,611 | 10,510 | 24,751 | 477,181 | 30,030 | 52,311 |

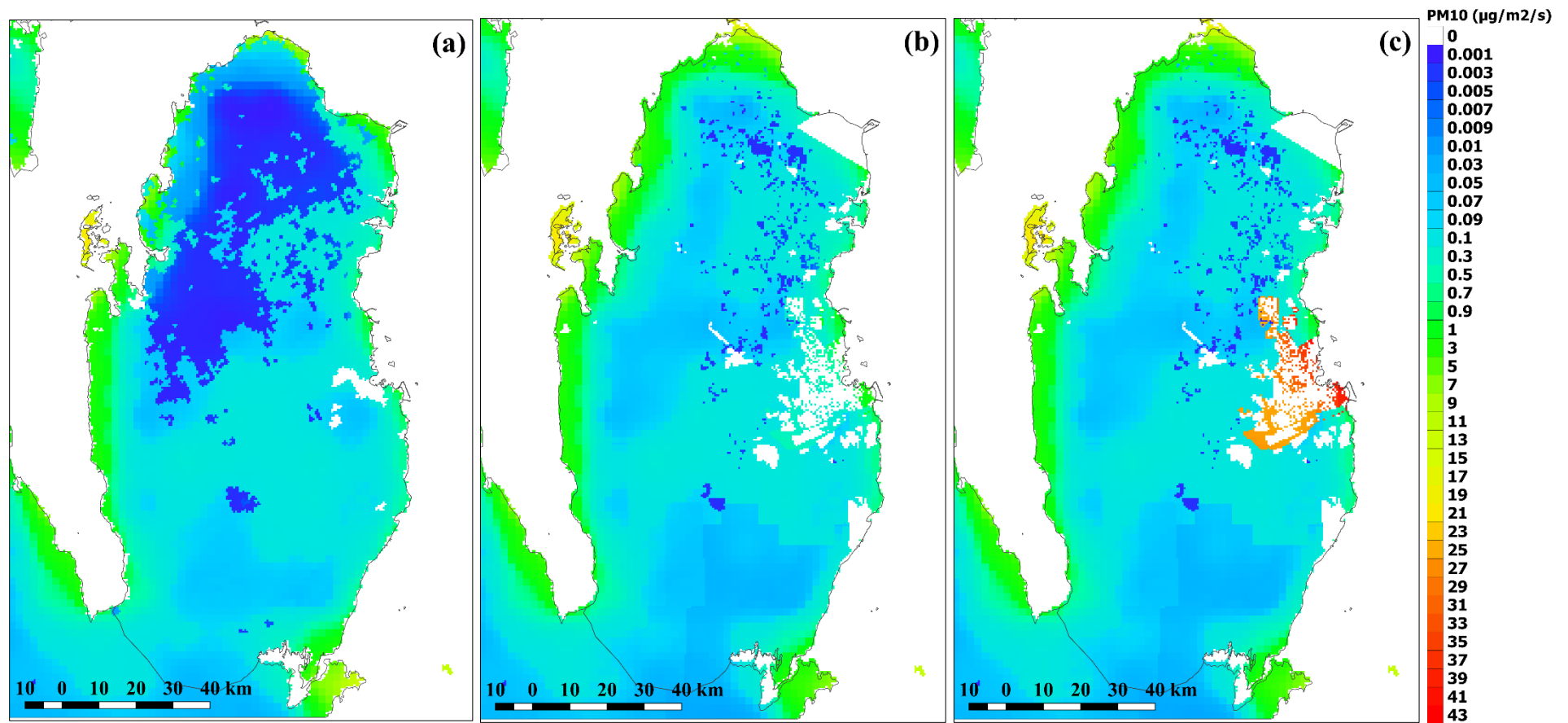


Figure 6.4 Mean emission fluxes of windblown PM₁₀ ($\mu\text{g m}^{-2} \text{s}^{-1}$) over Qatar for the modelling period (January-December, 2015) – (a) Case 1, (b) Case 2, (c) Case 3 – as shown in Table 6.2.

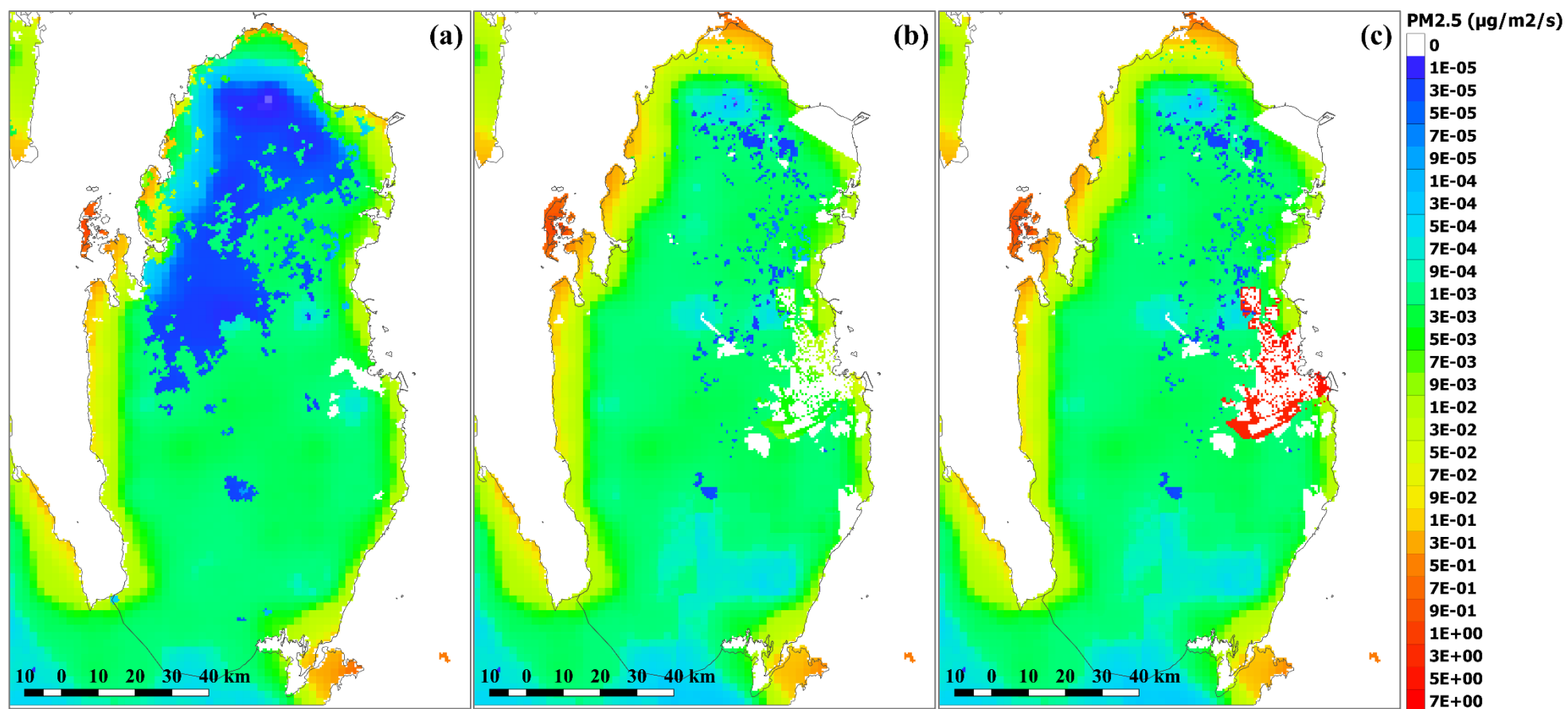


Figure 6.5 Mean emission fluxes of windblown PM_{2.5} ($\mu\text{g m}^{-2} \text{s}^{-1}$) over Qatar for the modelling period (January-December, 2015). (a) Case 1, (b) Case 2, (c) Case 3

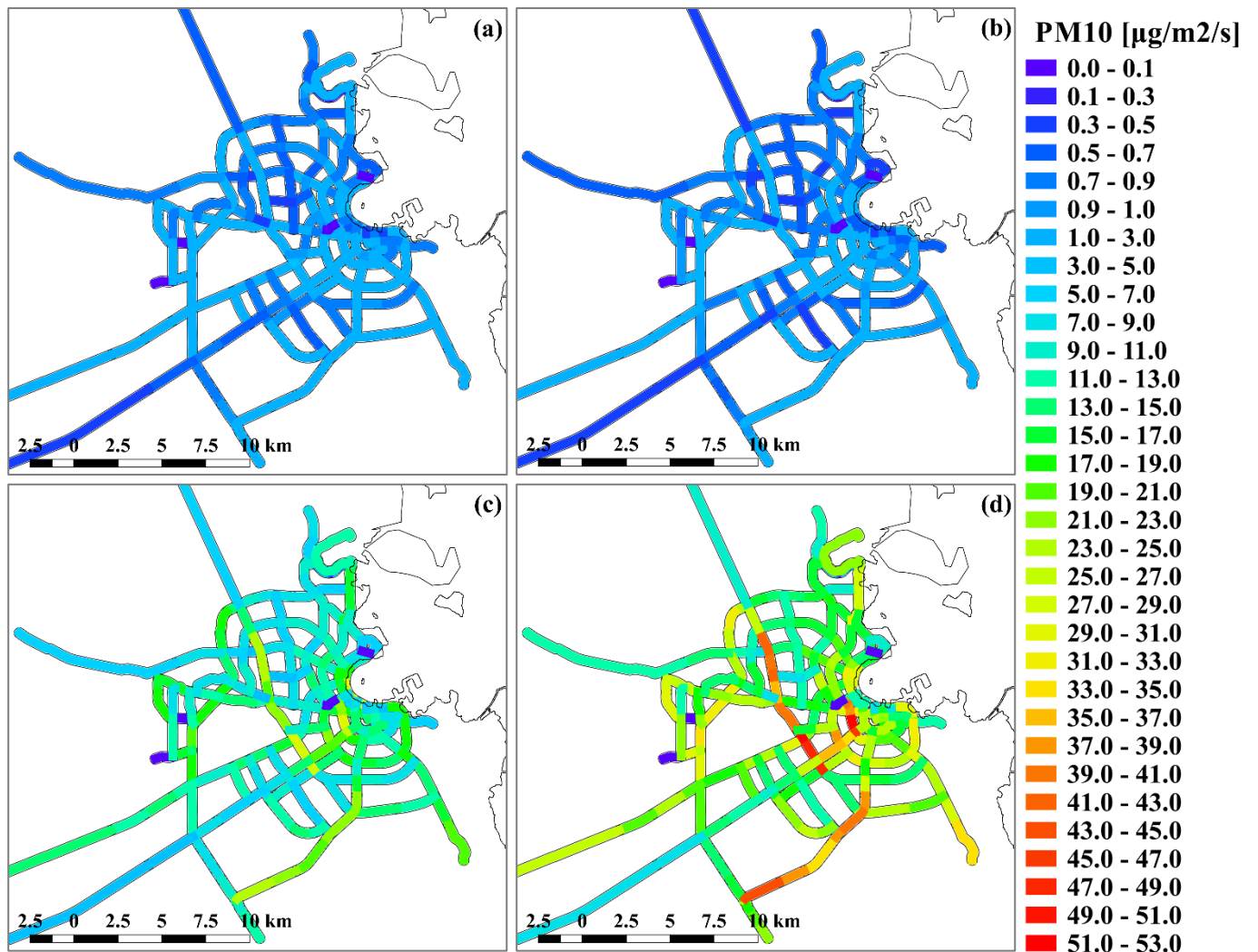


Figure 6.6 Mean emission fluxes of PM₁₀ ($\mu\text{g m}^{-2} \text{s}^{-1}$) emitted from VEX (left) and VfPM (right) along Doha's major road network. (a and b) show Cases 1 and 2, (c and d) show Case 3.

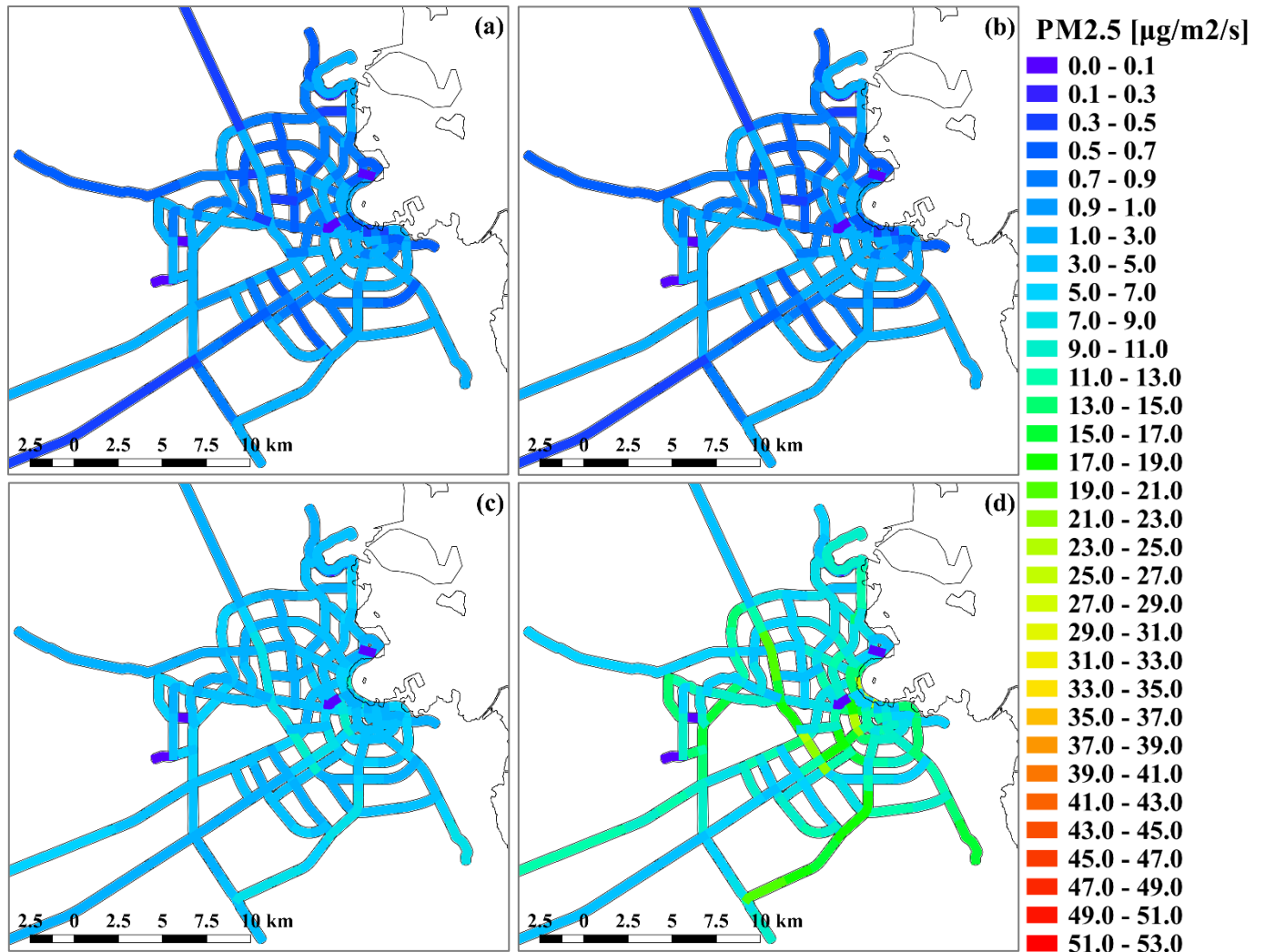


Figure 6.7 Mean emission fluxes of PM_{2.5} ($\mu\text{g m}^{-2} \text{s}^{-1}$) emitted from exhaust (left) and non-exhaust (right) traffic along Doha's major road network. (a) and (b) Case 1&2, (c) and (d) Case 3

6.3.2 Modelled Concentrations

The contribution of fPM on the PM airborne levels is examined over the metropolitan area of Doha rather than the whole of Qatar since most of the population resides there. In brief, the concentration levels follow similar trends and differences driven by the trends in the emission fluxes for both the barren land and traffic-induced PM. Figure 6.8 depicts the estimated annual mean concentrations of PM₁₀ (PM_{2.5} in Figure 6.9) attributed to barren land emissions which are on average 10-15 times higher using our approach (Case 3) compared to the Schaap model (Cases

1 and 2). More specifically this contribution is around 20.0 to 146.0 $\mu\text{g m}^{-3}$ for PM_{10} (3.5-20.0 $\mu\text{g m}^{-3}$ for $\text{PM}_{2.5}$) and exceeds the WHO recommended value of 20 $\mu\text{g m}^{-3}$ for total airborne PM_{10} (10 $\mu\text{g m}^{-3}$ for $\text{PM}_{2.5}$) almost all over the metropolitan area. A more detailed examination of the contour plots reveals the effect of the different LULC maps and of the inclusion of in-the-city barren land on the calculations. Both Cases 1 and 2 (Figure 6.8a and b) show the highest levels at the South-West part of the city, but Case 1 is missing the North-Western high levels due to the significantly different LULC in the North-Western side of the peninsula (see Figure 6.1). On the other hand, Case 3 (Figure 6.8c) shows more and stronger hot-spots owed to the inclusion of the barren land spaces, comprised active and non-active construction sites, within the metropolitan area.

The impact of road traffic (VEX and VfPM) on PM_{10} levels is illustrated in Figure 6.10 (Figure 6.11 for $\text{PM}_{2.5}$). As expected the highest impacts are observed along the three main pathways: (i) the Doha expressway, the longest and busiest highway that connects the southern and northern urban areas as well as the metropolitan area with the northern rural and industrial areas of Qatar, followed by (ii) the Muntazah road which leads to the small industrial area southwest of the city and features both intense traffic and large numbers of heavy-duty vehicles, and finally (iii) the Furousiya road, another major road with high traffic and close to busy shopping centres. In Cases 1 and 2, which are based on the literature EFs, the concentration levels are quite similar with small differences attributed to the different LULC data and consequently the different local wind velocities. On the other hand, the predicted levels in Case 3, based on our approach, are around ten times higher VEX (compared to the other cases) contributing 35% of $\text{PM}_{2.5}$ (90% in Case 2), and 19 times higher VfPM contributing 48% of $\text{PM}_{2.5}$ (42% in Case 2).

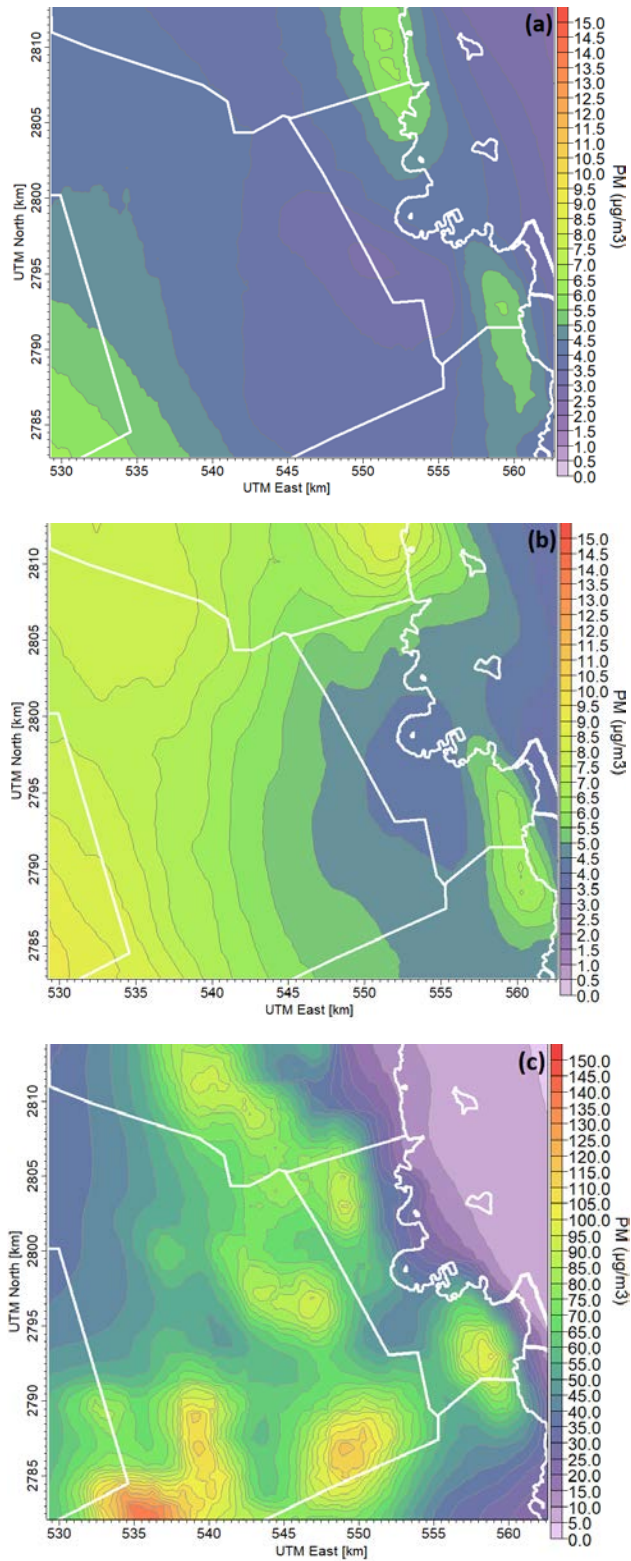


Figure 6.8 The annual mean PM₁₀ ($\mu\text{g m}^{-3}$) contributions from barren lands predicted by CALPUFF model over Doha. (a) Case 1, (b) Case 2, (c) Case 3.

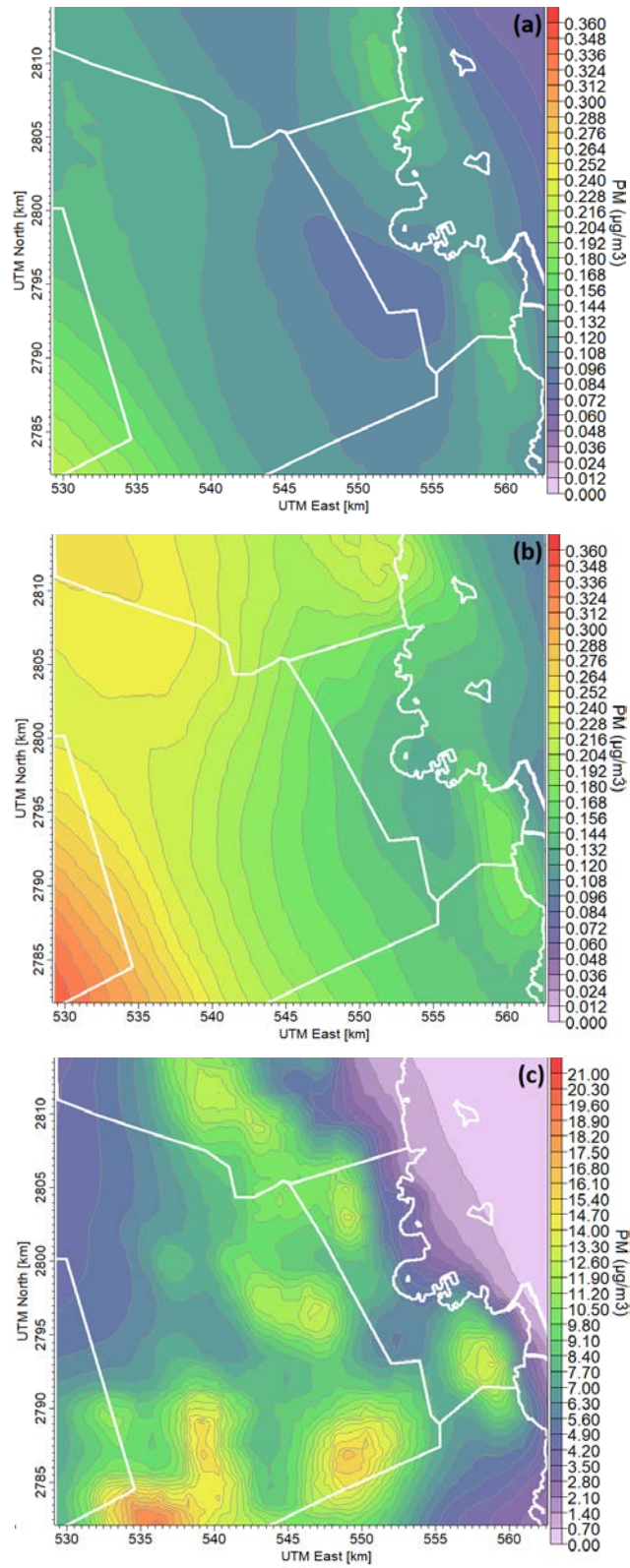


Figure 6.9 The annual mean PM_{2.5} ($\mu\text{g m}^{-3}$) contributions from barren lands predicted by CALPUFF model over Doha. (a) Case 1, (b) Case 2, (c) Case 3.

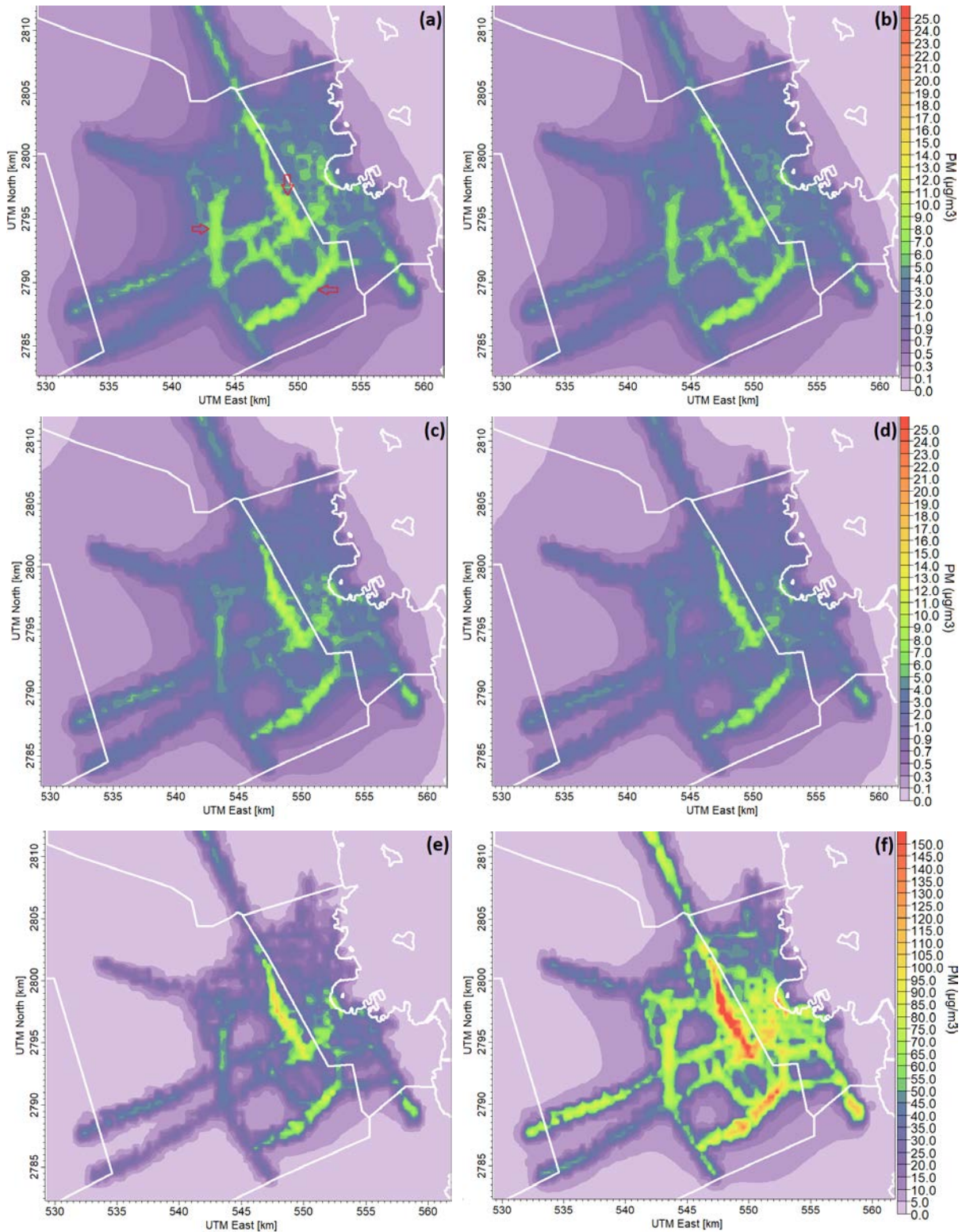


Figure 6.10 The annual mean PM₁₀ ($\mu\text{g m}^{-3}$) contributions from VEX (left) and VfPM (right) predicted by CALPUFF model over Doha. Case 1 (a & b), Case 2 (c & d), Case 3 (e & f). The highest emissions roads are marked in (a).

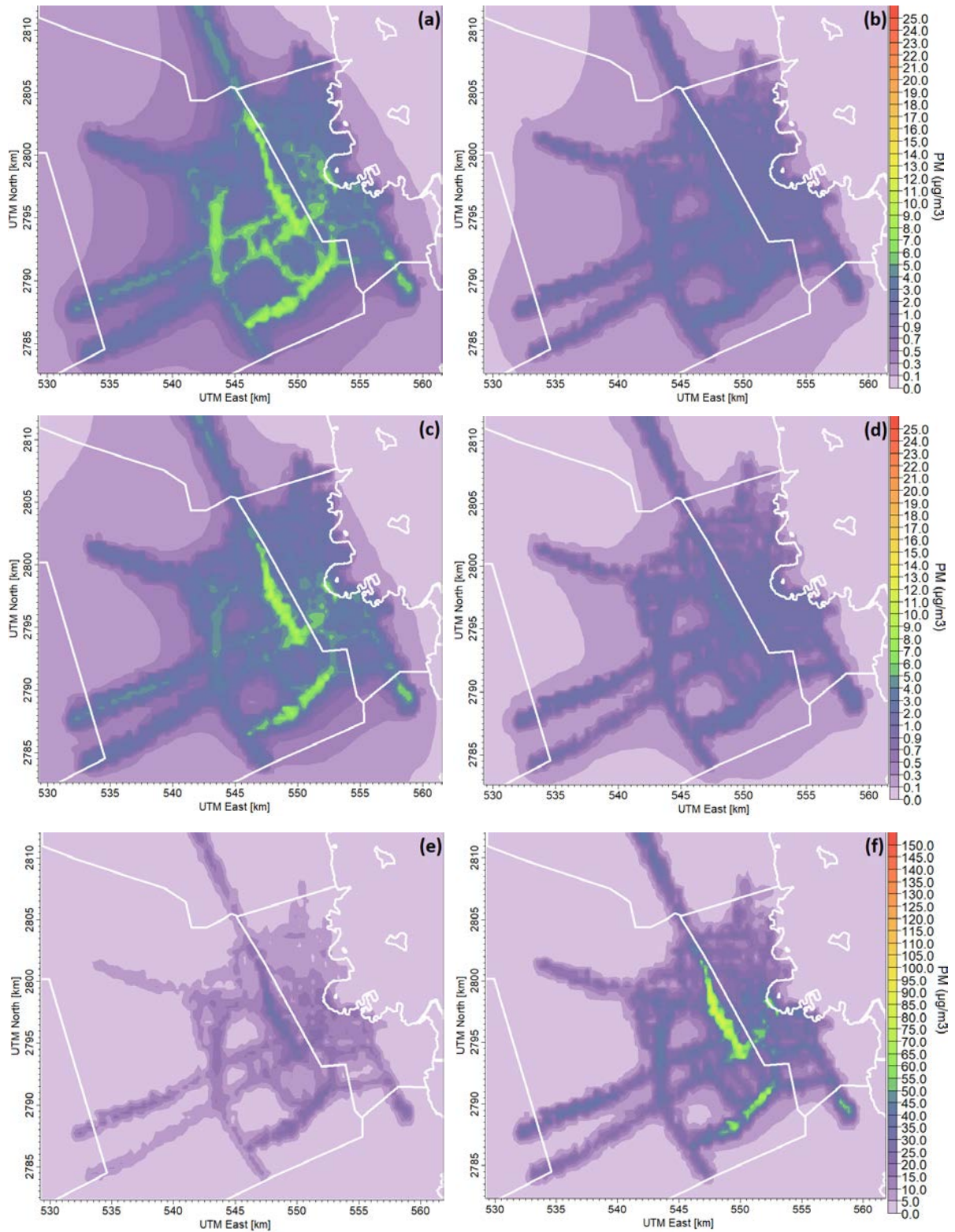


Figure 6.11 The annual mean PM_{2.5} ($\mu\text{g m}^{-3}$) contributions from VEX (left) and VfPM (right) predicted by CALPUFF model over Doha. Case 1 (a & b), Case 2 (c & d), Case 3 (e & f).

6.3.3 Contribution to Airborne PM levels

In this section, we compare the modelling results with the measurements collected during the previous field campaign (refer to Section 5.2.2). It has to be noted that the total calculated fPM, herein, accounts only for the contributions from the barren lands and VfPM, and neglects VEX and transboundary/regional sources that have similar profiles (i.e., composition). On the other hand, the measured PM accounts for all source contributions (i.e., including sea salt, secondary aerosols and crustal material). The time series plots of 24h average concentrations (Figure 6.12) show that Cases 1 and 2 severely underestimate the fPM contributions for both PM₁₀ and PM_{2.5}. Case 3 still underestimates both fractions but with a lower deviation compared to Cases 1 and 2. This is expected since the measured concentrations account for more sources than fPM. For Case 3, the average modelled fPM concentrations for PM₁₀ and PM_{2.5} for the duration of the campaign (April to June 2015) were around 109.0 $\mu\text{g m}^{-3}$ and 30.1 $\mu\text{g m}^{-3}$, while the monthly averages were 107 $\mu\text{g m}^{-3}$ and 26.7 for April, 105.8 $\mu\text{g m}^{-3}$ and 28.4 for May, and 115.3 $\mu\text{g m}^{-3}$ and 37.1 for June. As shown in Figure 6.12, there are exceptions where 24h average PM₁₀ from Case 3 seem to match (or exceed) measurements (~ 8% of days). We couldn't detect a pattern for this behaviour, although it points to an underestimation by the measuring unit during these occurrences.

The pollution roses in Figure 6.13 show that the highest measured PM₁₀ concentrations were associated with NW winds and notable contributions from N-NE, while the highest modelled concentrations (Case 3) are shown to the NE. On the other hand, the highest modelled PM_{2.5} concentrations were associated with NE winds, while the highest measured concentrations were associated with the Eastern winds corresponding to the adjacent trafficked road and the coastline (~ 1.1 km to the east). The standard deviation plots of modelled concentrations (seen in Figure 6.13) show a stronger deviation of PM_{2.5} to the East which indicates a missing contribution,

probably due to the removal of VEX or the missing sea salt component. The standard deviation plot indicates that (in addition to VEX) there is a high deviation between modelled and measured concentrations due to NW winds $\geq 4 \text{ m s}^{-1}$ (24 h average) suggesting an underestimation by our model during stronger wind conditions.

In an effort to further interpret the results of our modelling cases, we performed a comparison between the CALMET meteorological data used in this study, and the meteorological data estimated by the WRF model from April to June 2015 at two locations in Doha; the field campaign site and the Doha International Airport. The WRF has been repeatedly used in modelling natural dust from the broader study area and performed satisfactorily with different modelling schemes (Beegum et al., 2016; Fountoukis et al., 2016; Kontos et al., 2018; Menut et al., 2013). On the other hand, the MM5 data processed by CALMET have reportedly underestimated wind speeds in similar simulations (Athanasopoulou et al., 2010). The wind rose plots (Figure C1 in Appendix C) demonstrate that the wind speeds processed by WRF show higher values from the prevailing wind directions (N-NW) compared to CALMET. This is also clear in the scatter plots (Figure C2; Appendix C) where CALMET model predicted lower wind speeds (maximum 24h average of 5.4 m/s), while WRF 24h average wind speeds reached up to 9.2 m/s. This could explain the underestimation of the emissions outside the metropolitan area in this work compared to previous studies.

6.3.4 Sensitivity of the Health Impact Assessment

Finally, the health impact of fPM was estimated by calculating the burden of mortality (combining modelled annual concentrations and population data per grid cell) relative to the WHO's recommended guideline levels. For Cases 1 and 2, the PM concentration levels were below the WHO's guidelines, which implies that none of the in-Qatar fPM sources, i.e., VfPM and barren

land, could be considered responsible for noteworthy health impact. On the contrary, using the modelling approaches in Case 3, the annual all-cause mortalities attributable to short-term exposure to fugitive PM₁₀ are estimated to be around 57 deaths (2.5% of the annual deaths in Qatar in 2015), compared to 21 deaths assuming the annual concentrations reported by WHO (Case 0). Our estimated annual mortality percentage was close to the annual percentage reported for Valladolid (2.2%), a city in Spain with a population of 300,000, for short-term exposure to PM₁₀ during the period from 1999 to 2008 (Arranz et al., 2014). Most of the recent epidemiological studies, however, focus on the effects of fine particles (PM_{2.5}) as they pose higher risk to human health. For example, Faridi et al. (2018) found that PM_{2.5} contributed to 7.6-11.3% of the annual mortality in Tehran between 2006 and 2015. Balakrishnan et al. (2019) recently estimated the burden of disease associated with air pollution (including PM and household pollution) in every state of India. They reported that 12.5% of the total deaths in India in 2017 were attributed to air pollution (6.8% from PM_{2.5} exposure alone).

Furthermore, Figure 6.14 presents the spatial distribution of the ratio of the estimated excess deaths per 0.25 km² using Case 3 modelling approach to Case 0 (i.e., the WHO's approach assumes that the whole population is exposed to the same concentration levels). As shown in Figure 6.14, the estimated ratios ranged between -0.6 and 11.0 for PM₁₀ (mean=1.8; median=1.7), and seem to be positive almost all over the metropolitan area. In other words, fPM could be considered responsible for up to 11.0 times higher short-term mortalities using Case 3 approach. Even when we use the average concentration for Case 3, the excess mortality was estimated to be 44 deaths, and Case 3/Case 0 mortality ratio ~ 2.2. Moreover, data from the World Bank suggests that the average death rate in Qatar in 2015 is 78.04 years. Following these data, the number of Years of Life Lost (YLL) is estimated as 4,448 years in 2015 for mortalities attributable to fugitive PM₁₀

from Case 3 (compared to 1,639 from WHO's reported concentration). YLL is a complementary estimate that considers the years of life lost due to premature mortality. These results support that findings of Anenberg et al (2010) and others (Samoli et al., 2008) who found that burden of disease estimates are sensitive to concentration thresholds and concentration–mortality relationships.

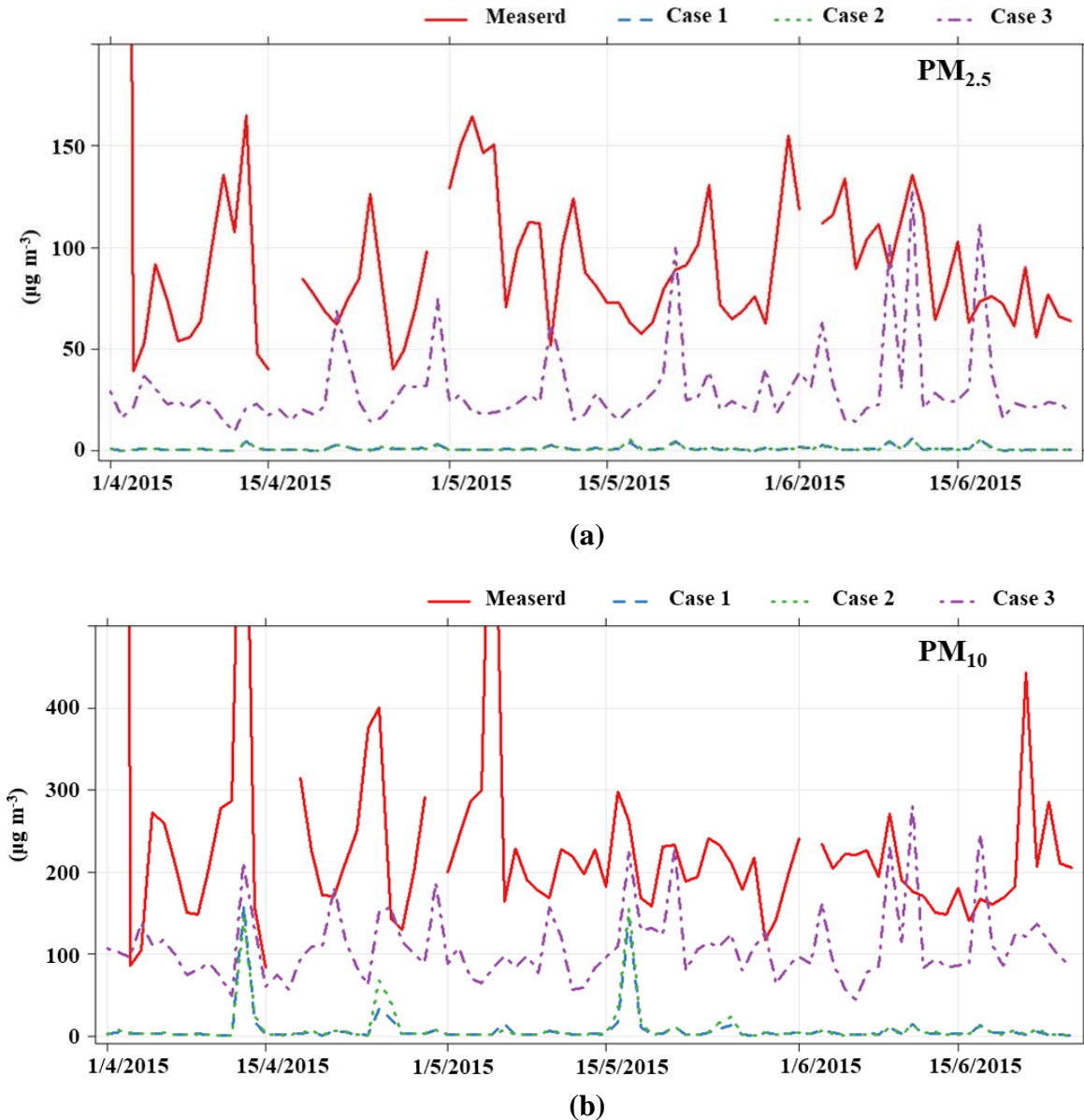


Figure 6.12 Time series comparing modelled and measured concentrations of (a) $PM_{2.5}$ and (b) PM_{10} .

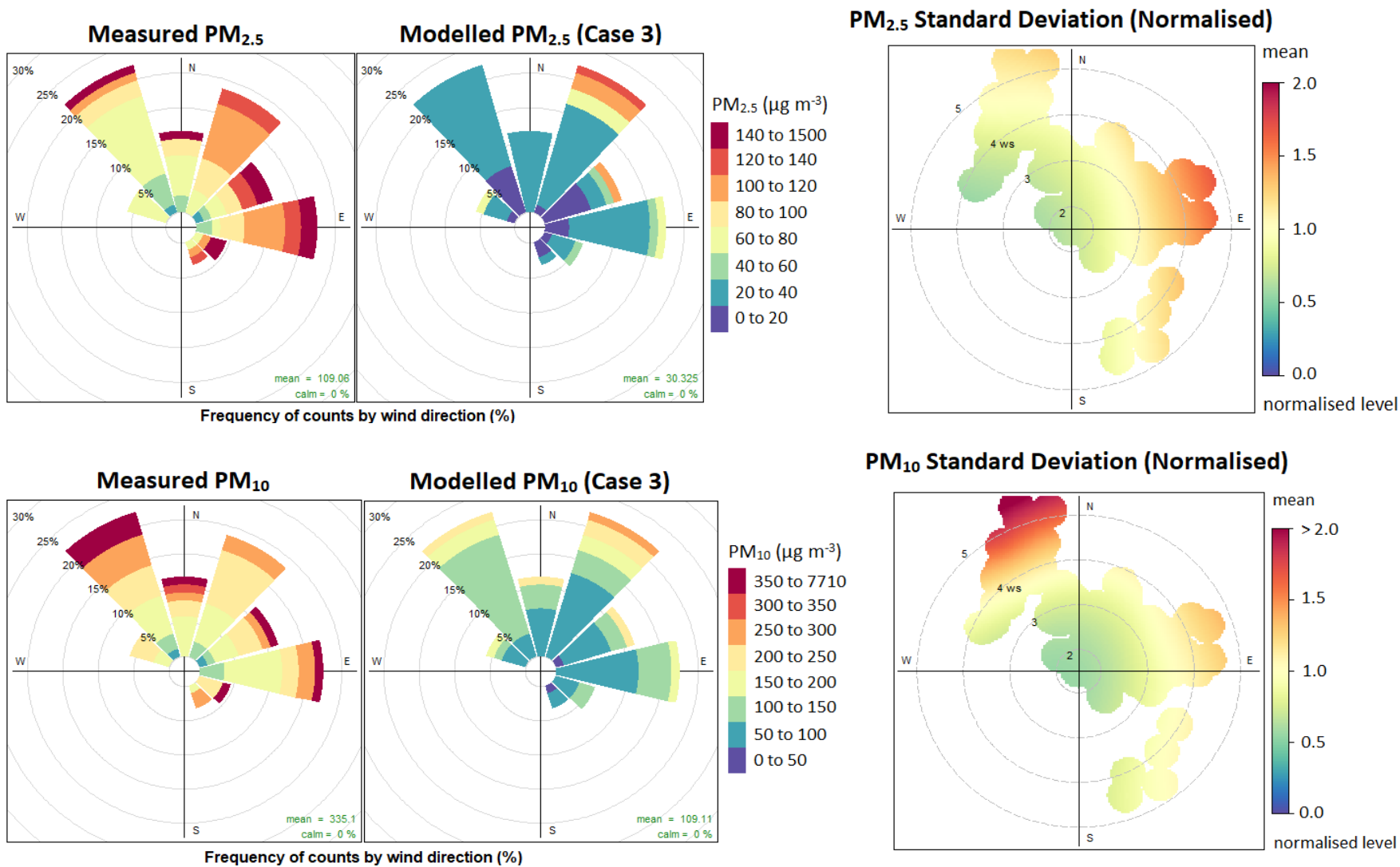


Figure 6.13 Pollution roses showing the measured and modelled (Case 3) concentration by wind direction. The right side shows polar plots of the standard deviation of modelled concentrations (normalised by the mean)

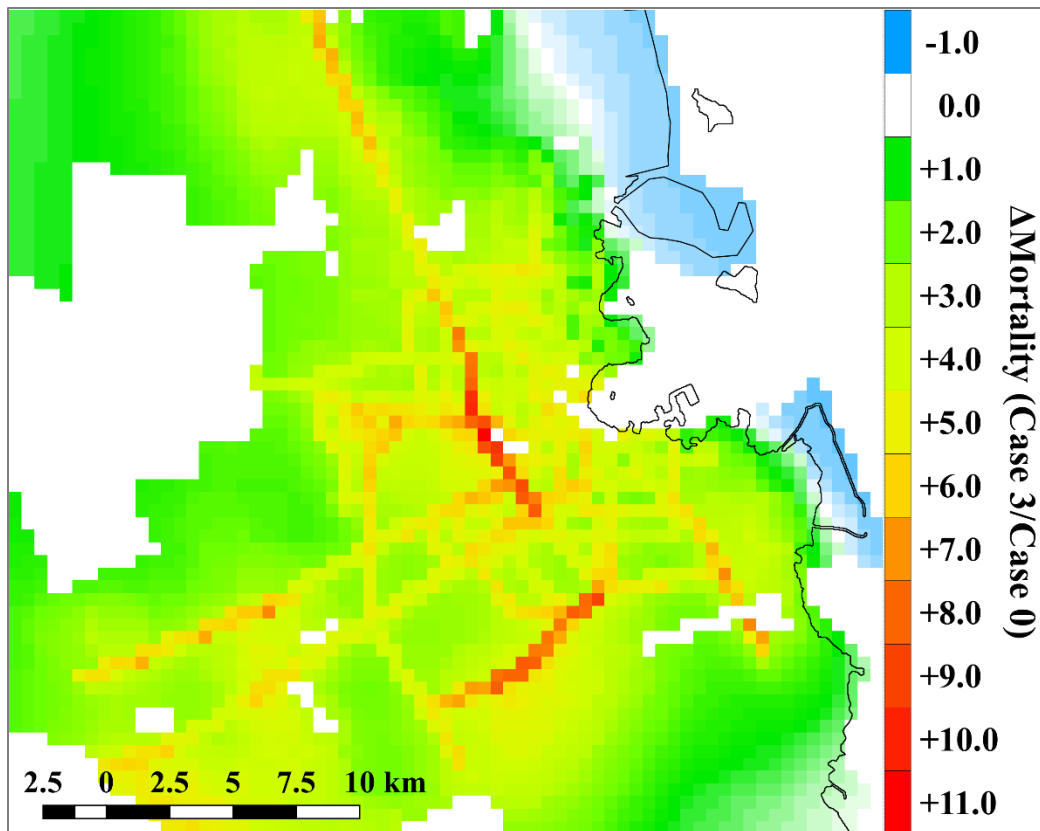


Figure 6.14 The ratio of Case 3 to Case 0 (WHO) expected mortalities (per 0.25 km²) attributable to outdoor fugitive PM₁₀.

6.4 Chapter Summary and Conclusions

We modelled fPM emissions from two common sources in areas with dry arid climates (barren/exposed lands and road traffic). We used a combination of our own developed emission models, literature models, and alternating LULC data for the state of Qatar. Four modelling cases were presented: (i) a baseline case (Case 0) with concentration levels obtained from WHO database, (ii) Case 1 using a basic LULC map and literature models, (iii) Case 2 using an improved LULC map and literature models, and (iv) Case 3 using an improved LULC and our own developed emission models.

For the greater metropolitan area of Doha, the estimated PM₁₀ emission fluxes from barren lands using our own model (Case 3) ranged from 0.05 to 42.0 $\mu\text{g m}^{-2} \text{s}^{-1}$ (1×10^{-3} to 6.0 $\mu\text{g m}^{-2} \text{s}^{-1}$

for the $PM_{2.5}$), which is considerably higher than the emissions predicted using just the literature model (emissions were between 0.03 to 2.0 $\mu\text{g m}^{-2} \text{s}^{-1}$ for Case 1 (7×10^{-4} to 0.05 $\mu\text{g m}^{-2} \text{s}^{-1}$ for the $PM_{2.5}$) and 0.03 to 3.2 $\mu\text{g m}^{-2} \text{s}^{-1}$ for Case 2 (5×10^{-4} to 0.09 $\mu\text{g m}^{-2} \text{s}^{-1}$ for the $PM_{2.5}$)). The estimated emission fluxes outside the city were predicted using the literature model and showed high spatial variability ranging between $1 \times 10^{-3} \mu\text{g m}^{-2} \text{s}^{-1}$ and 22 $\mu\text{g m}^{-2} \text{s}^{-1}$ for PM_{10} (1×10^{-5} to 1 $\mu\text{g m}^{-2} \text{s}^{-1}$ for the $PM_{2.5}$). For traffic sources, our model showed significantly higher emissions and higher variability between exhaust (VEX) and non-exhaust (VfPM) for both PM_{10} and $PM_{2.5}$ compared to literature model. The annual fPM concentrations predicted by Cases 1 and 2 were insignificant, while Case 3 exceeded the WHO guidelines for all sources. The locations of the highest impact were consistent with the improved LULC and were identified near the large exposed areas within the city and along the busiest roads of Doha. Overall, the literature models substantially underestimated the measured concentrations, while the results of our models showed a lower deviation. The calculated EBD, following the WHO methodology, was about 11.0 times higher short-term excess mortalities compared to the measurements reported by WHO.

These above results confirm that compliance with WHO guidelines will significantly reduce mortality cases that could be attributed to local fPM sources, and gives an indication of the number of mortalities that can be avoided if the target concentrations are achieved. Moreover, further studies are needed to assess an individual's exposure to fPM, with the account of other fPM sources such as sea salt.

Chapter 7 **Summary, Conclusions and Future Work**

The aim of this chapter is to present a summary and the conclusions drawn from the preceding chapters. It also highlights research gaps and presents recommendations for future research.

7.1 Summary

Air quality is progressively recognized as a critical issue for human health and is a subject for which comprehensive global emission data are missing. One of the main environmental challenges in arid and semi-arid regions is the PM emissions emitted by fugitive sources (i.e., fPM). The meteorology and low vegetation cover of arid regions make them highly susceptible to wind-blown particles. In addition, the massive expansion in road networks has led to increased non-exhaust PM emissions from anthropogenic sources. In order to support regulatory purposes and design control strategies, emissions have to be consistently monitored and estimated. One way to quantify emissions is using the empirical factors developed by well-established environmental institutions. However, information on fPM emissions in the currently available inventories is limited, compared to a large number of different sources that can produce fPM emissions and only available for the developed regions. Furthermore, using analogues factors may results in inaccuracies when applied to certain surfaces of interest.

This research aimed to develop EFs and models, better representative of the areas with arid climates, by utilizing field measurements, source characterization techniques, dispersion modelling and statistical tools. Chapter 1 provided the background, motivation, objectives and approach of this thesis. Chapter 2 provides a comprehensive literature review of the existing knowledge on the topic and relevant literature studies. The chapter also highlights the significance

of fPM in areas with arid desert climates, especially from local sources, and their substantial impact on the health and the environment. Chapter 3 gives a summary of the instruments, analysis methods and models used to achieve the objectives of this research. Chapters 4-6 presents the results obtained from the field measurements and the subsequent post processing of the results. The overall conclusions of the results are described in Section 7.2 and recommendations for future research are presented in Section 7.3.

7.1.1 Flux Estimation of fPM Emissions from loose Soils (Calcsols)

The currently available emission models for windblown dust were developed for certain geographical regions and weather conditions of Europe and North America, which may lead to inaccuracies when applied to regions with desert arid climate. Two months field measurements (of PM over a size range of 0.25 to 32 μm) collected from a construction site at rest were used. The FDM was implemented to calculate PM concentrations and obtain their emission fluxes in an iterative procedure. The model results were fitted to a power function, which expresses the wind velocity dependence. The goodness of fit results shows a better performance for larger particles. The obtained power factors were in the same range of those reported in the literature for similar sources. The modelled concentrations for PM₁₀ fall within the FAC2 (factor of two) of the measured.

7.1.2 Estimation of Vehicle-Induced fPM Emissions

Vehicle-induced particulate matter (PM) emissions contributed are a significant contributor to roadside pollutants in urban environments. We investigated and proposed EFs and models for vehicle-induced exhaust (VEX) and fugitive (VfPM) particulate matter emissions representative of areas with arid climates. PNCs, PMCs and integrated samples were collected for a period of three months for both PM₁₀ and PM_{2.5} next to a trafficked road in the city of Doha, Qatar. Using

PMF modelling on the elemental data of the samples, six distinct PM sources were identified: traffic exhaust, dust resuspension, fresh and aged sea salt, secondary aerosols, and fuel oil/shipping. Dispersion modelling and regression analysis were combined to derive EFs (linear analysis) and models (non-linear analysis) for the total traffic fleet (heavy and light duty). The non-linear regression provided an emission model for VfPM, dependent on meteorological parameters, having similar performance to the linear model, but increased the p-value indicating a weak hypothesis.

7.1.3 The Impact of fPM on Air Quality and Health in Dry-Arid Areas

We modelled fPM emissions from the two studied sources in areas with dry arid climates (barren/exposed lands and road traffic). We used a combination of our own developed emission models, literature models, and alternating land use/land cover (LULC) data for the state of Qatar. Four modelling cases were presented: (i) a baseline case (Case 0) with concentration levels obtained from WHO database, (ii) Case 1 using a basic LULC map and literature models, (iii) Case 2 using an improved LULC map and literature models, and (iv) Case 3 using an improved LULC and our own developed emission models. Finally, the health impact of fPM was estimated by combining modelled annual concentrations and population data per grid cell (of the modelling domain) relative to the WHO's recommend guideline levels

7.2 Conclusions

The key conclusions obtained from the overall analysis covered in the chapters of this thesis area summarised below:

- The fPM emission fluxes calculated for in city exposed lands (construction sites) yield a power law function, which expresses the wind velocity dependence. Fitted power function was considered acceptable given that adjusted R^2 values varied from 0.13 for the smaller particles

and up to 0.69 for the larger ones. These factors are in the same range of those reported in the literature for similar sources.

- The results of PMF modelling suggested that resuspension is the main contributor of mass PM in the urban site (29.2%), followed by fresh sea salt (27.5%), exhaust traffic (14.5%), secondary aerosols (13.7%), aged sea salt (8.0%), and finally fuel oil/shipping (7.1%). This result indicates the significance of fPM.
- Linear and non-linear emission models were derived for traffic VEX and VfPM. The best fitted EF for VEX using linear regression ranged from 620 to 730 mg VKT⁻¹ (adjusted R² ~0.84), and for VfPM from 1080 to 1410 mg VKT⁻¹ (Adjusted R² ~ 0.7)
- Modelling results of fPM from barren lands and VfPM showed a significant annual contribution from barren lands (~ 90% of the total predicted fPM).
- The calculated EBD, following the WHO methodology, found that the estimated mortalities from short-term exposure to fugitive PM₁₀ reaches up to 11 times higher compared to mortalities calculated with a constant concentration reported by WHO.
- The outcome of this work is expected to contribute to the improvement of PM emission inventories by focusing on an overlooked but significant pollution source, especially in dry and arid regions, and often located very close to residential areas and sensitive population groups. Further campaigns are recommended to reduce the uncertainty and include more fPM sources (e.g., earthworks) and other types of soil.

7.3 Recommendations for Future Research

The subject of this research offers a sound basis for future work to further understand the behaviour of fPM. For example, more studies are necessary to reduce the uncertainty in estimating

the fugitive emissions from similar sources. Here are some recommendations to be considered for future research:

(1) The effect of LULC data, as shown in the findings of Chapter 6, indicates that further studies covering a diverse range of soil types in different geographical settings is needed. Surface characteristics are critical in estimating fPM emissions.

(2) For vehicle-induced PM, future field campaigns should include multiple streets with different traffic patterns, consider the road surface dust load, incorporate gaseous pollutants as tracers of VEX emissions, and further validate the effect of meteorological data.

(3) Since there is a wide range of fPM sources in arid areas, in which some of them proved to be significant (e.g. sea salt and active construction activities), future studies should aim to widen the investigation to include more sources. Further field measurements are recommended to perform in different meteorological conditions and diverse urban/rural environments to capture the collective impact of natural and anthropogenic fPM sources in arid areas. With the aid of other tools (e.g., dispersion modelling), these investigations should result in better EFs and models for the estimation of fPM emissions.

(3) Expand the work to cover multiyear analysis. This will help capture the seasonal variations of fPM and provide a better understanding of the long-term effects of fPM. Health assessments, in particular, should emphasize on individual exposures especially in sensitive groups such as children.

(4) Combine the individual EFs and models into an online emission inventory system for fPM sources. The online system should combine the emission models and apply them on a nested grid covering the study area (e.g., Middle East) with a selected spatial resolution. The model will process LULC and soil texture maps according to the user defined model grid and projections and performs a number of calculations in each grid cell (e.g., calculate the percentage coverage of each

soil type in the grid cell) to estimate the gridded temporally resolved emissions. This inventory will provide essential background information for the use in atmospheric modelling systems and the development of abatement strategies and policies on both the local (i.e., Qatar) and regional scales.

References

- Aatmeeyata, Kaul, D.S., Sharma, M., 2009. Traffic generated non-exhaust particulate emissions from concrete pavement: A mass and particle size study for two-wheelers and small cars. *Atmospheric Environment* 43, 5691-5697.
- Abbass, R.A., Kumar, P., El-Gendy, A., 2018. An overview of monitoring and reduction strategies for health and climate change related emissions in the Middle East and North Africa region. *Atmospheric Environment* 175, 33-43.
- Abdeen, Z., Qasrawi, R., Heo, J., Wu, B., Shpund, J., Vanger, A., Sharf, G., Moise, T., Brenner, S., Nassar, K., Saleh, R., Al-Mahasneh, Q.M., Sarnat, J.A., Schauer, J.J., 2014. Spatial and temporal variation in fine particulate matter mass and chemical composition: the Middle East Consortium for Aerosol Research Study. *The Scientific World Journal* 2014, 16.
- Abdul-Wahab, S.A., 2006. Impact of fugitive dust emissions from cement plants on nearby communities. *Ecological Modelling* 195, 338-348.
- Abu-Allaban, M., Gillies, J.A., Gertler, A.W., Clayton, R., Proffitt, D., 2003. Tailpipe, resuspended road dust, and brake-wear emission factors from on-road vehicles. *Atmospheric Environment* 37, 5283-5293.
- Abu Allaban, M., Lowenthal, D.H., Gertler, A.W., Labib, M., 2007. Sources of PM10 and PM2.5 in Cairo's ambient air. *Environmental Monitoring and Assessment* 133, 417-425.
- Al-Dabbous, A.N., Kumar, P., 2014. Number and size distribution of airborne nanoparticles during summertime in Kuwait: First observations from the middle east. *Environmental Science and Technology* 48, 13634-13643.
- Al-Dabbous, A.N., Kumar, P., 2015. Source apportionment of airborne nanoparticles in a Middle Eastern city using positive matrix factorization. *Environmental Science: Processes & Impacts* 17, 802-812.
- Al Senafi, F., Anis, A., 2015. Shamals and climate variability in the Northern Arabian/Persian Gulf from 1973 to 2012. *International Journal of Climatology* 35, 4509-4528.
- Alfaro, S.C., Gomes, L., 2001. Modeling mineral aerosol production by wind erosion: Emission intensities and aerosol size distributions in source areas. *Journal of Geophysical Research Atmospheres* 106, 18075-18084.
- Alghamdi, M.A., 2016. Characteristics and risk assessment of heavy metals in airborne PM10 from residential area of northern Jeddah city, Saudi Arabia. *Polish Journal of Environmental Studies* 25, 939-949.

- Alolayan, M.A., Brown, K.W., Evans, J.S., Bouhamra, W.S., Koutrakis, P., 2013. Source apportionment of fine particles in Kuwait City. *Science of The Total Environment* 448, 14-25.
- Amato, F., Alastuey, A., Karanasiou, A., Lucarelli, F., Nava, S., Calzolari, G., Severi, M., Becagli, S., Gianelle, V.L., Colombi, C., Alves, C., Custódio, D., Nunes, T., Cerqueira, M., Pio, C., Eleftheriadis, K., Diapouli, E., Reche, C., Minguillón, M.C., Manousakas, M.I., Maggos, T., Vratolis, S., Harrison, R.M., Querol, X., 2016a. AIRUSE-LIFE+: a harmonized PM speciation and source apportionment in five southern European cities. *Atmos. Chem. Phys.* 16, 3289-3309.
- Amato, F., Cassee, F.R., Denier van der Gon, H.A.C., Gehrig, R., Gustafsson, M., Hafner, W., Harrison, R.M., Jozwicka, M., Kelly, F.J., Moreno, T., Prevot, A.S.H., Schaap, M., Sunyer, J., Querol, X., 2014. Urban air quality: The challenge of traffic non-exhaust emissions. *Journal of Hazardous Materials* 275, 31-36.
- Amato, F., Favez, O., Pandolfi, M., Alastuey, A., Querol, X., Moukhtar, S., Bruge, B., Verlhac, S., Orza, J.A.G., Bonnaire, N., Le Priol, T., Petit, J.F., Sciare, J., 2016b. Traffic induced particle resuspension in Paris: Emission factors and source contributions. *Atmospheric Environment* 129, 114-124.
- Amato, F., Karanasiou, A., Moreno, T., Alastuey, A., Orza, J.A.G., Lumbreras, J., Borge, R., Boldo, E., Linares, C., Querol, X., 2012. Emission factors from road dust resuspension in a Mediterranean freeway. *Atmospheric Environment* 61, 580-587.
- Amato, F., Pandolfi, M., Moreno, T., Furger, M., Pey, J., Alastuey, A., Bukowiecki, N., Prevot, A.S.H., Baltensperger, U., Querol, X., 2011. Sources and variability of inhalable road dust particles in three European cities. *Atmospheric Environment* 45, 6777-6787.
- Amato, F., Pandolfi, M., Viana, M., Querol, X., Alastuey, A., Moreno, T., 2009. Spatial and chemical patterns of PM10 in road dust deposited in urban environment. *Atmospheric Environment* 43, 1650-1659.
- Amato, F., Querol, X., Johansson, C., Nagl, C., Alastuey, A., 2010. A review on the effectiveness of street sweeping, washing and dust suppressants as urban PM control methods. *Science of the Total Environment* 408, 3070-3084.
- Anderson, J.O., Thundiyil, J.G., Stolbach, A., 2012. Clearing the air: A review of the effects of Particulate Matter air pollution on human health. *Journal of Medical Toxicology* 8, 166-175.
- Andreão, W.L., Albuquerque, T.T.A., Kumar, P., 2018. Excess deaths associated with fine particulate matter in Brazilian cities. *Atmospheric Environment* 194, 71-81.

- Anenberg, S.C., Horowitz, L.W., Tong, D.Q., West, J.J., 2010. An Estimate of the Global Burden of Anthropogenic Ozone and Fine Particulate Matter on Premature Human Mortality Using Atmospheric Modeling. *Environmental Health Perspectives* 118, 1189-1195.
- AQEG, 2007. Air quality and climate change: A UK perspective. Report by the Air Quality Expert Group (AQEG). Department for Environment, Food and Rural Affairs (Defra). <http://www.defra.gov.uk/environment/airquality/aqeg>.
- Argyropoulos, C.D., Hassan, H., Kumar, P., Kakosimos, K.E., 2019. Measurements and modelling of particulate matter building ingress during a severe dust storm event. *Building and Environment*, 106441.
- Arranz, M.C., Moreno, M.F.M., Medina, A.A., Capitán, M.A., Vaquer, F.C., Gómez, A.A., 2014. Health impact assessment of air pollution in Valladolid, Spain. *BMJ Open* 4, e005999.
- Athanasopoulou, E., Protonotariou, A., Papangelis, G., Tombrou, M., Mihalopoulos, N., Gerasopoulos, E., 2016. Long-range transport of Saharan dust and chemical transformations over the Eastern Mediterranean. *Atmospheric Environment* 140, 592-604.
- Athanasopoulou, E., Tombrou, M., Russell, A.G., Karanasiou, A., Eleftheriadis, K., Dandou, A., 2010. Implementation of road and soil dust emission parameterizations in the aerosol model CAMx: Applications over the greater Athens urban area affected by natural sources. *Journal of Geophysical Research: Atmospheres* 115.
- Azarmi, F., Kumar, P., Mulheron, M., Colaux, J.L., Jeynes, C., Adhami, S., Watts, J.F., 2015. Physicochemical characteristics and occupational exposure to coarse, fine and ultrafine particles during building refurbishment activities. *Journal of Nanoparticle Research* 17, 343.
- Baayoun, A., Itani, W., El Helou, J., Halabi, L., Medlej, S., El Malki, M., Moukhadder, A., Aboujaoude, L.K., Kabakian, V., Mounajed, H., Mokalled, T., Shihadeh, A., Lakkis, I., Saliba, N.A., 2019. Emission inventory of key sources of air pollution in Lebanon. *Atmospheric Environment* 215, 116871.
- Bagnold, R.A., 1941. *The physics of blown sand and desert dunes*. London: Methuen and Co., Ltd. Dova publications, Inc., Mineola, New York.
- Bagnold, R.A., 1973. *The physics of blown sand and desert dunes*. by R.A. Bagnold. London : Chapman & Hall, 1973.
- Balakrishnan, K., Dey, S., Gupta, T., Dhaliwal, R.S., Brauer, M., Cohen, A.J., Stanaway, J.D., Beig, G., Joshi, T.K., Aggarwal, A.N., Sabde, Y., Sadhu, H., Frostad, J., Causey, K., Godwin, W., Shukla, D.K., Kumar, G.A., Varghese, C.M., Muraleedharan, P., Agrawal, A., Anjana, R.M., Bhansali, A., Bhardwaj, D., Burkart, K., Cercy, K., Chakma, J.K., Chowdhury, S., Christopher, D.J., Dutta, E., Furtado, M., Ghosh, S., Ghoshal, A.G., Glenn, S.D., Guleria, R., Gupta, R., Jeemon, P., Kant, R., Kant, S., Kaur, T., Koul, P.A., Krish,

- V., Krishna, B., Larson, S.L., Madhipatla, K., Mahesh, P.A., Mohan, V., Mukhopadhyay, S., Mutreja, P., Naik, N., Nair, S., Nguyen, G., Odell, C.M., Pandian, J.D., Prabhakaran, D., Prabhakaran, P., Roy, A., Salvi, S., Sambandam, S., Saraf, D., Sharma, M., Shrivastava, A., Singh, V., Tandon, N., Thomas, N.J., Torre, A., Xavier, D., Yadav, G., Singh, S., Shekhar, C., Vos, T., Dandona, R., Reddy, K.S., Lim, S.S., Murray, C.J.L., Venkatesh, S., Dandona, L., 2019. The impact of air pollution on deaths, disease burden, and life expectancy across the states of India: the Global Burden of Disease Study 2017. *The Lancet Planetary Health* 3, e26-e39.
- Bang, K.M., Mazurek, J.M., Wood, J.M., White, G.E., Hendricks, S.A., Weston, A., 2015. Silicosis mortality trends and new exposures to respirable crystalline silica — United States, 2001–2010, Morbidity and Mortality Weekly Report (MMWR). U.S. Department of Health and Human Services Centers for Disease Control and Prevention, Centers for Disease Control and Prevention
- Barlow, J., 2014. Progress in observing and modelling the urban boundary layer. *Urban Climate* 10, 216-240.
- Beegum, S.N., Gherboudj, I., Chaouch, N., Couvidat, F., Menut, L., Ghedira, H., 2016. Simulating aerosols over Arabian Peninsula with CHIMERE: Sensitivity to soil, surface parameters and anthropogenic emission inventories. *Atmospheric Environment* 128, 185-197.
- Belis, C.A., Karagulian, F., Amato, F., Almeida, M., Artaxo, P., Beddows, D.C.S., Bernardoni, V., Bove, M.C., Carbone, S., Cesari, D., Contini, D., Cuccia, E., Diapouli, E., Eleftheriadis, K., Favez, O., El Haddad, I., Harrison, R.M., Hellebust, S., Hovorka, J., Jang, E., Jorquera, H., Kammermeier, T., Karl, M., Lucarelli, F., Mooibroek, D., Nava, S., Nøjgaard, J.K., Paatero, P., Pandolfi, M., Perrone, M.G., Petit, J.E., Pietrodangelo, A., Pokorná, P., Prati, P., Prevot, A.S.H., Quass, U., Querol, X., Saraga, D., Sciare, J., Sfetsos, A., Valli, G., Vecchi, R., Vestenius, M., Yubero, E., Hopke, P.K., 2015. A new methodology to assess the performance and uncertainty of source apportionment models II: The results of two European intercomparison exercises. *Atmospheric Environment* 123, 240-250.
- Bener, A., Dogan, M., Ehlayel, M.S., Shanks, N.J., Sabbah, A., 2009. The impact of air pollution on hospital admission for respiratory and cardiovascular diseases in an oil and gas-rich country. *Eur Ann Allergy Clin Immunol* 41, 80–84.
- Berger, J., Denby, B., 2011. A generalised model for traffic induced road dust emissions. Model description and evaluation. *Atmospheric Environment* 45, 3692-3703.
- Brauer, M., 2002. Air pollution from traffic and the development of respiratory infections and asthmatic and allergic symptoms in children. *American Journal of Respiratory & Critical Care Medicine* 166, 1092-1098.
- Brown, K.W., Bouhamra, W., Lamoureux, D.P., Evans, J.S., Koutrakis, P., 2008. Characterization of particulate matter for three sites in Kuwait. *Journal of the Air and Waste Management Association*.

- Brunekreef, B., Forsberg, B., 2005. Epidemiological evidence of effects of coarse airborne particles on health. *European Respiratory Journal* 26, 309-318.
- Bu-Olayan, A.H., Thomas, B.V., 2012. Dispersion model on PM_{2.5} fugitive dust and trace metals levels in Kuwait governorates. *Environmental Monitoring and Assessment* 184, 1731-1737.
- Bukowiecki, N., Lienemann, P., Hill, M., Furger, M., Richard, A., Amato, F., Prévôt, A.S.H., Baltensperger, U., Buchmann, B., Gehrig, R., 2010. PM₁₀ emission factors for non-exhaust particles generated by road traffic in an urban street canyon and along a freeway in Switzerland. *Atmospheric Environment* 44, 2330-2340.
- Burnett, R.T., Arden Pope Iii, C., Ezzati, M., Olives, C., Lim, S.S., Mehta, S., Shin, H.H., Singh, G., Hubbell, B., Brauer, M., Ross Anderson, H., Smith, K.R., Balmes, J.R., Bruce, N.G., Kan, H., Laden, F., Prüss-Ustün, A., Turner, M.C., Gapstur, S.M., Diver, W.R., Cohen, A., 2014. An integrated risk function for estimating the global burden of disease attributable to ambient fine particulate matter exposure. *Environmental Health Perspectives* 122, 397-403.
- Chaaban, F., 2008. Air quality in: Tolba, M.K., Saab, N.W. (Eds.), *Arab Environment: Future Challenges*
- Chatenet, B., Marticorena, B., Gomes, L., Bergametti, G., 1996. Assessing the microped size distributions of desert soils erodible by wind. *Sedimentology* 43, 901-911.
- Chatzimichailidis, A.E., Kakosimos, K.E., Assael, M.J., 2014. Use of dispersion modelling for the assessment of primary particulate matter sources on the air quality of Greater Thessaloniki Area. *Fresenius Environmental Bulletin* 23.
- Chowdhuri, A., Gupta, C.K., 2017. Assessment of particulate matter (PM) concentrations at a typical construction site in Bangalore. *International Research Journal of Environment Science* 6, 14-18.
- Cohen, A.J., Anderson, H.R., Ostro, B., Pandey, K.D., Krzyzanowski, M., Künzli, N., Gutschmidt, K., Pope, A., Romieu, I., Samet, J.M., Smith, K., 2005. The global burden of disease due to outdoor air pollution. *Journal of Toxicology and Environmental Health - Part A* 68, 1301-1307.
- Cohen, A.J., Brauer, M., Burnett, R., Anderson, H.R., Frostad, J., Estep, K., Balakrishnan, K., Brunekreef, B., Dandona, L., Dandona, R., Feigin, V., Freedman, G., Hubbell, B., Jobling, A., Kan, H., Knibbs, L., Liu, Y., Martin, R., Morawska, L., Pope, C.A., Shin, H., Straif, K., Shaddick, G., Thomas, M., van Dingenen, R., van Donkelaar, A., Vos, T., Murray, C.J.L., Forouzanfar, M.H., 2017. Estimates and 25-year trends of the global burden of disease attributable to ambient air pollution: an analysis of data from the Global Burden of Diseases Study 2015. *The Lancet* 389, 1907-1918.

- Coskuner, G., Jassim, M.S., Munir, S., 2018. Characterizing temporal variability of PM_{2.5}/PM₁₀ ratio and its relationship with meteorological parameters in Bahrain. *Environmental Forensics* 19, 315-326.
- Cowherd Jr., C., Kinsey, J.S., 1986. Identification, assessment, and control of fugitive particulate emissions, in: USEPA (Ed.). United States Environmental Protection Agency.
- Crippa, M., Guizzardi, D., Muntean, M., Schaaf, E., Dentener, F., van Aardenne, J.A., Monni, S., Doering, U., Olivier, J.G.J., Pagliari, V., Janssens-Maenhout, G., 2018. Gridded emissions of air pollutants for the period 1970–2012 within EDGAR v4.3.2. *Earth System Science* 120, 1987-2013.
- Dahl, A., Gharibi, A., Swietlicki, E., Gudmundsson, A., Bohgard, M., Ljungman, A., Blomqvist, G., Gustafsson, M., 2006. Traffic-generated emissions of ultrafine particles from pavement–tire interface. *Atmospheric Environment* 40, 1314-1323.
- Denby, B.R., Sundvor, I., 2012. NORTRIP model development and documentation: NON-exhaust Road TRaffic Induced Particle emission modelling. Norwegian Institute for Air Research (NILU), Kjeller, Norway.
- Denby, B.R., Sundvor, I., Johansson, C., Pirjola, L., Ketzel, M., Norman, M., Kupiainen, K., Gustafsson, M., Blomqvist, G., Kauhaniemi, M., Omstedt, G., 2013. A coupled road dust and surface moisture model to predict non-exhaust road traffic induced particle emissions (NORTRIP). Part 2: Surface moisture and salt impact modelling. *Atmospheric Environment* 81, 485-503.
- Diapouli, E., Manousakas, M.I., Vratolis, S., Vasilatou, V., Pateraki, S., Bairachtari, K.A., Querol, X., Amato, F., Alastuey, A., xE, Karanasiou, A.A., Lucarelli, F., Nava, S., Calzolari, G., Gianelle, V.L., Colombi, C., Alves, C., xE, lia, Cust, xF, dio, D., Pio, C., Spyrou, C., Kallos, G.B., Eleftheriadis, K., 2017. AIRUSE-LIFE +: estimation of natural source contributions to urban ambient air PM_{sub.10} and PM_{sub.2.5} concentrations in southern Europe - implications to compliance with limit values. *Atmospheric Chemistry and Physics* 17, 3673.
- Draxler, R.R., 2001. Estimating PM₁₀ air concentrations from dust storms in Iraq, Kuwait and Saudi Arabia. *Atmospheric environment* (1994) 35, 4315-4330.
- Driussi, C., Jansz, J., 2006. Technological options for waste minimisation in the mining industry. *Journal of Cleaner Production* 14, 682-688.
- Du, K., Yuen, W., Wang, W., Rood, M.J., Varma, R.M., Hashmonay, R.A., Kim, B.J., Kemme, M.R., 2011. Optical remote sensing to quantify fugitive particulate mass emissions from stationary short-term and mobile continuous sources: Part II. Field applications. *Environmental Science & Technology* 45, 666-672.

- EEA, 2016. EMEP/EEA air pollutant emission inventory guidebook. European Environment Agency
- Engelbrecht, J.P., Jayanty, R.K.M., 2013. Assessing sources of airborne mineral dust and other aerosols, in Iraq. *Aeolian Research* 9, 153-160.
- Engelbrecht, J.P., McDonald, E.V., Gillies, J.A., Jayanty, R.K.M., Casuccio, G., Gertler, A.W., 2009a. Characterizing mineral dusts and other aerosols from the Middle East—Part 1: Ambient Sampling. *Inhalation Toxicology* 21, 297-326.
- Engelbrecht, J.P., McDonald, E.V., Gillies, J.A., Jayanty, R.K.M.J., Casuccio, G., Gertler, A.W., 2009b. Characterizing mineral dusts and other aerosols from the Middle East-Part 2: grab samples and re-suspensions. *Inhalation Toxicology* 21, 327-336.
- Ettouney, R.S., Abdul-Wahab, S., Elkilani, A.S., 2009. Emissions inventory, ISCST, and neural network modelling of air pollution in Kuwait. *International Journal of Environmental Studies* 66, 181-194.
- Etyemezian, V., Ahonen, S., Nikolic, D., Gillies, J., Kuhns, H., Gillette, D., Veranth, J., 2004. Deposition and Removal of Fugitive Dust in the Arid Southwestern United States: Measurements and Model Results. *Journal of the Air & Waste Management Association* (1995) 54, 1099-1111.
- Etyemezian, V., Kuhns, H., Gillies, J., Chow, J., Hendrickson, K., McGown, M., Pitchford, M., 2003a. Vehicle-based road dust emission measurement (III):: effect of speed, traffic volume, location, and season on PM10 road dust emissions in the Treasure Valley, ID. *Atmospheric Environment* 37, 4583-4593.
- Etyemezian, V., Kuhns, H., Gillies, J., Green, M., Pitchford, M., Watson, J., 2003b. Vehicle-based road dust emission measurement: I—methods and calibration. *Atmospheric Environment* 37, 4559-4571.
- Eyring, V., Köhler, H.W., van Aardenne, J., Lauer, A., 2005. Emissions from international shipping: 1. The last 50 years. *Journal of Geophysical Research: Atmospheres* 110.
- Fan, Z.T., Meng, Q., Weisel, C., Laumbach, R., Ohman-Strickland, P., Shalat, S., Hernandez, M.Z., Black, K., 2009. Acute exposure to elevated PM2.5 generated by traffic and cardiopulmonary health effects in healthy older adults. *Journal of Exposure Science and Environmental Epidemiology* 19, 525-533.
- FAO, 2014. World reference base for soil resources 2014, international soil classification system for naming soils and creating legends for soil maps, World Soil Resources Reports. Food and Agriculture Organization of the United Nations, p. 191.

- Farahat, A., 2016. Air pollution in the Arabian Peninsula (Saudi Arabia, the United Arab Emirates, Kuwait, Qatar, Bahrain, and Oman): causes, effects, and aerosol categorization. *Arabian Journal of Geosciences* 9, 1-17.
- Faridi, S., Shamsipour, M., Krzyzanowski, M., Künzli, N., Amini, H., Azimi, F., Malkawi, M., Momeniha, F., Gholampour, A., Hassanvand, M.S., Naddafi, K., 2018. Long-term trends and health impact of PM_{2.5} and O₃ in Tehran, Iran, 2006–2015. *Environment International* 114, 37-49.
- Fountoukis, C., Ackermann, L., Ayoub, M., Gladich, I., Hoehn, R., Skillern, A., 2016. Impact of atmospheric dust emission schemes on dust production and concentration over the Arabian Peninsula. *Modeling Earth Systems and Environment* 2.
- García-Rico, L., Meza-Figueroa, D., Jay Gandolfi, A., Del Río-Salas, R., Romero, F.M., Meza-Montenegro, M.M., 2016. Dust–metal sources in an urbanized arid zone: implications for health-risk assessments. *Archives of Environmental Contamination and Toxicology* 70, 522-533.
- Gehrig, R., Hill, M., Buchmann, B., Imhof, D., Weingartner, E., Baltensperger, U., 2004. Separate determination of PM₁₀ emission factors of road traffic for tailpipe emissions and emissions from abrasion and resuspension processes. *International Journal of Environment and Pollution* 22, 312-325.
- Gillette, D.A., Adams, J., Muhs, D., Kihl, R., 1982. Threshold friction velocities and rupture moduli for crusted desert soils for the input of soil particles into the air. *Journal of Geophysical Research: Oceans* 87, 9003-9015.
- Gillette, D.A., Fryrear, D.W., Gill, T.E., Ley, T., Cahill, T.A., Gearhart, E.A., 1997. Relation of vertical flux of particles smaller than 10 μm to total aeolian horizontal mass flux at Owens Lake. *Journal of Geophysical Research Atmospheres* 102, 26,009-26,015.
- Gkatzoflias, D., Kouridis, C., Ntziachristos, L., Samaras, Z., 2006. COPERT 4: Computer programme to calculate emissions from road transport. European Environment Agency.
- Goel, A., Kumar, P., 2015. Characterisation of nanoparticle emissions and exposure at traffic intersections through fast–response mobile and sequential measurements. *Atmospheric Environment* 107, 374-390.
- Gopaldaswami, N., Kakosimos, K., Vèchot, L., Olewski, T., Mannan, M.S., 2015. Analysis of meteorological parameters for dense gas dispersion using mesoscale models. *Journal of Loss Prevention in the Process Industries* 35, 145-156.
- Goudie, A.S., 2014. Desert dust and human health disorders. *Environment International* 63, 101-113.

- Grantz, D.A., Garner, J.H.B., Johnson, D.W., 2003. Ecological effects of particulate matter. *Environment International* 29, 213-239.
- Grigoratos, T., Gustafsson, M., Eriksson, O., Martini, G., 2018. Experimental investigation of tread wear and particle emission from tyres with different treadwear marking. *Atmospheric Environment* 182, 200-212.
- Grigoratos, T., Martini, G., 2015. Brake wear particle emissions: a review. *Environmental Science and Pollution Research* 22, 2491-2504.
- Grimm, 2009. Manual, Enviro Check 365. Grimm Aerosol Technik GmbH & Co. KG, Germany.
- Gualtieri, M., Mantecca, P., Cetta, F., Camatini, M., 2008. Organic compounds in tire particle induce reactive oxygen species and heat-shock proteins in the human alveolar cell line A549. *Environment International* 34, 437-442.
- Hamdan, N.M., Alawadhi, H., Jisrawi, N., 2015. Elemental and chemical analysis of PM10 and PM2.5 indoor and outdoor pollutants in the UAE. *International Journal of Environmental Sciences and Development* 6.
- Hamidi, M., Kavianpour, M.R., Shao, Y., 2013. Synoptic analysis of dust storms in the Middle East. *Asia-Pacific Journal of Atmospheric Sciences* 49, 279-286.
- Hamidi, M., Kavianpour, M.R., Shao, Y., 2014. Numerical simulation of dust events in the Middle East. *Aeolian Research* 13, 59-70.
- Hamza, W., Enan, M.R., Al-Hassini, H., Stuut, J.-B., de-Ber, D., 2011. Dust storms over the Arabian Gulf: a possible indicator of climate changes consequences. *Aquatic Ecosystem Health & Management* 14, 260-268.
- Harrison, R.M., Bousiotis, D., Mohorjy, A.M., Alkhalaf, A.K., Shamy, M., Alghamdi, M., Khoder, M., Costa, M., 2017. Health risk associated with airborne particulate matter and its components in Jeddah, Saudi Arabia. *Science of The Total Environment* 590-591, 531-539.
- Harrison, R.M., Jones, A.M., Gietl, J., Yin, J., Green, D.C., 2012. Estimation of the contributions of brake dust, tire wear, and resuspension to nonexhaust traffic particles derived from atmospheric measurements. *Environmental Science and Technology* 46, 6523-6529.
- Hassan, H., 2015. Developing emission factors of fugitive Particulate Matter emissions for construction sites in the Middle East. Texas A & M University, Master's thesis. Available electronically from <http://hdl.handle.net/1969.1/155039>.
- Hassan, H., Abraham, M., Kumar, P., Kakosimos, K.E., 2017a. Sources and emissions of fugitive Particulate Matter in: Kumar, P. (Ed.), *Airborne Particles: Origin, Emissions and Health Impacts* Nova Science Publishers, Inc., pp. 21-35.

- Hassan, H., Kumar, P., Kakosimos, K.E., 2017b. Emissions modelling and impact assessment of fugitive Particulate Matter in arid and semi-arid region, 18th International Conference on Harmonisation within Atmospheric Dispersion Modelling for Regulatory Purposes, Bologna, Italy.
- Hassan, H., Saraga, D., Kumar, P., Kakosimos, K.E., under review. Vehicle-induced fugitive Particulate Matter emissions in a city of arid desert climate. *Atmospheric Environment*.
- Hassan, H.A., Kumar, P., Kakosimos, K.E., 2016. Flux estimation of fugitive particulate matter emissions from loose Calcisols at construction sites. *Atmospheric Environment* 141, 96-105.
- HBEFA, 2014. The Handbook Emission Factors for Road Transport (HBEFA v.3.2).
- Heal, M.R., Kumar, P., Harrison, R.M., 2012. Particles, air quality, policy and health. *Chemical Society Reviews* 41, 6606-6630.
- Heo, J., Wu, B., Abdeen, Z., Qasrawi, R., Sarnat, J.A., Sharf, G., Shpund, K., Schauer, J.J., 2017. Source apportionments of ambient fine particulate matter in Israeli, Jordanian, and Palestinian cities. *Environmental Pollution* 225, 1-11.
- Huang, J., Minnis, P., Lin, B., Wang, T., Yi, Y., Hu, Y., Sun-Mack, S., Ayers, K., 2006. Possible influences of Asian dust aerosols on cloud properties and radiative forcing observed from MODIS and CERES. *Geophysical Research Letters* 33.
- Hussein, T., Johansson, C., Karlsson, H., Hansson, H.C., 2008. Factors affecting non-tailpipe aerosol particle emissions from paved roads: On-road measurements in Stockholm, Sweden. *Atmospheric Environment* 42, 688-702.
- Hussein, T., Juwhari, H., Al Kuisi, M., Alkattan, H., Lahlouh, B., Al-Hunaiti, A., 2018. Accumulation and coarse mode aerosol concentrations and carbonaceous contents in the urban background atmosphere in Amman, Jordan. *Arabian Journal of Geosciences* 11, 617.
- INFRAS, 2007. Handbook Emission Factors for Road Transport (HBEFA).
- Issa, N.S.C., Al Abbar, S.D., 2015. Sustainability in the Middle East: achievements and challenges. *International Journal of Sustainable Building Technology and Urban Development* 6, 34-38.
- Kakosimos, K.E., Assael, M.J., Katsarou, A.S., 2011. Application and evaluation of AERMOD on the assessment of particulate matter pollution caused by industrial activities in the Greater Thessaloniki area. *Environmental Technology* 32, 593-608.
- Kakosimos, K.E., Hertel, O., Ketzel, M., Berkowicz, R., 2010. Operational Street Pollution Model (OSPM) – a review of performed application and validation studies, and future prospects. *Environmental Chemistry* 7, 485-503.

- Kalenderski, S., Stenchikov, G., Zhao, C., 2013. Modeling a typical winter-time dust event over the Arabian Peninsula and the Red Sea. *Atmospheric Chemistry and Physics* 13, 1999-2014.
- Kara, M., Mangir, N., Bayram, A., Elbir, T., 2014. A spatially high resolution and activity based emissions inventory for the metropolitan area of Istanbul, Turkey. *Aerosol and Air Quality Research* 14, 10-20.
- Ketzel, M., Omstedt, G., Johansson, C., Düring, I., Pohjola, M., Oettl, D., Gidhagen, L., Wählin, P., Lohmeyer, A., Haakana, M., Berkowicz, R., 2007. Estimation and validation of PM_{2.5}/PM₁₀ exhaust and non-exhaust emission factors for practical street pollution modelling. *Atmospheric Environment* 41, 9370-9385.
- Khodeir, M., Shamy, M., Alghamdi, M., Zhong, M., Sun, H., Costa, M., Chen, L., Maciejczyk, P., 2012. Source apportionment and elemental composition of PM_{2.5} and PM₁₀ in Jeddah City, Saudi Arabia. *Atmospheric Pollution Research* 3, 331-340.
- Kholdebarin, A., Biati, A., Moattar, F., Shariat, S.M., 2015. Outdoor PM₁₀ source apportionment in metropolitan cities—a case study. *Environmental Monitoring and Assessment* 187, 49.
- Kinsey, J.S., Linna, K.J., Squier, W.C., Muleski, G.E., Cowherd Jr., C., 2004. Characterization of the fugitive particulate emissions from construction mud/dirt carryout. *Journal of the Air and Waste Management Association* 54, 1394-1404.
- Kontos, S., Liora, N., Giannaros, C., Kakosimos, K., Poupkou, A., Melas, D., 2018. Modeling natural dust emissions in the central Middle East: Parameterizations and sensitivity. *Atmospheric Environment* 190, 294-307.
- Kouyoumdjian, H., Saliba, N.A., 2006. Mass concentration and ion composition of coarse and fine particles in an urban area in Beirut: effect of calcium carbonate on the absorption of nitric and sulfuric acids and the depletion of chloride. *Atmospheric Chemistry and Physics* 6, 1865-1877.
- Krasnov, H., Katra, I., Koutrakis, P., Friger, M.D., 2014. Contribution of dust storms to PM₁₀ levels in an urban arid environment. *Journal of the Air and Waste Management Association* 64, 89-94.
- Krasnov, H., Katra, I., Novack, V., Vodonos, A., Friger, M.D., 2015. Increased indoor PM concentrations controlled by atmospheric dust events and urban factors. *Building and Environment* 87, 169-176.
- Krecl, P., Targino, A.C., Landi, T.P., Ketzel, M., 2018. Determination of black carbon, PM_{2.5}, particle number and NO_x emission factors from roadside measurements and their implications for emission inventory development. *Atmospheric Environment* 186, 229-240.

- Kuenen, J., van der Gon, H., Visschedijk, A., Dröge, R., van Gijlswijk, R., 2011. MACC European emission inventory for the years 2003-2007. The Netherlands Organisation.
- Kumar, P., Imam, B., 2013. Footprints of air pollution and changing environment on the sustainability of built infrastructure. *Science of the Total Environment* 444, 85-101.
- Kumar, P., Morawska, L., 2014. Recycling concrete: An undiscovered source of ultrafine particles. *Atmospheric Environment* 90, 51-58.
- Kumar, P., Morawska, L., Birmili, W., Paasonen, P., Hu, M., Kulmala, M., Harrison, R.M., Norford, L., Britter, R., 2014. Ultrafine particles in cities. *Environment International* 66, 1-10.
- Kumar, P., Mulheron, M., Som, C., 2012. Release of ultrafine particles from three simulated building processes. *Journal of Nanoparticle Research* 14, 1-14.
- Kumar, P., Pirjola, L., Ketzel, M., Harrison, R.M., 2013. Nanoparticle emissions from 11 non-vehicle exhaust sources – A review. *Atmospheric Environment* 67, 252-277.
- Kwak, J., Lee, S., Lee, S., 2014. On-road and laboratory investigations on non-exhaust ultrafine particles from the interaction between the tire and road pavement under braking conditions. *Atmospheric Environment* 97, 195-205.
- Laurent, B., Marticorena, B., Bergametti, G., Léon, J.F., Mahowald, N.M., 2008. Modeling mineral dust emissions from the Sahara desert using new surface properties and soil database. *Journal of Geophysical Research: Atmospheres* 113.
- Lawrence, S., Sokhi, R., Ravindra, K., 2016. Quantification of vehicle fleet PM10 particulate matter emission factors from exhaust and non-exhaust sources using tunnel measurement techniques. *Environmental Pollution* 210, 419-428.
- Lee, J.H., Hopke, P.K., Holsen, T.M., Polissar, A.V., 2005. Evaluation of continuous and filter-based methods for measuring PM2.5 mass concentration. *Aerosol Science and Technology* 39, 290-303.
- Lenschow, P., 2001. Some ideas about the sources of PM10. *Atmospheric Environment* 35, S23.
- Lim, C.C., Thurston, G.D., Shamy, M., Alghamdi, M.r., Khoder, M., Mohorjy, A.M., Alkhalaf, A.K., Brocato, J., Chen, L.C., Costa, M., 2018. Temporal variations of fine and coarse particulate matter sources in Jeddah, Saudi Arabia. *Journal of the Air & Waste Management Association* 68, 123-138.
- Liora, N., Markakis, K., Poupkou, A., Giannaros, T.M., Melas, D., 2015. The natural emissions model (NEMO): Description, application and model evaluation. *Atmospheric Environment* 122, 493-504.

- Liora, N., Poupkou, A., Giannaros, T.M., Kakosimos, K.E., Stein, O., Melas, D., 2016. Impacts of natural emission sources on particle pollution levels in Europe. *Atmospheric Environment* 137, 171-185.
- MacKinnon, D.J., Clow, G.D., Tigges, R.K., Reynolds, R.L., Chavez, J.P.S., 2004. Comparison of aerodynamically and model-derived roughness lengths (zo) over diverse surfaces, central Mojave Desert, California, USA. *Geomorphology* 63, 103-113.
- Markakis, K., Im, U., Unal, A., Melas, D., Yenigun, O., Incecik, S., 2012. Compilation of a GIS based high spatially and temporally resolved emission inventory for the greater Istanbul area. *Atmospheric Pollution Research* 3, 112-125.
- Marticorena, B., Bergametti, G., 1995. Modeling the atmospheric dust cycle: 1. Design of a soil-derived dust emission scheme. *Journal of Geophysical Research: Atmospheres* 100, 16,415-416,430.
- Marticorena, B., Bergametti, G., Aumont, B., Callot, Y., N'Doumé, C., Legrand, M., 1997. Modeling the atmospheric dust cycle: 2. Simulation of Saharan dust sources. *Journal of Geophysical Research: Atmospheres* 102, 4387-4404.
- Massoud, R., Shihadeh, A.L., Roumié, M., Youness, M., Gerard, J., Saliba, N., Zaarour, R., Abboud, M., Farah, W., Saliba, N.A., 2011. Intraurban variability of PM10 and PM2.5 in an Eastern Mediterranean city. *Atmospheric Research* 101, 893-901.
- MDPS, 2015. Chapter VIII: Transport and communications statistics (2015).
- Menut, L., Pérez, C., Haustein, K., Bessagnet, B., Prigent, C., Alfaro, S., 2013. Impact of surface roughness and soil texture on mineral dust emission fluxes modeling. *Journal of Geophysical Research: Atmospheres* 118, 6505-6520.
- Ministry for the Environment, N.Z., 2001. Good practice guide for preparing emissions inventories, Ministry for the Environment, New Zealand.
- Mokalled, T., Le Calvé, S., Badaro-Saliba, N., Abboud, M., Zaarour, R., Farah, W., Adjizian-Gérard, J., 2018. Identifying the impact of Beirut airport's activities on local air quality - Part I: Emissions inventory of NO2 and VOCs. *Atmospheric Environment* 187, 435-444.
- Mori, Y., 1986. Evaluation of several 'single-pass' estimators of the mean and the standard deviation of wind direction. *Journal of Climate and Applied Meteorology* 25, 1387-1397.
- Munir, S., Habeebullah, T.M., Mohammed, A.M.F., Morsy, E.A., Rehan, M., Ali, K., 2017. Analysing PM2.5 and its association with PM10 and meteorology in the arid climate of Makkah, Saudi Arabia. *Aerosol and Air Quality Research* 17, 453-464.

- Naddafi, K., Hassanvand, M., Yunesian, M., Momeniha, F., Nabizadeh, R., Faridi, S., Gholampour, A., 2012. Health impact assessment of air pollution in megacity of Tehran, Iran. *Iranian Journal of Environmental Health Science & Engineering* 9, 28.
- Namdari, S., Karimi, N., Sorooshian, A., Mohammadi, G., Sehatkashani, S., 2018. Impacts of climate and synoptic fluctuations on dust storm activity over the Middle East. *Atmospheric Environment* 173, 265-276.
- Nasser, Z., Salameh, P., Nasser, W., Abbas, L.A., Elias, E., Leveque, A., 2015. Outdoor Particulate Matter (PM) and associated cardiovascular diseases in the Middle East. *International Journal of Occupational Medicine and Environmental Health* 28, 641-661.
- Nayebare, S., Aburizaiza, O.S., Khwaja, H.A., Siddique, A., Hussain, M.M., Zeb, J., Khatib, F., Carpenter, D.O., Blake, D.R., 2016. Chemical characterization and source apportionment of PM_{2.5} in Rabigh, Saudi Arabia. *Aerosol and Air Quality Research* 16, 3114-3129.
- Nayebare, S.R., Aburizaiza, O.S., Siddique, A., Carpenter, D.O., Hussain, M.M., Zeb, J., Aburizaiza, A.J., Khwaja, H.A., 2018. Ambient air quality in the holy city of Makkah: A source apportionment with elemental enrichment factors (EFs) and factor analysis (PMF). *Environmental Pollution* 243, 1791-1801.
- Nelin, T.D., Joseph, A.M., Gorr, M.W., Wold, L.E., 2012. Direct and indirect effects of particulate matter on the cardiovascular system. *Toxicology Letters* 208, 293-299.
- Nemmar, A., Hoet, P.H.M., Vanquickenborne, B., Dinsdale, D., Thomeer, M., Hoylaerts, M.F., Vanbilloen, H., Mortelmans, L., Nemery, B., 2002. Passage of inhaled particles into the blood circulation in humans. *Circulation* 105, 411-417.
- Neuman, C.M., 2003. Effects of temperature and humidity upon the entrainment of sedimentary particles by wind. *Boundary-Layer Meteorology* 108, 61-89.
- Neuman, C.M., Boulton, J.W., Sanderson, S., 2009. Wind tunnel simulation of environmental controls on fugitive dust emissions from mine tailings. *Atmospheric Environment* 43, 520-529.
- Nickling, W.G., Gillies, J.A., 1989. Emission of fine-grained particulates from desert soils, in: Leinen, M., Sarnthein, M. (Eds.), *Paleoclimatology and Paleometeorology: Modern and Past Patterns of Global Atmospheric Transport*. Springer Netherlands, pp. 133-165.
- Nickovic, S., Kallos, G., Papadopoulos, A., Kakaliagou, O., 2001. A model for prediction of desert dust cycle in the atmosphere. *Journal of Geophysical Research: Atmospheres* 106, 18113-18129.
- Niemeyer, T.C., Gillette, D.A., Deluisi, J.J., Kim, Y.J., Niemeyer, W.F., Ley, T., Gill, T.E., Ono, D., 1999. Optical depth, size distribution and flux of dust from Owens Lake, California. *Earth Surface Processes and Landforms* 24, 463-479.

- Norris, G., Duvall, R., Brown, S., Bai, S., 2014. EPA Positive Matrix Factorization (PMF) 5.0 fundamentals and user guide, in: Agency, U.S.E.P. (Ed.).
- NPI, 1999. Emission estimation technique manual for cement manufacturing, National Pollutant Inventory (NPI). Australian Government, Department of the Environment.
- NPI, 2005. Improvement of NPI fugitive particulate matter emission estimation techniques, National Pollutant Inventory (NPI): Australian Government, Department of the Environment, 2005.
- NSAI, 2014. Ambient air - Standard gravimetric measurement method for the determination of the PM10 or PM2.5 mass concentrations of suspended Particulate Matter (Irish Standard EN12341:2014). National Standards Authority of Ireland.
- Omstedt, G., Bringfelt, B., Johansson, C., 2005. A model for vehicle-induced non-tailpipe emissions of particles along Swedish roads. *Atmospheric Environment* 39, 6088-6097.
- Ono, D., 2006. Application of the Gillette model for windblown dust at Owens Lake, CA. *Atmospheric Environment* 40, 3011-3021.
- Ono, D., Kiddo, P., Howard, C., Davis, G., Richmond, K., 2011. Application of a combined measurement and modeling method to quantify windblown dust emissions from the exposed playa at Mono Lake, California. *Journal of the Air and Waste Management Association* 61, 1036-1045.
- Ostro, B., 2004. Outdoor air pollution: assessing the environmental burden of disease at national and local levels. Geneva, World Health Organization (WHO environmental burden of disease series, no. 5).
- Paatero, P., 1997. Least squares formulation of robust non-negative factor analysis. *Chemometrics and Intelligent Laboratory Systems* 37, 23-35.
- Paatero, P., Hopke, P.K., Song, X.-H., Ramadan, Z., 2002. Understanding and controlling rotations in factor analytic models. *Chemometrics and Intelligent Laboratory Systems* 60, 253-264.
- Padoan, E., Ajmone-Marsan, F., Querol, X., Amato, F., 2018. An empirical model to predict road dust emissions based on pavement and traffic characteristics. *Environmental Pollution* 237, 713-720.
- Pandolfi, M., Gonzalez-Castanedo, Y., Alastuey, A., de la Rosa, J.D., Mantilla, E., de la Campa, A.S., Querol, X., Pey, J., Amato, F., Moreno, T., 2011. Source apportionment of PM10 and PM2.5 at multiple sites in the strait of Gibraltar by PMF: impact of shipping emissions. *Environmental Science and Pollution Research* 18, 260-269.

- Pant, P., Harrison, R.M., 2013. Estimation of the contribution of road traffic emissions to particulate matter concentrations from field measurements: A review. *Atmospheric Environment* 77, 78-97.
- Pérez, N., Pey, J., Reche, C., Cortés, J., Alastuey, A., Querol, X., 2016. Impact of harbour emissions on ambient PM10 and PM2.5 in Barcelona (Spain): Evidences of secondary aerosol formation within the urban area. *Science of the Total Environment* 571, 237-250.
- Pey, J., Pérez, N., Cortés, J., Alastuey, A., Querol, X., 2013. Chemical fingerprint and impact of shipping emissions over a western Mediterranean metropolis: Primary and aged contributions. *Science of the Total Environment* 463-464, 497-507.
- Pirjola, L., Johansson, C., Kupiainen, K., Stojiljkovic, A., Karlsson, H., Hussein, T., 2010. Road dust emissions from paved roads measured using different mobile systems. *Journal of the Air and Waste Management Association* 60, 1422-1433.
- Polissar, A.V., Hopke, P.K., Harris, J.M., 2001. Source regions for atmospheric aerosol measured at Barrow, Alaska. *Environmental Science and Technology* 35, 4214-4226.
- Polissar, A.V., Hopke, P.K., Paatero, P., Malm, W.C., Sisler, J.F., 1998. Atmospheric aerosol over Alaska: 2. Elemental composition and sources. *Journal of Geophysical Research: Atmospheres* 103, 19045-19057.
- Pope, C.A., 3rd, Burnett, R.T., Thun, M.J., Calle, E.E., Krewski, D., Ito, K., Thurston, G.D., 2002. Lung cancer, cardiopulmonary mortality, and long-term exposure to fine particulate air pollution. *JAMA* 287, 1132-1141.
- Pope, F.D., Gatari, M., Ng'ang'a, D., Poynter, A., Blake, R., 2018. Airborne particulate matter monitoring in Kenya using calibrated low-cost sensors. *Atmospheric Chemistry and Physics* 18, 15403-15418.
- Pope III, C.A., Dockery, D.W., 2006. Health effects of fine particulate air pollution: lines that connect. *Journal of the Air and Waste Management Association* 56, 709-742.
- Pouliot, G., Pierce, T., Denier van der Gon, H., Schaap, M., Moran, M., Nopmongcol, U., 2012. Comparing emission inventories and model-ready emission datasets between Europe and North America for the AQMEII project. *Atmospheric Environment* 53, 4-14.
- Prabha, J., 2006. Comparison and performance evaluation of dispersion models FDM and ISCST3 for a gold mine at Goa. *Journal of Industrial Pollution Control* 22, 297-303.
- Prakash, P.J., Stenchikov, G., Kalenderski, S., Osipov, S., Bangalath, H., 2015. The impact of dust storms on the Arabian Peninsula and the Red Sea. *Atmospheric Chemistry and Physics* 15, 199.
- PSA, 2018. 2018 Report of the Qatar Planning and Statistics Authority.

- Qiao, F., Li, Q., Lei, Y., 2018. Particulate Matter caused health risk in an urban area of the Middle East and the challenges in reducing its anthropogenic emissions. *Environment Pollution and Climate Change* 2, 145.
- QMD, Climate Information for Doha. Qatar Meterology Department, Civil Aviation Authority, <http://qweather.gov.qa/>.
- Rasheed, A., Aneja, V.P., Ayyer, A., Rafique, U., 2015. Measurement and analysis of fine Particulate Matter (PM_{2.5}) in urban areas of Pakistan. *Aerosol and Air Quality Research*.
- Rashki, A., Eriksson, P.G., Rautenbach, C.J.d.W., Kaskaoutis, D.G., Grote, W., Dykstra, J., 2013. Assessment of chemical and mineralogical characteristics of airborne dust in the Sistan region, Iran. *Chemosphere* 90, 227-236.
- Reff, A., Eberly, S.I., Bhave, P.V., 2007. Receptor modeling of ambient Particulate Matter data using Positive Matrix Factorization: review of existing methods. *Journal of the Air and Waste Management Association* 57, 146-154.
- Riccio, A., Chianese, E., Monaco, D., Costagliola, M.A., Perretta, G., Prati, M.V., Agrillo, G., Esposito, A., Gasbarra, D., Shindler, L., Brusasca, G., Nanni, A., Pozzi, C., Magliulo, V., 2016. Real-world automotive particulate matter and PAH emission factors and profile concentrations: Results from an urban tunnel experiment in Naples, Italy. *Atmospheric Environment* 141, 379-387.
- Roney, J.A., White, B.R., 2006. Estimating fugitive dust emission rates using an environmental boundary layer wind tunnel. *Atmospheric Environment* 40, 7668-7685.
- Saab, N., 2017. AFED (2017). Arab Environment in 10 Years in: Saab, N. (Ed.), Annual Report of Arab Forum for Environment and Development, Beirut, Lebanon. Technical Publications.
- Saliba, N., Massoud, R., 2011. A comparative review of PM Levels, sources, and their likely fates in the Eastern Mediterranean region, in: Zereini F., W.C.L.S.E. (Ed.), *Urban Airborne Particulate Matter*. Springer Berlin Heidelberg, Environmental Science and Engineering, pp. 3-17.
- Samoli, E., Peng, R., Ramsay, T., Pipikou, M., Touloumi, G., Dominici, F., Burnett, R., Cohen, A., Krewski, D., Samet, J., Katsouyanni, K., 2008. Acute effects of ambient particulate matter on mortality in Europe and North America: results from the APHENA study. *Environmental Health Perspectives* 116, 1480-1486.
- Sanderson, R.S., Neuman, C.M., Boulton, J.W., 2014. Windblown fugitive dust emissions from smelter slag. *Aeolian Research* 13, 19-29.

- Sanf elix, V., Escrig, A., L opez-Lilao, A., Celades, I., Monfort, E., 2015. On the source inversion of fugitive surface layer releases. Part I. Model formulation and application to simple sources. *Atmospheric Environment* 109, 171-177.
- Sanf elix, V., Escrig, A., L opez-Lilao, A., Celades, I., Monfort, E., 2017. On the source inversion of fugitive surface layer releases. Part II. Complex sources. *Atmospheric Environment* 158, 27-35.
- Saraga, D., Maggos, T., Sadoun, E., Fthenou, E., Hassan, H., Tsiouri, V., Karavoltsos, S., Sakellari, A., Vasilakos, C., Kakosimos, K., 2017. Chemical characterization of indoor and outdoor Particulate Matter (PM_{2.5}, PM₁₀) in Doha, Qatar. *Aerosol and Air Quality Research* 17, 1156–1168.
- Saraga, D.E., Tolis, E.I., Maggos, T., Vasilakos, C., Bartzis, J.G., 2019. PM_{2.5} source apportionment for the port city of Thessaloniki, Greece. *Science of the Total Environment* 650, 2337-2354.
- Sarnat, J.A., Moise, T., Shpund, J., Liu, Y., Pachon, J.E., Qasrawi, R., Abdeen, Z., Brenner, S., Nassar, K., Saleh, R., Schauer, J.J., 2010. Assessing the spatial and temporal variability of fine particulate matter components in Israeli, Jordanian, and Palestinian cities. *Atmospheric Environment* 44, 2383-2392.
- Sassen, K., DeMott, P.J., Prospero, J.M., Poellot, M.R., 2003. Saharan dust storms and indirect aerosol effects on clouds: CRYSTAL-FACE results. *Geophysical Research Letters* 30.
- Schaap, M., Manders, A.M.M., Hendriks, E.C.J., Cnossen, J.M., Segers, A.J.S., Denier van der Gon, H.A.C., Jozwicka, M., Sauter, F., Velders, G., Matthijsen, J., Bultjes, P.J.H., 2009. Regional modelling of particulate matter for the Netherlands, Technical background report BOP 500099008. Netherlands Environmental Assessment Agency, (PBL).
- Scott, P.K., Proctor, D., 2008. Soil suspension/dispersion modeling methods for estimating health-based soil cleanup levels of hexavalent chromium at chromite ore processing residue sites. *Journal of the Air and Waste Management Association* 58, 384-403.
- Shahsavani, A., Naddafi, K., Jafarzade Haghighifard, N., Mesdaghinia, A., Yunesian, M., Nabizadeh, R., Arahami, M., Sowlat, M.H., Yarahmadi, M., Saki, H., Alimohamadi, M., Nazmara, S., Motevalian, S.A., Goudarzi, G., 2012. The evaluation of PM₁₀, PM_{2.5}, and PM₁ concentrations during the Middle Eastern Dust (MED) events in Ahvaz, Iran, from april through september 2010. *Journal of Arid Environments* 77, 72-83.
- Shaltout, A.A., Boman, J., Al-Malawi, D.-a.R., Shehadeh, Z.F., 2013. Elemental composition of PM_{2.5} particles sampled in industrial and residential areas of Taif, Saudi Arabia. *Aerosol and Air Quality Research* 13, 1356-1364.
- Shaltout, A.A., Hassan, S.K., Karydas, A.G., Zaki, Z.I., Mostafa, N.Y., Kregsamer, P., Wobrauschek, P., Strelı, C., 2018. Comparative elemental analysis of fine particulate

- matter (PM_{2.5}) from industrial and residential areas in Greater Cairo-Egypt by means of a multi-secondary target energy dispersive X-ray fluorescence spectrometer. *Spectrochimica Acta Part B: Atomic Spectroscopy* 145, 29-35.
- Shamy, M., Alghamdi, M., Khoder, M.I., Mohorjy, A.M., Alkhatim, A.A., Alkhalaf, A.K., Brocato, J., Chen, L.C., Thurston, G.D., Lim, C.C., Costa, M., 2018. Association between exposure to ambient air particulates and metabolic syndrome components in a Saudi Arabian population. *Int J Environ Res Public Health* 15, 27.
- Shao, Y., 2009. *Physics and modelling of wind erosion*. S.l. : Springer.
- Shao, Y., Raupach, M.R., Findlater, P.A., 1993. Effect of saltation bombardment on the entrainment of dust by wind. *Journal of Geophysical Research: Atmospheres* 98, 12719-12726.
- Shaw, W.J., Jerry Allwine, K., Fritz, B.G., Rutz, F.C., Rishel, J.P., Chapman, E.G., 2008. An evaluation of the wind erosion module in DUSTRAN. *Atmospheric Environment* 42, 1907-1921.
- Shirmohammadi, F., Wang, D., Hasheminassab, S., Verma, V., Schauer, J.J., Shafer, M.M., Sioutas, C., 2017. Oxidative potential of on-road fine particulate matter (PM_{2.5}) measured on major freeways of Los Angeles, CA, and a 10-year comparison with earlier roadside studies. *Atmospheric Environment* 148, 102-114.
- Shraim, A.M., Alenazi, D.A., Abdel-Salam, A.-S.G., Kumar, P., 2016. Loading rates of dust and metals in residential houses of arid and dry climatic regions. *Aerosol and Air Quality Research* 16, 2462-2473.
- Sindhwan, R., Goyal, P., Kumar, S., Kumar, A., 2015. Anthropogenic emission inventory of criteria air pollutants of an urban agglomeration - National Capital Region (NCR), Delhi. *Aerosol and Air Quality Research* 15, 1681-1697.
- Sivacoumar, R., Mohan Raj, S., Chinnadurai, S.J., Jayabalou, R., 2009. Modeling of fugitive dust emission and control measures in stone crushing industry. *Journal of Environmental Monitoring* 11, 987-997.
- Soleimani, Z., Parhizgari, N., Dehdari Rad, H., Akhoond, M.R., Kermani, M., Marzouni, M.B., Goudarzi, H., Goudarzi, G., 2015. Normal and dusty days comparison of culturable indoor airborne bacteria in Ahvaz, Iran. *Aerobiologia* 31, 127-141.
- Sowlat, M.H., Naddafi, K., Yunesian, M., Jackson, P.L., Lotfi, S., Shahsavani, A., 2013. PM₁₀ source apportionment in Ahvaz, Iran, using Positive Matrix Factorization. *CLEAN – Soil, Air, Water* 41, 1143-1151.
- Taghvaei, S., Sowlat, M.H., Mousavi, A., Hassanvand, M.S., Yunesian, M., Naddafi, K., Sioutas, C., 2018. Source apportionment of ambient PM_{2.5} in two locations in central Tehran using

- the Positive Matrix Factorization (PMF) model. *Science of The Total Environment* 628-629, 672-686.
- Tan, C., Fang, W., 2018. Mapping the wind hazard of global tropical cyclones with parametric wind field models by considering the effects of local factors. *International Journal of Disaster Risk Science* 9, 86-99.
- Terrouche, A., Ali-Khodja, H., Talbi, M., Bencharif-Madani, F., Charron, A., Derradji, A., 2015. Roadside PM10 and associated metals in Constantine, Algeria. *International Journal of Environmental Studies* 72, 74-86.
- Thorpe, A., Harrison, R.M., 2008. Sources and properties of non-exhaust particulate matter from road traffic: A review. *Science of the Total Environment* 400, 270-282.
- Thorpe, A.J., Harrison, R.M., Boulter, P.G., McCrae, I.S., 2007. Estimation of particle resuspension source strength on a major London road. *Atmospheric Environment* 41, 8007-8020.
- Thurston, G.D., Spengler, J.D., 1985. A quantitative assessment of source contributions to inhalable particulate matter pollution in metropolitan Boston. *Atmospheric Environment* (1967) 19, 9-25.
- Tolis, E.I., Saraga, D.E., Filiou, K.F., Tziavos, N.I., Tsioulos, C.P., Dinas, A., Bartzis, J.G., 2015. One-year intensive characterization on PM2.5 nearby port area of Thessaloniki, Greece. *Environmental Science and Pollution Research* 22, 6812-6826.
- Trivedi, R., Chakraborty, M.K., Tewary, B.K., 2009. Dust dispersion modeling using fugitive dust model at an opencast coal project of Western Coalfields Limited, India. *Journal of Scientific and Industrial Research* 68, 71-78.
- Tsiouri, V., Kakosimos, K.E., Kumar, P., 2015. Concentrations, sources and exposure risks associated with particulate matter in the Middle East Area—a review. *Air Quality, Atmosphere and Health* 8, 67-80.
- USEPA, 1987. Reference method for the determination of Particulate Matter as PM10 in the atmosphere, 40 CFR Appendix J to Part 50, in: Agency, U.E.P. (Ed.), *Federal Register*.
- USEPA, 1995. AP 42: Compilation of air pollutant emission factors U.S. Environmental Protection Agency.
- USEPA, 2000. Meteorological monitoring guidance for regulatory modeling applications. U.S. Environmental Protection Agency, Office of Air and Radiation, Office of Air Quality Planning and Standards, Research Triangle Park, NC.
- USEPA, 2004. Chemical Mass Balance (CMB) Model. United States Environmental Protection Agency.

- USEPA, 2005. Revision to the guideline on air quality models: adoption of a preferred general purpose (flat and complex terrain) dispersion model and other revisions. US Environmental Protection Agency 70, 68218-68261.
- USEPA, 2006. AP 42: Compilation of air pollutant emission factors, fifth edition, volume 1. Chapter 13: Miscellaneous sources. .
- USEPA, 2008. EPA's Report on the Environment (ROE) (2008 final report), U.S. Environmental Protection Agency, Washington, D.C., pp. NTIS PB2008-112484.
- USEPA, 2009. Integrated Science Assessment (ISA) for Particulate Matter, U.S. Environmental Protection Agency, Washington, DC.
- USEPA, 2011. Rule for limiting fugitive Particulate Matter emissions, 40 CFR 49.126, in: Agency, U.E.P. (Ed.), Federal Register.
- USEPA, 2014. National Emissions Inventory (NEI) US Environmental Protection Agency.
- USEPA, 2015. Motor Vehicle Emission Simulator (MOVES). United States Environmental Protection Agency.
- USEPA, 2016. Motor Vehicle Emission Simulator. MOVES2014a user guide EPA report EPA-420-B-16-085. Office of Transportation and Air Quality.
- USGS, 2000. Global Land Cover Characteristics (GLCC) data base version 2.0. United States Geological Survey, <https://www.usgs.gov/media/images/global-land-cover-characteristics-data-base-version-20>.
- Valavanidis, A., Fiotakis, K., Vlachogianni, T., 2008. Airborne Particulate Matter and human health: toxicological assessment and importance of size and composition of particles for oxidative damage and carcinogenic mechanisms. Taylor & Francis Group, pp. 339-362.
- Venkatram, A., 2000. A critique of empirical emission factor models: a case study of the AP-42 model for estimating PM10 emissions from paved roads. Atmospheric Environment 34, 1-11.
- Vodonos, A., Friger, M., Katra, I., Avnon, L., Krasnov, H., Koutrakis, P., Schwartz, J., Lior, O., Novack, V., 2014. The impact of desert dust exposures on hospitalizations due to exacerbation of chronic obstructive pulmonary disease. Air Quality, Atmosphere & Health 7, 433-439.
- Waked, A., Afif, C., Seigneur, C., 2012. An atmospheric emission inventory of anthropogenic and biogenic sources for Lebanon. Atmospheric Environment 50, 88-96.
- West, I., Al-Mulla, M.M., 2013. Qatar - geology, sabkhas, evaporites and desert environments.

- WHO, 2005. WHO Air Quality Guidelines for Particulate Matter, Ozone, Nitrogen Dioxide and Sulfur Dioxide - Global Update 2005, in: Organization, W.H. (Ed.), http://www.who.int/phe/health_topics/outdoorair/outdoorair_aqg/en/.
- WHO, 2016a. Ambient air pollution: a global assessment of exposure and burden of disease, in: Organization, W.H. (Ed.), <https://www.who.int/phe/publications/air-pollution-global-assessment/en/>.
- WHO, 2016b. WHO global urban ambient air pollution database (update 2016), http://www.who.int/phe/health_topics/outdoorair/databases/cities/en/.
- Winges, K.D., 1991. User's guide for the Fugitive Dust Model (FDM) revised: user's instructions. US Environmental Protection Agency, Report (EPA-910/9-88-202R); TRC Environmental Consultants.
- Winiwarter, W., Kuhlbusch, T.A.J., Viana, M., Hitzenberger, R., 2009. Quality considerations of European PM emission inventories. *Atmospheric Environment* 43, 3819-3828.
- WRAP, 2006. Wrap Fugitive Dust Handbook. Prepared by Countess Environmental, Westlake Village, California, for Western Governors' Association, Denver, Colorado US: Western Regional Air Partnership.
- Wu, Z., Zhang, X., Wu, M., 2016. Mitigating construction dust pollution: state of the art and the way forward. *Journal of Cleaner Production* 112, 1658-1666.
- Yu, Y., Notaro, M., Kalashnikova, O.V., Garay, M.J., 2016. Climatology of summer Shamal wind in the Middle East. *Journal of Geophysical Research: Atmospheres* 121, 289-305.
- Yuen, W., Du, K., Koloutsou-Vakakis, S., Rood, M.J., Kim, B.J., Kemme, M.I.R., Hashmonay, R.A., Meister, C., 2015. Fugitive Particulate Matter emissions to the atmosphere from tracked and wheeled vehicles in a desert region by hybrid-optical remote sensing. *Aerosol and Air Quality Research* 15, 1613-1626.
- Yuwono, A.S., Amaliah, L., Rochimawati, N.R., Kurniawan, A., Mulyanto, B., 2014. Determination of emission factors for soil borne dustfall and suspended particulate in ambient air. *ARPN Journal of Engineering and Applied Sciences* 9, 1417-1422.

Appendix A

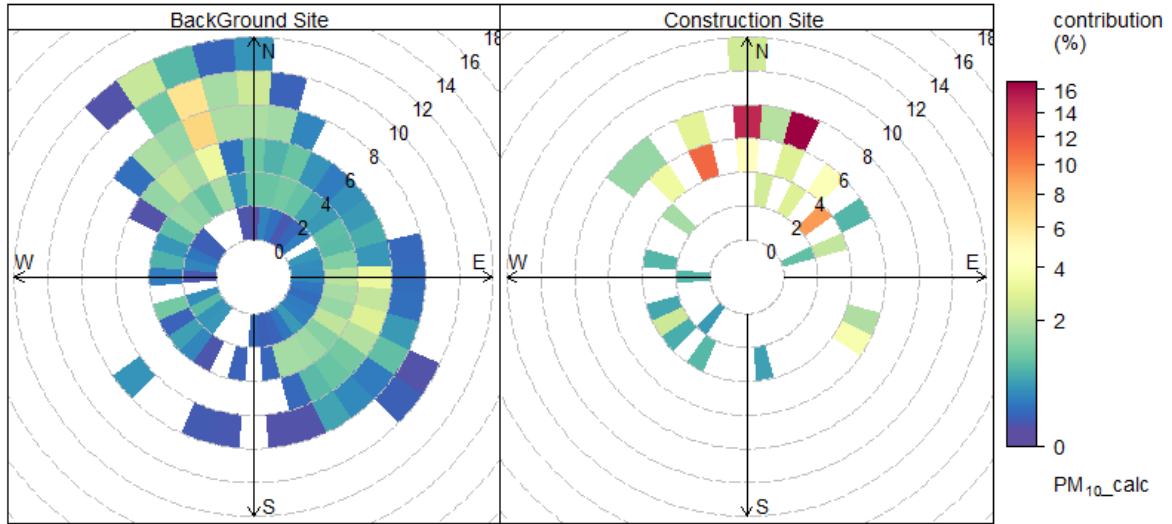


Figure A1 Contribution plot showing the contribution (%) from each wind sector to the mean PM₁₀

Appendix B

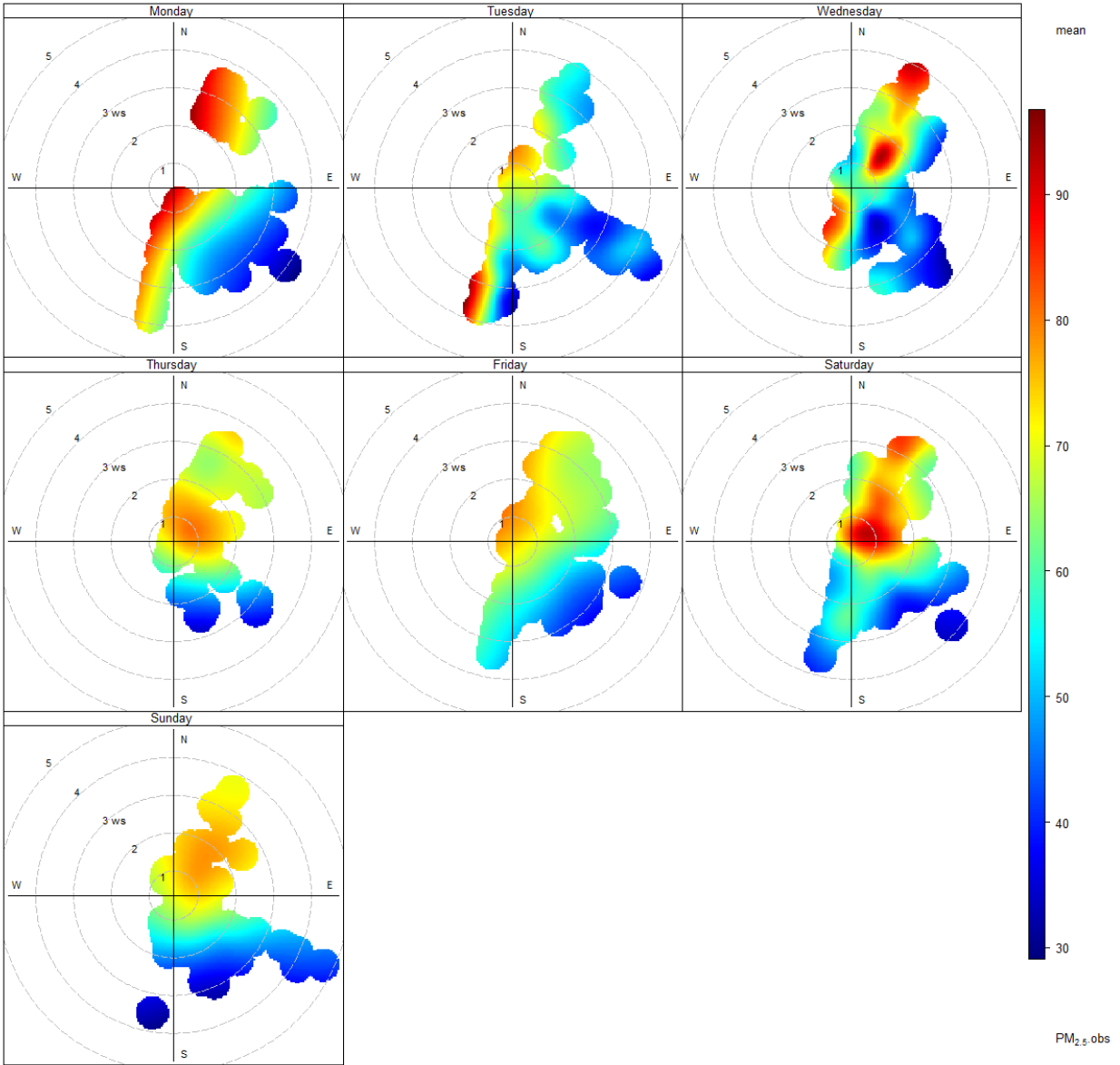
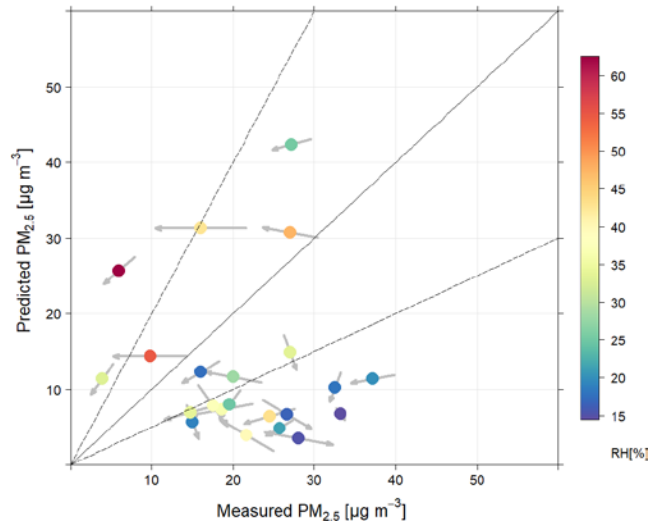
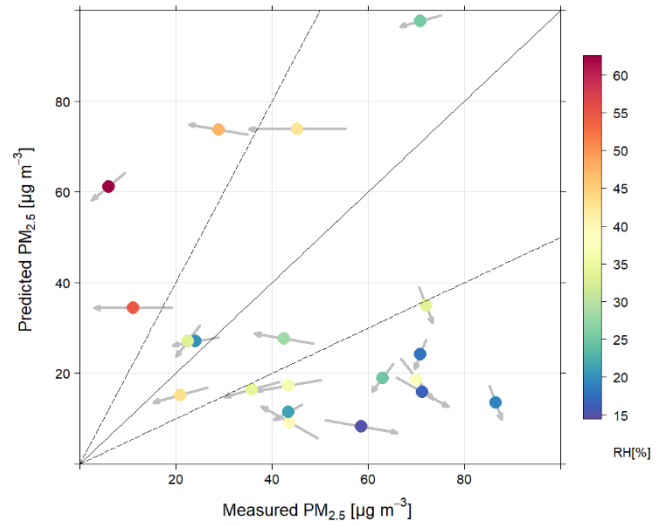


Figure B1 PM_{2.5} weekday pollution roses (with PM₁₀ threshold <160 $\mu\text{g m}^{-3}$)



(a) PM_{2.5} VEX linear model



(b) PM_{2.5} VfPM linear model

Figure B2 Scatter plot examples of the measured vs predicted (a) VEX and (b) VfPM PM_{2.5} concentration levels with the estimated EFs. Vectors correspond to the daily wind speed and prevailing direction, and colours the average relative humidity [%].

Appendix C

This appendix provides a list of Schaap model equations used for the calculation of Aeolian dust emissions (Section 6.2.2.1) and additional details for the formulations used in the model parameterizations for windblown dust (Schaap et al., 2009).

- The uncorrected threshold friction velocity:

$$u_{th,u}^*(D_p) = \left\{ \begin{array}{ll} \frac{0.129C}{(1.928(aD_p^x + b)^{0.092} - 1)^{0.5}} & \text{for } 0.03 < \text{Re} < 10 \\ 0.12C[1 - 0.0858(-0.0617((aD_p^x + b) - 10))] & \text{for } \text{Re} > 10 \end{array} \right\}$$

Where, $a = 1331 \text{cm}^{-x}$, $b = 0.38$, $x = 1.56$

- The threshold friction velocity is modified by the drag partitioning (f_{eff}):

$$u_{th}^*(D_p, z_0, z_{0s}) = u_{th,u}^*(D_p) \frac{f_w}{f_{eff}(z_0, z_{0s})}$$

where f_{eff} is calculated as:

$$f_{eff} = 1 - \left(\frac{\ln\left(\frac{z_0}{z_{0s}}\right)}{\ln\left(0.35\left(\frac{10}{z_{0s}}\right)\right)} \right)$$

- Horizontal flux of saltating particles ($\text{g m}^{-2} \text{s}^{-1}$):

$$F_h = \frac{K_l \rho_{air}}{g} u^{*3} \left(1 - \frac{u_{th}^*(D_p)}{u^*} \right) \left(1 + \frac{u_{th}^*(D_p)}{u^*} \right)^2$$

Comparison between CALMET-processed (MM5) and WRF-processed Meteorology data:

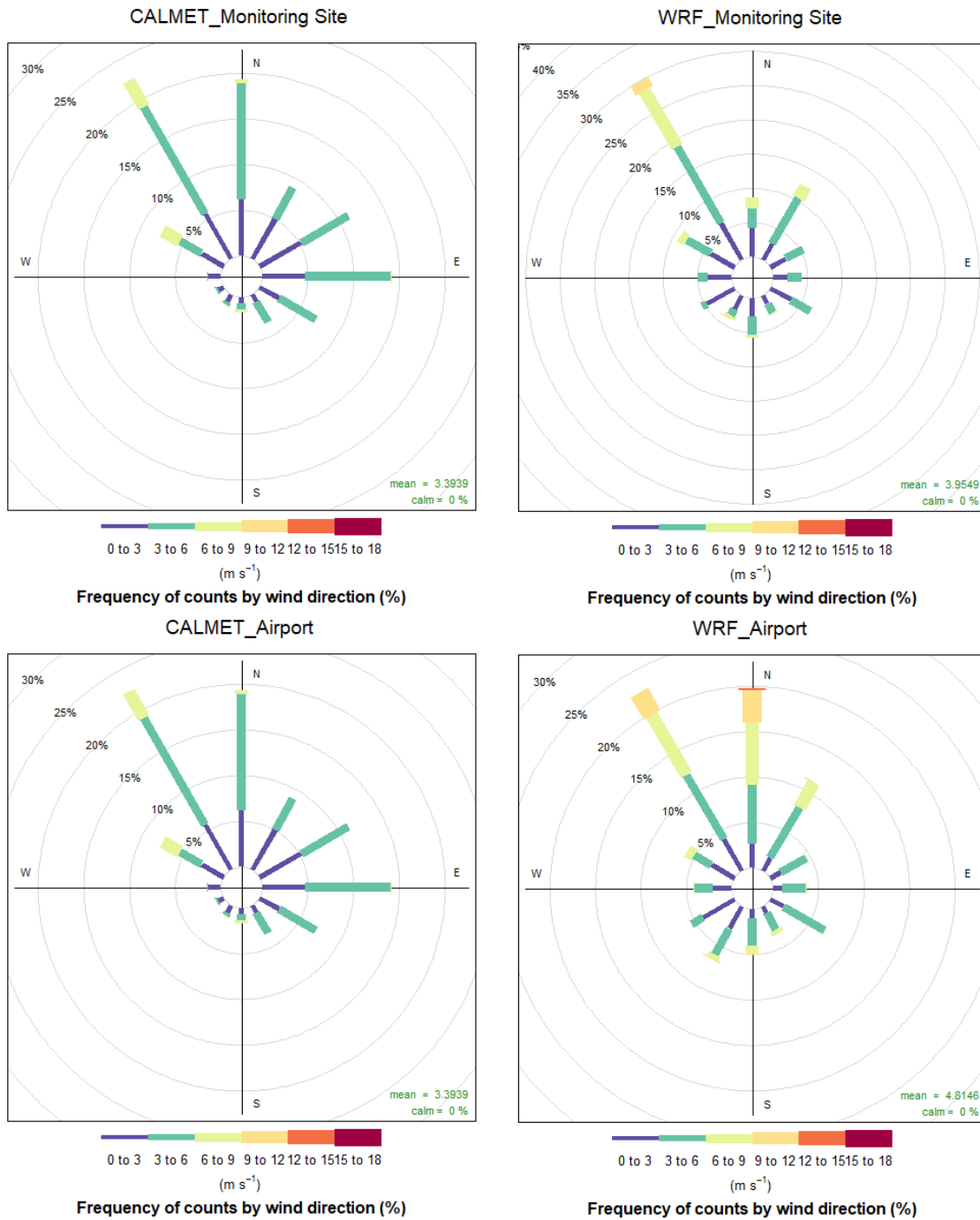


Figure C1 Wind roses comparing the meteorology data from CALMET and WRF models two locations within Doha city: (i) monitoring site and (ii) Doha International Airport

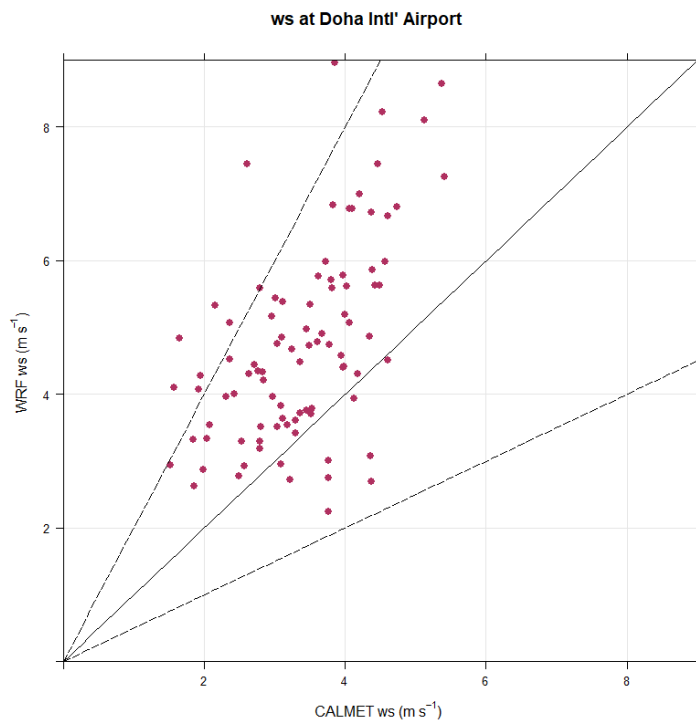
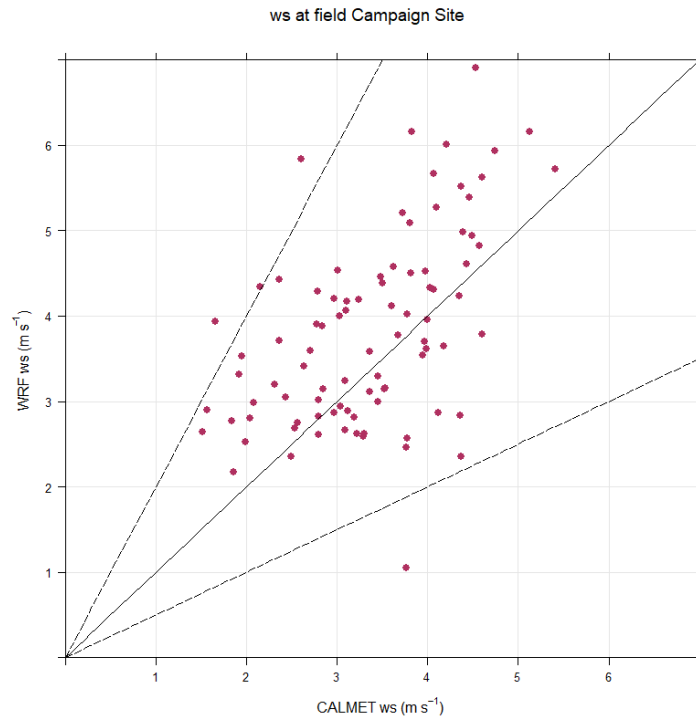


Figure C2 Scatter plots of wind speeds (u_{10}) predicted by CALMET and WRF models at two urban sites in Doha city: (i) the monitoring site and (ii) Doha International Airport